BRILLOUIN SCATTERING IN CUBIC CRYSTALS USING LASERS

by

KLAUS FRITSCH

B.S., Georgetown University

(1961)

SUBMITTED IN PARTIAL FULFILLMENT OF THE

REQUIREMENTS FOR THE DEGREE OF

MASTER OF SCIENCE

at the

MASSACHUSETTS INSTITUTE OF TECHNOLOGY

January, 1965

Signature of Author . . . . . .
Department of Physics, January 18, 1965

Certified by . . . . . .
Thesis Supervisor

Accepted by . . . . . .
Chairman, Departmental Committee
on Graduate Students

BRILLOUIN SCATTERING IN CUBIC CRYSTALS

USING LASERS

Klaus Fritsch

Submitted to the Department of Physics on January 18, 1965, in partial fulfillment of the requirements for the degree of Master of Science.

ABSTRACT

It is often desirable to make a detailed study of lattice vibrations in crystals. The well-known ultrasonic pulse methods yield precise information concerning the velocities of propagation of the elastic waves and the elastic constants in the ultrasonic region. These methods are adequate provided one is interested in a few principal directions of propagation only.

A technique is described here which makes use of the process of Brillouin scattering using a laser light source to make feasible a detailed and precise study of lattice vibrations in the hypersonic region (2 - 50 kMc). The main advantages of this method are:

(1) Ability to go to very high frequencies

(2) Absence of acoustic excitation

(3) Simplicity of obtaining the angular dependence of the sound velocities

(4) Possibility of measuring the polarization fraction of mixed modes

Using a low power laser the Brillouin spectra of light scattered inelastically from lattice vibrations were observed in three cubic crystals (KI, KCl and RbCl) for many directions of propagation of the elastic waves in the {110} planes. From this set of data the velocities of the elastic waves were calculated as a function of the direction of propagation. A computer was used to render those values for the three cubic elastic constants which made the root mean square deviation between the theoretical curve for the velocity and the experimental values a minimum.

Thesis Supervisor: George B. Benedek

Associate Professor of Physics

ACKNOWLEDGEMENTS

I would like to express my gratitude to Professor George B. Benedek, who showed a large amount of patience in supervising and guiding this project.

I also wish to make known my appreciation to the Department of Physics whose Graduate Assistantship made this work possible.

I am very grateful to Tom Greytak who wrote the computer program for me and to Joe Lastovka for many helpful discussions.

I wish to acknowledge the fine and speedy work done by Al Pukt who built the sample holder and by Janis A. Kalnajs in supplying and polishing several single crystals.

I am also grateful for the assistance and cooperation of Miss H. Fleischmann, who typed the manuscript.

Brookline, Massachusetts K.F.
January, 1965

TABLE OF CONTENTS

LIST OF FIGURES

LIST OF TABLES

Chapter I

BRILLOUIN SCATTERING

1.1 Introduction

This thesis presents a study of inelastic scattering of light by thermal phonons in cubic crystals using a laser as source of the incident radiation.

A study of Brillouin spectra in solids is instructive because it yields information on the elastic properties and the lattice vibrations in the solid entirely in the absence of accoustic excitation. For example, R. S. Krishnan[1] used Brillouin scattering to find effective elastic constants for a number of crystals for several simple propagation directions.

In this thesis I will undertake a more detailed study of the Brillouin spectrum as a function of the propagation direction in several cubic crystals. This will immediately give information on the velocities as a function of the propagation direction and hence information concerning the elastic constants.

1.2 Comparison with previous work

Brillouin scattering, a type of scattering analogous to thermal diffuse scattering of x rays[2] and coherent inelastic scattering of neutrons[3], was first described by L. Brillouin[4] in 1922. It was first observed experimentally in a solid, crystalline quartz, by E. Gross[5] in 1930.

In the years following 1930 many Indian physicists studied the Brillouin spectra of liquids and solids[6]. With solids, exposure times of the order of eighty hours using a mercury arc source were not exceptional due to the weak scattering of most solids. Clearly, this exposure time had to be shortened drastically for a project requiring many data points. Recently, it was shown by G. B. Benedek et al[7] and simultaneously by R. Y. Chiao and B. P. Stoicheff[8] that spectra of this type can be recorded in minutes with photoelectric equipment provided a laser is used as source of the incident radiation.

1.3 Choice of crystals

This research was limited to cubic crystals because of theoretical simplicity (only three independent elastic constants enter the calculations) and because there were transparent compounds available in large single crystals which show moderately strong spectra and are sufficiently hard. The latter requirement is necessitated by the fact that the resolution of the equipment was limited to about 1.3 parts in 10^6 in wavelength. Therefore, for results of the desired accuracy, the Brillouin peaks had to be separated from the unshifted Rayleigh component by a certain minimum wavelength interval. It was found that the alkali halides fulfilled both requirements.

1.4 Frequency change in the scattered radiation

We may describe Brillouin scattering of light by the following two processes:

1) Phonon annihilation - An incident photon of frequency ν_i and wave vector $\underset{\sim}{k}_i$ annihilates a thermal phonon of frequency ν_σ and wave vector $\underset{\sim}{k}_\sigma$ propagating in the solid. The incident photon has gained energy and emerges with increased frequency ν_s ($\nu_s > \nu_i$) and wave vector $\underset{\sim}{k}_s$. This process is referred to as Anti-Stokes scattering in the Raman effect.

2) Phonon creation - An incident photon of frequency ν_i and wave vector $\underset{\sim}{k}_i$ creates a phonon of frequency ν_σ and wave vector $\underset{\sim}{k}_\sigma$. The scattered photon has lost energy and emerges with decreased frequency ν_s ($\nu_s < \nu_i$) and wave vector $\underset{\sim}{k}_s$. This is referred to as Stokes scattering in the Raman effect. Clearly, in the absence of thermal excitation, only the second process can occur.

If the scattering phonon belongs to one of the acoustic branches of the phonon spectrum of the solid, the scattering is called Brillouin scattering. This is the process we will consider here. If the scattering phonon belongs to an optical branch, the scattering is usually called Raman scattering.

Let us now derive the frequency shift. Energy and momentum conservation yields:

$$\nu_s = \nu_i \pm \nu_\sigma \qquad (1.1)$$

$$\underset{\sim}{k}_s = \underset{\sim}{k}_i + \underset{\sim}{k}_\sigma$$

If we call the scattering angle θ, we have

$$k_\sigma^2 = k_s^2 + k_i^2 - 2 k_s k_i \cos\theta \tag{1.2}$$

The dispersion relation for elastic waves is

$$k_\sigma = \frac{2\pi}{\lambda_\sigma} = \frac{2\pi \nu_\sigma}{v_j(\underset{\sim}{k}_\sigma, \nu_\sigma)} \qquad (j = 1, 2, 3 \text{ indicates the branch}) \tag{1.3}$$

where v_j is the velocity of the acoustic wave in the material. This is, in general, a function of the frequency and the propagation direction. The dispersion relation for light is

$$k_i = \frac{2\pi}{\lambda_i} = \frac{2\pi n_i \nu_i}{c}$$
$$k_s = \frac{2\pi}{\lambda_s} = \frac{2\pi n_s \nu_s}{c} \tag{1.4}$$

where n_i and n_s are the indices of refraction of the crystal at frequency ν_i and ν_s respectively.

After substitution of Eqs. (1.3) and (1.4) into Eq. (1.2) we obtain

$$\frac{\nu_\sigma^2}{v^2} = \frac{n_s^2 \nu_s^2}{c^2} + \frac{n_i^2 \nu_i^2}{c^2} - 2\frac{\nu_i \nu_s n_i n_s}{c^2}\cos\theta$$

But $\nu_\sigma^2 = (\nu_s - \nu_i)^2$ from Eq. (1.1) and

$$\nu_s^2 \left(\frac{c^2}{v^2} - n_s^2\right) + \nu_i^2 \left(\frac{c^2}{v^2} - n_i^2\right) - 2\nu_s \nu_i \left(\frac{c^2}{v^2} - n_i n_s \cos\theta\right) = 0$$

Since c/v is of the order of 10^5,

$$\nu_s^2 + \nu_i^2 - 2\nu_s\nu_i \tilde{\approx} 0$$

and we see that $\nu_s \tilde{\approx} \nu_i$. Therefore, $\underset{\sim}{k}_s$ and $\underset{\sim}{k}_i$ are almost equal in magnitude and we may approximate:

$$k_\sigma^2 = 2\, k_i^2 (1 - \cos\theta) = 4\, k_i^2 \sin^2(\theta/2)$$

$$k_\sigma = 2\, k_i \sin(\theta/2) \qquad (1.5)$$

Using Eqs. (1.3) and (1.4)

$$\nu_\sigma = \frac{2v_j\,(\underset{\approx}{k}_\sigma, \nu_\sigma)\, n_i\, \nu_i}{c} \sin\theta/2$$

and upon substitution into Eq. (1.1) we finally get

$$\nu_s = \nu_i \left[1 \pm \frac{2v_j\,(\underset{\approx}{k}_\sigma, \nu_\sigma)\, n_i}{c} \sin\theta/2\right] \qquad (1.6)$$

$$j = 1, 2, 3$$

This result can be derived in a very simple manner by considering the frequency change of the incident photon caused by scattering off a moving soundwave. The frequency shift is just the Doppler shift of the incident photon as it is "reflected" from the wavefront of a sound wave moving with velocity v toward the photon or away from it.

There is also the unshifted component at frequency ν_i. Calculation of the scattered intensity shows that if the polarizability is a scalar, then only the longitudinal component of the phonon polarization contributes to the scattering (see Ch. IV, 4.5).

To get an idea of the instrumental resolution necessary for observing the frequency shifts indicated by Eq. (1.6) let us make a calculation using some representative numbers. Since v/c is of the order of 10^5, $n \sim 1$ and $\nu_i \sim 5 \times 10^{14}$ cps (6328 Å),

$$\Delta\nu = | \nu_i \pm \nu_s | = 2 (v/c) n \nu_i \sin (\theta/2)$$

$$\sim 2 \times 10^5 \times 5 \times 10^{14} \times 0.707 \sim 7 \text{ kMc}$$

for 90° scattering. Depending upon the particular crystal and the mode of propagation under consideration we expect the frequency shift to vary between about 5 and 15 kMc for 90° scattering.

We notice that by changing the scattering angle θ we can sweep through the whole frequency range between 2 and 20 kMc for the alkali halides, up to 50 kMc for harder materials. Since the laser employed

in this experiment has a line width of $\sim$ 1 kMc at 6328 Å, we are able to resolve the scattering with good precision.

Chapter II

ELASTIC WAVES IN CUBIC CRYSTALS

2.1 Dependence of the velocity on the frequency and on the direction of propagation of the wave.

We would like to find a theoretical expression for the velocities v_j (j = 1, 2, 3) as a function of $\underset{\sim}{k}_\sigma$ and ν_σ. Let us consider the dispersion relation for elastic waves, Eq. (1.3), in greater detail. For experimental reasons we will limit ourselves to the {110} planes (the experimental setup for 90 degree scattering is relatively uncomplicated, passable intensities are attained and the shifts are big enough to be resolved).

The samples were mounted in such a way that $\underset{\sim}{k}_i$, $\underset{\sim}{k}_s$, and $\underset{\sim}{k}_\sigma$ lie in the {110} plane. As the crystal is rotated, the magnitude of $\underset{\sim}{k}_\sigma$ remains constant and only its direction changes so that $\underset{\sim}{k}_\sigma$ sweeps out all directions in the {110} plane. The wavelength of the phonons observed for the alkali halides was of the order of 3000 $\mathring{A}$.

Reference to Figs. 2.1 and 2.2 illuminates the above remarks. Fig. 2.1 shows the frequency ν_σ of the elastic waves, plotted as a function of the magnitude of $\underset{\sim}{k}_\sigma$ for $\underset{\sim}{k}_\sigma$ in the <001> direction. By studying the dependence of ν_σ on the scattering angle θ for a constant direction of propagation of the elastic waves one could map out

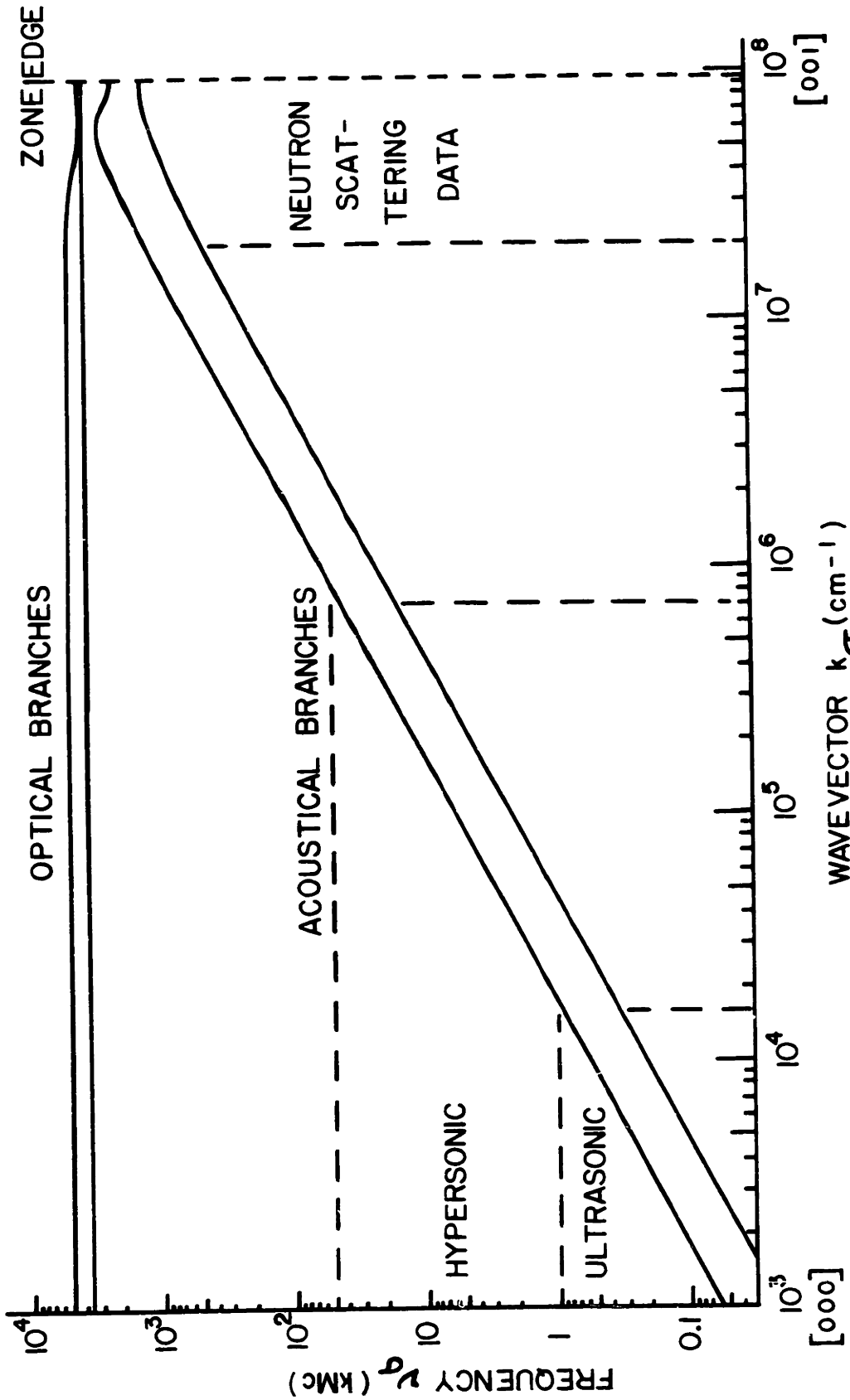

FIG. 2.1 FREQUENCY SHIFTS AS A FUNCTION OF $|k_\sigma|$ IN ⟨00l⟩ DIRECTION

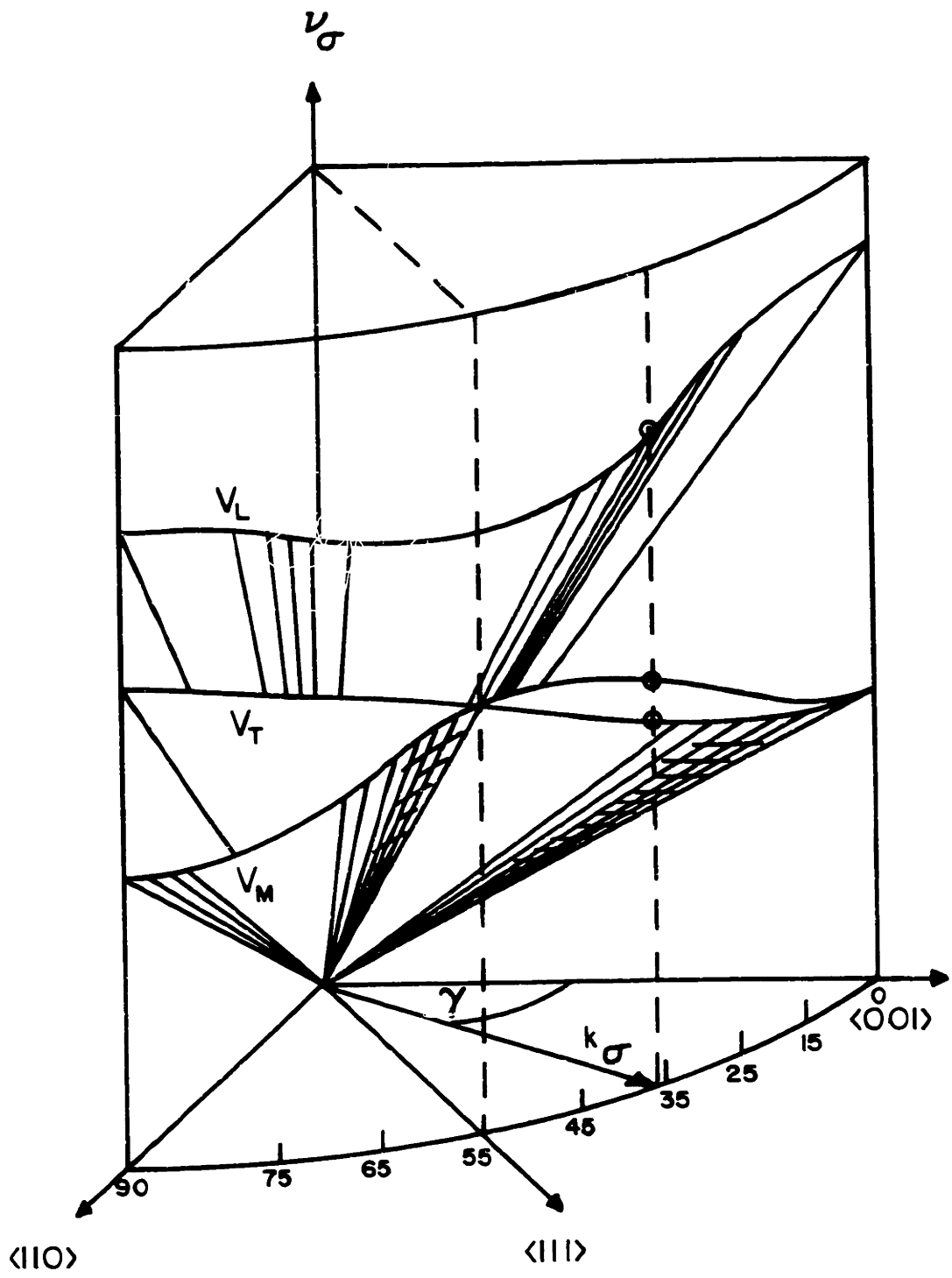

FIG. 2.2 FREQUENCY SHIFTS AS A FUNCTION OF γ FOR CONSTANT $|k_\sigma|$

the dispersion relation, Eq. (1.3), in the hypersonic region indicated in Fig. 2.1. Of course, the maximum frequency observable in a particular crystal is limited to $\nu_\sigma = 2\ v\ \nu_i\ n_i/c$ for backscattering ($\theta = 180°$). Therefore, one can go to higher frequencies in materials that have a high index of refraction and a low compressibility (large bulk modulus). From the dispersion curve one would then be able to find $2\ \pi\ d\nu_\sigma/dk_\sigma$, the group velocity. From neutron spectrometry experiments[9] one can get information on the dispersion curve between roughly 0.2 times the distance to the zone edge all the way up to the zone edge. The general shape of the dispersion curve for this region is shown for the alkali halides in Fig. 2.1.

Since the straight line extrapolation of the ultrasonic data joins up very well with the neutron spectrometry data one expects little dispersion in the hypersonic region.

In the experiment described here I have limited myself to 90 degree scattering. Therefore, the frequency shifts of the scattering in the {110} plane are measured as a function of the angle γ from the <001> direction. Since $|\underset{\sim}{k}_\sigma|$ is fixed, the experimental points fall on a cylinder of radius $|\underset{\sim}{k}_\sigma|$ perpendicular to the {110} plane. This is shown in Fig. 2.2 for potassium iodide. v_L, v_T, and v_M indicate the longitudinal, transverse, and mixed branch, respectively.

It was pointed out earlier that the sound frequencies are typically 7 kMc. Inasmuch as the cutoff frequency of the lattice is in the 3×10^3 kMc region, we may expect to be in the linear part of the phonon spectrum and may assume that the velocity is independent of the frequency (for a variation in frequency of about a factor of two). Then, the phase velocity will be equal to the group velocity, $v_p = v_g = 2\pi\nu_\sigma/k_\sigma$. Of course, if there should be a small amount of dispersion one would not be able to fit the experimental data to the theoretical curves which have been obtained with the assumption of no dispersion. This will be discussed more completely in Chapter IV.

We will now discuss the dependence of v_j on the propagation direction $\underset{\sim}{k}_\sigma$. At the same time the relation between v_j and the three cubic elastic constants c_{11}, c_{44}, and c_{12} will become clear.

In a cubic crystal we may write the generalized form of Hooke's law and the matrix of elastic stiffness constants (c_{im})[10] as follows:

$$S_i = \sum_m c_{im}\, \epsilon_m \tag{2.1}$$

and

$$(c_{im}) = \begin{bmatrix} c_{11} & c_{12} & c_{12} & 0 & 0 & 0 \\ c_{12} & c_{11} & c_{12} & 0 & 0 & 0 \\ c_{12} & c_{12} & c_{11} & 0 & 0 & 0 \\ 0 & 0 & 0 & c_{44} & 0 & 0 \\ 0 & 0 & 0 & 0 & c_{44} & 0 \\ 0 & 0 & 0 & 0 & 0 & c_{44} \end{bmatrix} \tag{2.2}$$

where i, m = 1, ..., 6. ε_m are the strain components and S_i the stress components.

$$\varepsilon_1 = e_{xx} = \partial u/\partial x,\ \varepsilon_2 = e_{yy} = \frac{\partial v}{\partial y},\ \varepsilon_4 = e_{yz} = \partial w/\partial y + \partial v/\partial z,\ \text{etc.}$$

$$S_1 = X_x,\ S_2 = Y_y,\ S_5 = Z_x,\ \text{etc.}$$

where the capital letter indicates the direction of the force and the subscript indicates the normal to the plane to which the force is applied.

In the kinetic case we must equate the inertial forces $\rho\ \partial^2 u/\partial t^2$, $\rho\ \partial^2 v/\partial t^2$, $\rho\ \partial^2 w/\partial t^2$ (ρ = density) to the surface forces. The equations of motion for the "elasto-kinetic case" are of the form

$$\rho\ \partial^2 u/\partial t^2 = \partial S_1/\partial x + \partial S_6/\partial y + \partial S_5/\partial z \qquad (2.3)$$

and similarly for v and w. Upon substitution of relations for plane waves

$$u = A_1 \exp i\ (\underset{\sim}{k} \cdot \underset{\sim}{r} - \omega t) \quad , \quad \text{etc.} \qquad (2.4)$$

into Eq. (2.3) we obtain a secular equation, a determinant determining the velocities of the three polarizations of waves of the acoustic branches:

$$\begin{vmatrix} c_{11}\alpha^2 + c_{44}\beta^2 + c_{44}\gamma^2 - \rho v^2 & \alpha\beta(c_{12} + c_{44}) & \alpha\gamma(c_{12} + c_{44}) \\ \alpha\beta(c_{12} + c_{44}) & c_{44}\alpha^2 + c_{11}\beta^2 + c_{44}\gamma^2 - \rho v^2 & \beta\gamma(c_{12} + c_{44}) \\ \alpha\gamma(c_{12} + c_{44}) & \beta\gamma(c_{12} + c_{44}) & c_{44}\alpha^2 + c_{44}\beta^2 + c_{11}\gamma^2 - \rho v^2 \end{vmatrix} = 0 \qquad (2.5)$$

where ρ is the density of the crystal and α, β, and γ are the cosines of the angles which the propagation direction makes with the x-, y-, and z-axis, respectively. This is treated in detail in a review article by Jules de Launay, "The Theory of Specific Heats and Lattice Vibrations" in Solid State Physics, Advances in Research and Applications[11]. It was pointed out before that $\underset{\sim}{k}_\sigma$ will always lie in the {110} plane, since we have limited ourselves to the {110} planes. Let γ be the cosine of the angle which $\underset{\sim}{k}_\sigma$ makes with the <001> direction. Obviously, then

$$\alpha = \beta = \sqrt{\frac{1 - \gamma^2}{2}}$$

and the velocity determinant (2.5) reduces to:

$$\begin{vmatrix} \frac{1}{2}[c_{11}+c_{44}+\gamma^2(c_{44}-c_{11})] - \rho v^2 & \frac{1-\gamma^2}{2}(c_{11}+c_{44}) & \gamma\sqrt{\frac{1-\gamma^2}{2}}(c_{12}+c_{44}) \\ \frac{1-\gamma^2}{2}(c_{11}+c_{44}) & \frac{1}{2}[c_{11}+c_{44}+\gamma^2(c_{44}-c_{11})] - \rho v^2 & \gamma\sqrt{\frac{1-\gamma^2}{2}}(c_{12}+c_{44}) \\ \gamma\sqrt{\frac{1-\gamma^2}{2}}(c_{12}+c_{44}) & \gamma\sqrt{\frac{1-\gamma^2}{2}}(c_{12}+c_{44}) & c_{44}+\gamma^2(c_{11}-c_{44}) - \rho v^2 \end{vmatrix} = 0 \qquad (2.6)$$

The three roots of this determinant are derived in the appendix.

They are v_T, v_L, and v_M :

$$v_T(\gamma) = \left[\frac{1}{2\rho}\right]^{1/2} [c_{11} - c_{12} + \gamma^2(2c_{44} + c_{12} - c_{11})]^{1/2} \qquad (2.7)$$

and

$$v_{L,\,M}^{(+,\,-)}(\gamma) = \left[\frac{1}{4\rho}\right]^{1/2} [4c_{44} + c_{11} + c_{12} + \gamma^2(c_{11} - 2c_{44} - c_{12}) \pm \{(c_{11} + c_{12})^2 + (2c_{44} + c_{12} - c_{11})[\gamma^2(8c_{44} + 14c_{12} + 6c_{11}) - \gamma^4(6c_{44} + 15c_{12} + 9c_{11})]\}^{1/2}]^{1/2} \qquad (2.8)$$

where T, M, and L are the branch indices (referred to previously by j = 1, 2, 3). T, M, and L indicate respectively that we are dealing with a completely transverse mode, a mixed mode, and an almost completely longitudinal mode. The longitudinal mode in Eq. (2.8) corresponds to the plus sign, the mixed mode to the minus sign. The curves obtained by plotting Eqs. (2.7) and (2.8) as a function of γ are shown in Fig. 2.2 for KI.

By using Eqs. (2.7) and (2.8) one can get the useful relation between the three velocity roots for any direction in the {110} planes (this is true for a wave-triplet in any direction):

$$\sum_{\nu=1}^{3} \rho v_\nu^2 = \rho \, (v_T^2 + v_M^2 + v_L^2)$$

$$= c_{11} + 2\, c_{44}$$

Eqs. (2.7) and (2.8) reduce to simple formulas along the <001>, <110>, and <111> direction. These velocities along with the corresponding polarizations of the modes are presented in Table I. In these directions, L is completely longitudinal, T and M are completely transverse waves. $\underset{\sim}{A}$ is the polarization vector of the waves with components A_x, A_y, and A_z. It is a unit vector. The fact that in the <001> and <111> directions $\underset{\sim}{A}_M$ and $\underset{\sim}{A}_T$ can be any two perpendicular unit vectors in the plane at right angles to $\underset{\sim}{A}_L$ is satisfied by using the variables S, M, and N in Table I which are arbitrary except for the constraint on their magnitude noted in Table I.

TABLE I

Velocities of propagation and polarizations in principal symmetry directions

Direction of propagation $\underset{\sim}{k}$	γ	v_L^2 (Longitudinal) $\underset{\sim}{A}_L$	v_M^2 (Transverse) $\underset{\sim}{A}_M$	v_T^2 (Transverse) $\underset{\sim}{A}_T$
$\underset{\sim}{k} = (k_x, k_y, k_z)$		$\underset{\sim}{A} = (A_x, A_y, A_z)$		
<001> $(0, 0, k)$	1	$\frac{c_{11}}{\rho}$ $(0, 0, 1)$	$\frac{c_{44}}{\rho}$ $(\sqrt{1 - S^2}, -S, 0)$ $0 \leq S \leq 1$	$\frac{c_{44}}{\rho}$ $(S, \sqrt{1 - S^2}, 0)$ $0 \leq S \leq 1$
<110> $(\frac{k}{\sqrt{2}}, \frac{k}{\sqrt{2}}, 0)$	0	$\frac{2c_{44} + c_{11} + c_{12}}{2\rho}$ $(\frac{1}{\sqrt{2}}, \frac{1}{\sqrt{2}}, 0)$	$\frac{c_{44}}{\rho}$ $(0, 0, 1)$	$\frac{c_{11} - c_{12}}{2\rho}$ $(\frac{1}{\sqrt{2}}, -\frac{1}{\sqrt{2}}, 0)$
<111> $(\frac{k}{\sqrt{3}}, \frac{k}{\sqrt{3}}, \frac{k}{\sqrt{3}})$	$\frac{1}{\sqrt{3}}$	$\frac{4c_{44} + 2c_{12} + c_{11}}{3\rho}$ $(\frac{1}{\sqrt{3}}, \frac{1}{\sqrt{3}}, \frac{1}{\sqrt{3}})$	$\frac{c_{44} + c_{11} - c_{12}}{3\rho}$ $\begin{bmatrix} M+2N \\ -(2M+N) \\ M-N \end{bmatrix} x \frac{1}{\sqrt{6(M^2+N^2+MN)}}$ $M, N \geq 0$	$\frac{c_{11} + c_{44} - c_{12}}{3\rho}$ $\begin{bmatrix} M \\ N \\ -(M+N) \end{bmatrix} x \frac{1}{\sqrt{2(M^2+N^2+MN)}}$ $M, N \geq 0$

2.2 Dependence of the velocity of propagation on the elastic constants

To obtain the best experimental values of the three cubic elastic constants inherent in the data we would like to find out how sensitive the velocity is to changes in c_{11}, c_{44} and c_{12} in the different directions of propagation. Consider Eq. (2.8). Since we are interested in the production of an error in the velocity by an error in the three elastic constants, we will investigate the following derivative:

$$\frac{\% \ \Delta v_{L_M}(\gamma)}{\% \ \Delta c_{11}(\gamma)} = \frac{\partial[\ln v_{L_M}(\gamma)]}{\partial[\ln c_{11}]} = \frac{c_{11}}{v_{L_M}(\gamma)} \frac{\partial v_{L_M}(\gamma)}{\partial c_{11}} \qquad (2.9)$$

Then, the larger $(\% \ \Delta v \ (\gamma))/(\% \ \Delta c_{11})$, the more sensitive the velocity is to a change in c_{11}. Clearly, if we want to determine the elastic constants to good precision we should make use of the directions where $(\partial \ln v \ (\gamma))/(\partial \ln c_{ij})$ is a maximum. In Figs. 2.3 and 2.4 the quantities $(\partial \ln v \ (\gamma))/(\partial \ln c_{11})$, $(\partial \ln v \ (\gamma))/(\partial \ln c_{44})$, $(\partial \ln v)/(\partial \ln c_{12})$, and $(\partial \ln v \ (\gamma))/(\partial \ln c)$ are displayed for the longitudinal root and for the mixed root as a function of γ ($c = 2 \ c_{44} + c_{12}$). The figures clearly show where the velocities are most sensitive to each of the three elastic constants. Consider Fig. 2.3. If we wanted to extract information on the elastic constants from a few directions of propagation using the longitudinal branch only, we would choose $\gamma = \cos (0°)$, for c_{11}, since $v \ (0°)$ depends only on c_{11}. c_{12} can be obtained from $v \ (55°)$ provided we know c_{44} and vice versa. Starting values for the three constants were obtained from these angles. Better values were

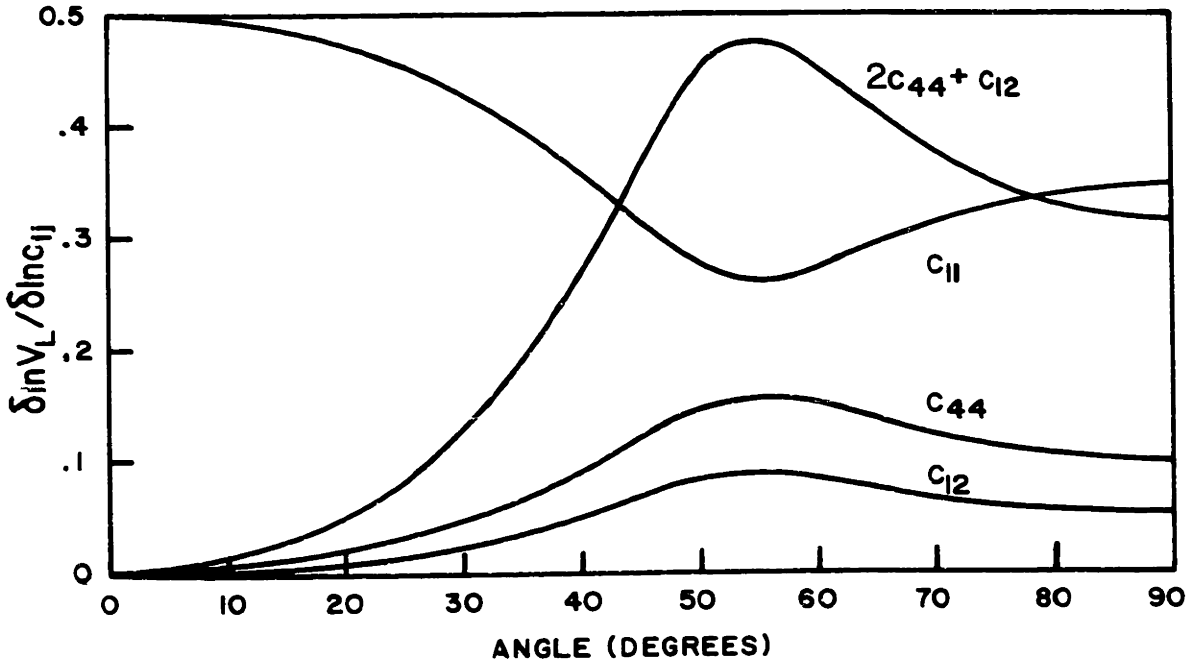

FIG. 2.3 SENSITIVITY OF $V_L(\gamma)$ TO CHANGES IN THE ELASTIC CONSTANTS (KI)

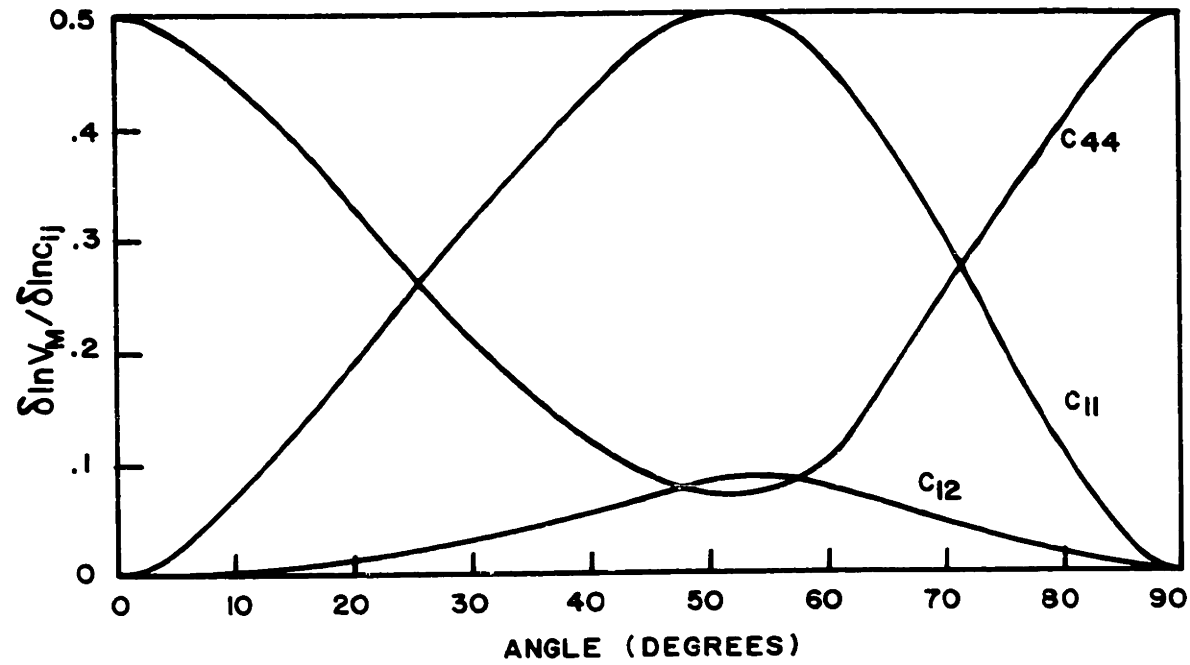

FIG. 2.4 SENSITIVITY OF $V_M(\gamma)$ TO CHANGES IN THE ELASTIC CONSTANTS (KI)

obtained by means of a least root mean square fit to the data. This will be discussed more fully in Chapter IV.

By studying Fig. 2.3 one realizes that c_{11} can be determined to 2% for an error of 1% in $v_L(\gamma)$ if just one data point (0°) is used. Since the sensitivity of $v_L(\gamma)$ to c_{11} never drops below 1/4 in the {110} plane, one can see that a least root mean squares fit should improve the accuracy in c_{11} substantially, approximately by a factor of $\sqrt{N}$ for N data points, provided, there is no dispersion. Fig. 2.3 indicates that c_{44} can be obtained to fairly good accuracy but even the least squares fitting procedure will not improve the accuracy of c_{12} very much, since $v_L(\gamma)$ is significantly dependent on c_{12} only between 50 and 60 degrees, and hence, only two data points are effective in determining c_{12}. The significance of the effective elastic constant $c = 2\,c_{44} + c_{12}$ will be discussed in Chapter IV.

One might think that the partially transverse branch v_M would yield better results for c_{12} and c_{44}. However, this branch was observed only for longitudinal admixtures greater than 20%. This corresponds to the region between $\gamma = \cos(25°)$ and $\gamma = \cos(45°)$. Since the precision in locating the position of this root was worse than that in locating the position of the longitudinal root, it would seem that nothing is gained in trying to get information on c_{12} and c_{44} from v_M. This point will be clarified in 4.2 .

2.3 Polarization of the phonons

It is important to know something about the polarization of the phonons, since only the longitudinal part of the polarization will contribute to the scattering. This can be understood in a rudimentary way by realizing that the light is scattered by local fluctuations in the density of the medium. Since a transverse wave will cause no first order changes in the density of the medium, we expect scattering only from longitudinal phonons.

Clearly, the polarizations for the three roots of the velocity determinantal equation as a function of γ are of considerable interest. These, of course, are just the eigenvectors corresponding to the eigenvalues v_M, v_T, and v_L. A derivation is given in the appendix. Only the results will be presented here. We define the polarization vectors as unit vectors $\underset{\sim}{A} = (A_x, A_y, A_z)$. The polarization for the transverse wave with velocity v_T is

$$\underset{\sim}{A}_T = (1/\sqrt{2}, -1/\sqrt{2}, 0) \tag{2.10}$$

This polarization is transverse, perpendicular to the z-axis, i.e. always perpendicular to the propagation direction for waves in the {110} planes. For v_L and v_M we have

$$\underset{\sim}{A}_{\substack{L \\ M}} = (1, 1, P_{\substack{L \\ M}}(\gamma)) \frac{1}{\sqrt{2 + P_{\substack{L \\ M}}^2(\gamma)}} \tag{2.11}$$

where

$$P_{L_M}(\gamma) = \frac{\gamma \sqrt{2\,(1-\gamma^2)(c_{12}+c_{44})}}{\rho v_{L_M}^2 - c_{44} + \gamma^2\,(c_{44}-c_{11})} \tag{2.11}$$

$$\text{and } P_L P_M = -2$$

We will define percentage of longitudinal admixture as

$$\%L = 100 \times \frac{\underset{\sim}{A} \cdot \underset{\sim}{k}}{|\underset{\sim}{k}|}$$

Hence

$$\%L_{L_M} = \frac{100}{\sqrt{2 + P_{L_M}^2}} \{\sqrt{2(1-\gamma^2)} + \gamma P_{L_M}\} \tag{2.12}$$

The percentage of longitudinal admixture is displayed in Fig. 2.5 for

$$\left.\begin{aligned} c_{11} &= 2.68 \\ c_{12} &= 0.44 \\ c_{44} &= 0.39 \end{aligned}\right\} \times 10^{11} \ \frac{\text{dynes}}{\text{cm}^2}$$

$$\rho = 3.13 \text{ gm/cm}^3.$$

These numbers are approximately correct for potassium iodide.

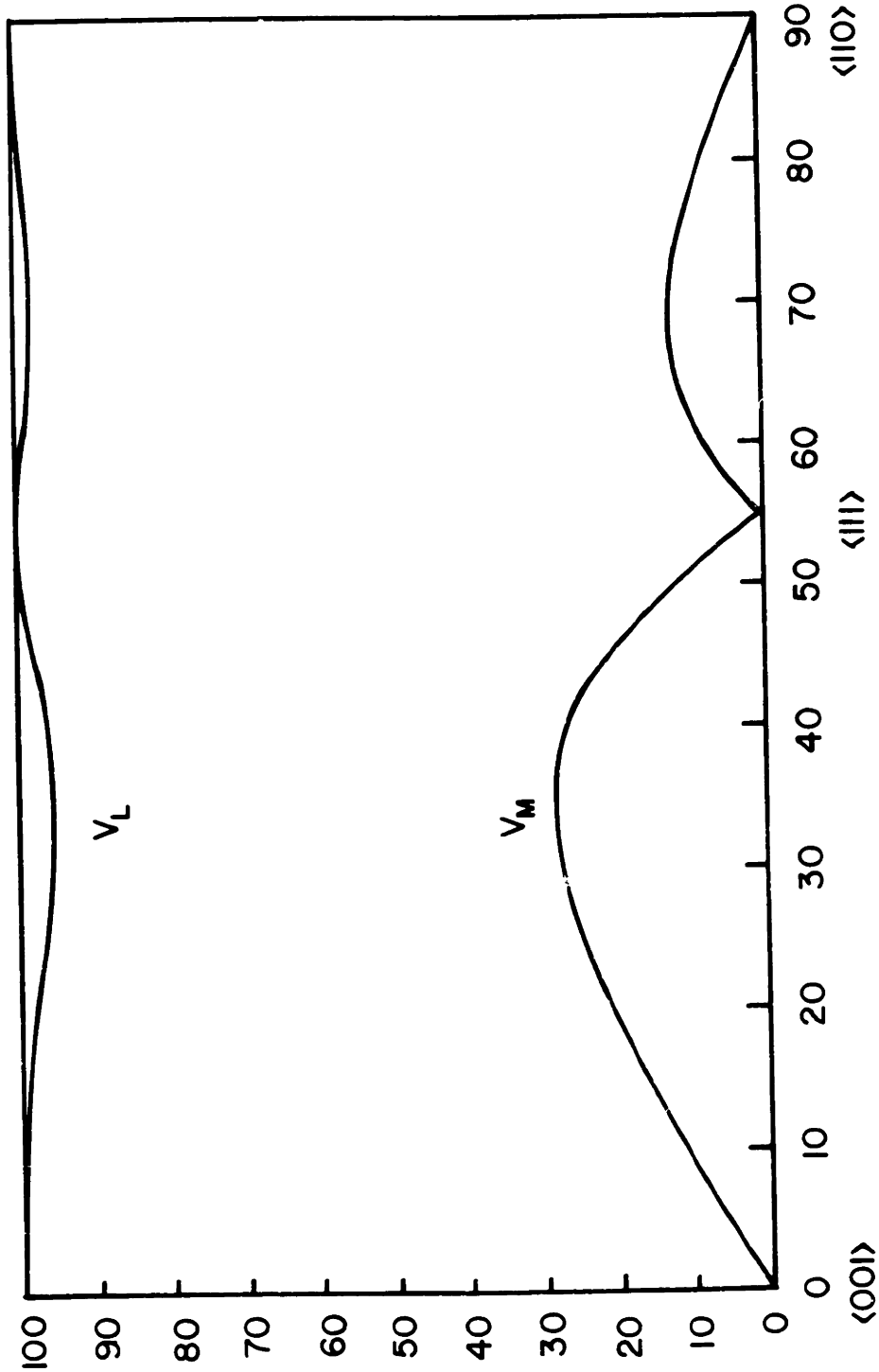

FIG. 2.5 LONGITUDINAL ADMIXTURE OF PHONON POLARIZATION (%)

Chapter III

EXPERIMENTAL SETUP

3.1 Description of the equipment

3.1.1 Optical equipment

The experimental setup is shown schematically in Fig. 3.1. A Spectra-Physics 10 milliwatt helium-neon laser (Model 115) is used as source of the incident radiation. The actual power entering the sample varies between 8 milliwatts for multimode operation and 2 milliwatts for uniphase operation of the laser. By use of the spectrograph it was determined that this laser power is concentrated into a 1 kMc wide spectral line at 6328 Å (the resolution of the spectrograph is about 600 Mc). The light leaving the laser with an angular divergence of less than 10 arc minutes is reflected up vertically by the prism P (see Fig. 3.1) and is focussed inside the sample by means of the short focal length lens L_1. The barely visible line of scattered light inside the sample, varying in diameter between approximately 0.05 mm and 0.5 mm, is then focussed onto the entrance slit S_1 of the spectrograph by the 25 cm focal length lens L_2.

Best placement of the sample and the lens L_2 is determined by two requirements. On the one hand one wants to send a maximum amount of scattered light into the spectrograph within a cone whose solid angle is determined by the aperture of mirror M_1. On the other hand, since

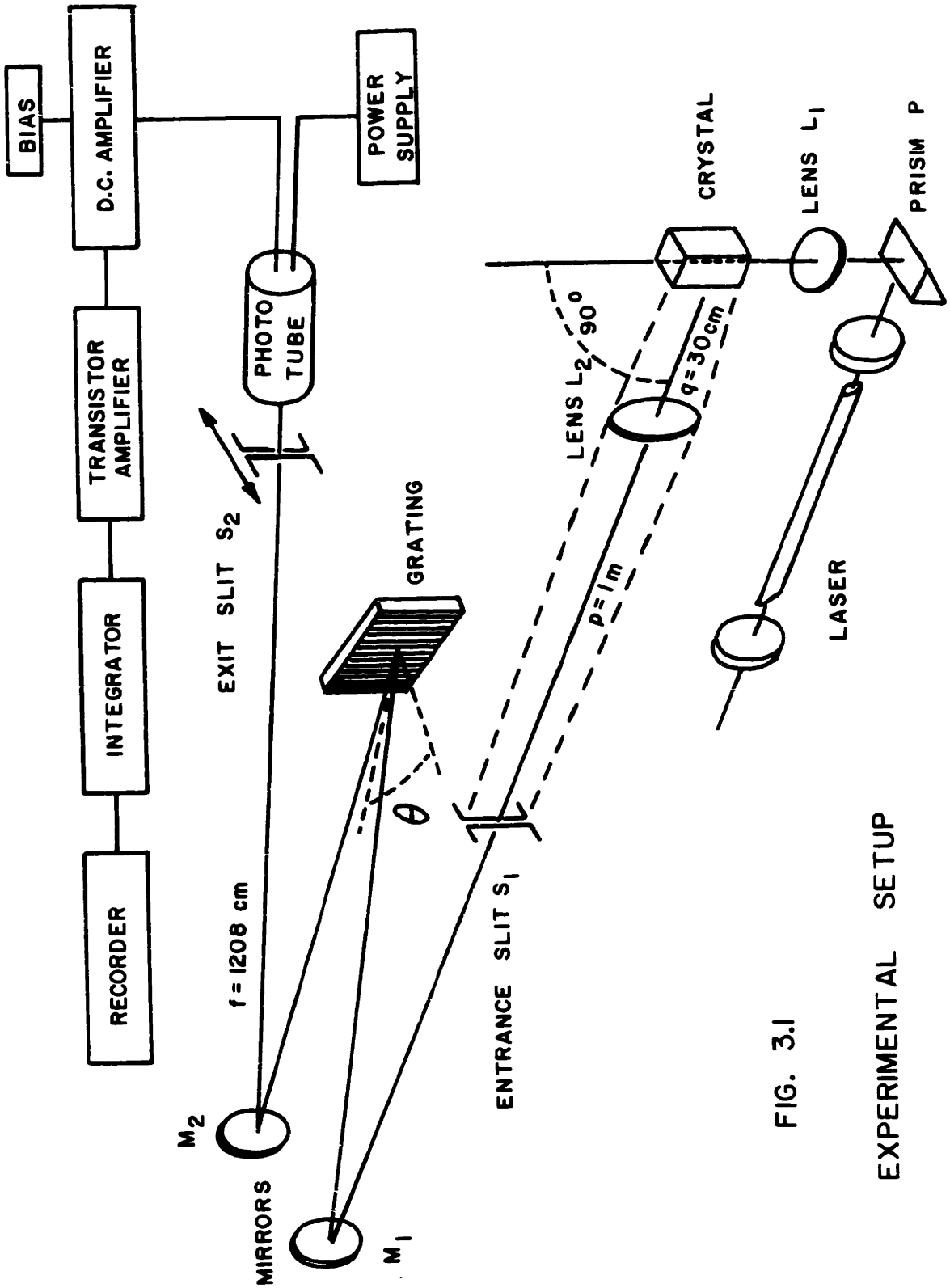

FIG. 3.1

EXPERIMENTAL SETUP

one is considering 90 degree scattering only, one wants to arrange the crystal and the lens L_2 such that a minimum of light scattered at angles other than 90 degrees is admitted into the spectrograph.

Let us look at the first requirement. So that the grating may gather a maximum amount of scattered light, the light beam entering the spectrograph should ideally be coneshaped with solid angle 3.4×10^{-4} sterradians. Actually, at high angles of diffraction the projected width of the grating is substantially smaller than the diameter of mirror M_1, and the solid angle will be correspondingly smaller. The basic area of the grating is 5" x 10" and the projected area of the grating is 5" x 10" x cos θ, where θ is the angle at which the grating is being used. Hence, the width of the incident beam should be 10" x cos θ and the height of the beam 5 inches. In this experiment the grating was used at 72 degrees corresponding to a solid angle of $2.2 \times 10^{-4} \times 0.309$ sterradians, i.e. 0.68×10^{-4} sterradians. Since the light entering the spectrograph has to pass through the entrance slit S_1, the requirement on the solid angle of the entering beam is to be interpreted as follows. In the horizontal plane the width of the beam inside the spectrograph is determined by the diffraction pattern due to the slit. Therefore, ideally, the entrance slit should be chosen such that the first diffraction minimum on either side of the center will fall at the edge of the projected grating area. Using this criterion,the ideal slit size is given by

$$\text{Slit width} = f\lambda/(2W \cos \theta)$$

where f is the focal length of the spectrograph, W is the width of the grating (10 inches), and θ is the grating angle. Hence with a 10 inch grating used at 72 degrees in a 1208 cm focal length spectrograph the ideal slit size would be 0.05 mm. In practice it is found that bigger slits have to be used for intensity reasons. As a matter of fact, in this experiment, a 0.25 mm slit had to be used throughout.

In the vertical plane the solid angle requirement can be satisfied by use of a lens L_2 which will give just the right divergence. The solid angle of light picked up can be changed by moving the crystal with respect to the lens L_2, whose focal length has to be chosen properly for every case, of course, so that the scattering line is focussed on the entrance slit. But another constraint enters. Inasmuch as the scattering line is focussed onto the entrance slit, light is lost unless the projected image has the size of the slit or is smaller. Since the width of the slit is 0.25 mm and the diameter of the beam roughly 0.1 mm in the case of good alignment, one needs a magnification of about 2.5. Use of a field lens directly in front of the entrance slit was not successful.

In aligning the optical system one has to remember that optimization of the solid angle of scattered light admitted into lens L_2 and best position as far as projection size is concerned, conflict. This can be understood quite simply. As the sample is brought closer to lens L_2, while at the same time the lens is moved further away from the entrance slit, the solid angle of scattered light admitted into the spectrograph is increased. At the same time, however, the

magnification increases and the image of the scattering line on the entrance slit becomes so big that a lot of light does not get into the spectrograph. If we call the (slit S_1 - lens L_2) distance p and the (lens L_2 - sample) distance q, (see Fig. 3.1) the magnification is given by $M = p/q$ when the scattering line is focussed on the slit. Let us call the solid angle of light admitted into the spectrograph Ω. Then, the solid angle picked up by the lens L_2 and arriving at the mirror M_1 is $\Omega' = \Omega p^2/q^2 = \Omega(p - f)^2/f^2$ for a lens of focal length f. We want to choose the position of the lens L_2 and that of the sample so that the projected image of the scattering line on the slit is barely larger than the slit, so that we get a clean-edged source. For a scattering line of 0.1 mm diameter and 1.0 cm length a magnification of 2.5 will yield an image 0.25 mm in diameter and 2.5 cm high. But this is exactly the size of the entrance slit. This is why the distances p and q were chosen in the ratio 10 : 3 as indicated in Fig. 3.1. The focal length is then obtained from $f = \frac{pq}{p + q}$. One must ask whether it would be profitable to increase the magnification further thus preventing a substantial amount of light focussed on the entrance slit from entering the spectrograph, but maybe increasing the solid angle accepted by lens L_2 sufficiently to overcome this loss. For example, if the magnification is increased by a factor of 2, only one fourth of the total light focussed onto the entrance slit enters the spectrograph. On the other hand the solid angle seen by lens L_2 increases by a factor of 4, roughly speaking. Actually, this is strictly true only for a slit of small

height. For the slit of 1 inch height used in this experiment the total solid angle of light picked up by the lens L_2 is smaller than indicated above. A good compromise position for lens L_2 and the sample can often only be found by experiment. A panel of six auto bulbs was constructed to fit over mirror M_1. With this it was possible to follow backward the six beams emerging from the entrance slit (each one due to one of the six bulbs), falling onto lens L_2 and being focussed as a line image of the slit inside the sample. This was very useful in the alignment, especially in the case of KCl where intensities were low.

It was explained before that the solid angle of scattered light seen by the spectrograph is roughly $\Omega' = p^2/q^2\Omega$. For $p/q = 2.5$ this is approximately 4.3×10^{-4} sterradians, where $\Omega = 0.68 \times 10^{-4}$ sterradians. Since the spectrograph accepts only a very small solid angle of the incident radiation about 90 degrees, the spectrograph sees mainly light scattered at 90 degrees. However, light is admitted through the circumference of the lens L_2 which yields a maximum deviation of the scattering angle from 90 degrees of about 3 degrees. It is easy to show that for 90 degree scattering $\Delta\nu = (\nu/2)\,\Delta\theta$ where $\Delta\nu$ is the frequency broadening associated with an acceptance angle $\Delta\theta$ centered about 90 degrees. Therefore, the total lineshape will be a convolution of the instrumental line shape, the shape due to the slits, the natural line shape and the broadening due to a large acceptance angle. This latter broadening for an opening angle of 6 degrees will be about 780 Mc for KCl,

580 Mc for KI, and 640 Mc for RbCl along the <001> direction. Since the sample is centered with respect to the spectrograph, this distribution about 90 degrees should be completely symmetrical. The expected natural width of the Brillouin components broadened by the above amount in frequency is not observable in this experiment, since the biggest contribution to the line shape was the rather wide 0.25 mm slit size (1.5 kMc).

The M.I.T. 1208 cm focal length grating spectrograph was used for the experiment with grating # 97, a 5" x 10" echelle with 300 lines/mm, blazed at 63 1/2 degrees ($\tan^{-1} 2$). The order of the spectrograph components is that of the "uncrossed" Czerny-Turner arrangement known for low astimatism. In this mounting a parallel beam of light impinges on the grating and the parallel diffracted beam is focussed by mirror M_2 in its focal plane. The grating used in the experiment is one of the best ones ruled at M.I.T. under interferometric control. Unfortunately, it produces a sharp satellite, whose intensity is roughly 1% of the parent line intensity, on the low wavelength side of the spectral lines. This satellite is probably caused by a "satellite grating", i.e. an extended area of the grating where the rulings are displaced collectively from their proper position. The problems caused by this satellite and their solution are discussed in 3.2.2. The grating is used at an angle of about 72 degrees in auto collimation (angles of incidence and diffraction are nearly equal) and in the tenth order. Since the grating is blazed at 63 1/2 degrees, it would have been

advantageous to use the grating at this angle. The grating is most efficient near the blaze angle and grating defects are less bothersome at this lower angle. Some preliminary experiments were done which indicated that at 59 degrees (ninth order) the efficiency was 40% as opposed to only 7% at 72 degrees. Nevertheless it was preferable to work in tenth order, since the dispersion is greater and alignment of the large slits and accuracy of the exit slit drive is not as critical as it would be in ninth order.

The diffracted light beam falls on the exit slit S_2. This slit is mounted on a carriage which can be driven horizontally along the focal plane of the spectrograph by means of a variable speed drive. The slit moves across the surface of a stationary photo-multiplier tube (RCA 7265, S-20 surface) which produces small anode currents proportional to the intensity of the impinging light.

3.1.2. Electronics

The anode current from the photo-multiplier tube is typically of the order of 3 millimicroamperes. This small current is amplified by a Hewlett-Packard 425 A d.c. amplifier. Its output is further amplified by a transistor amplifier used mainly to match the impedance of the strip-chart recorder. It is possible to buck out the d.c. part of the dark current of the photo-multiplier tube by means of a direct biasing circuit. This enables one to use the d.c. amplifier on a more sensitive scale. An integrating network is supplied between the transistor amplifier and the strip-chart recorder allowing integration times between 0.3 and 30 seconds.

3.1.3 Sample holder

In preliminary experiments it was found that there is a lot of extraneous scattering from the surface of the crystal at the locations where the laser beam enters the sample and where it leaves the sample. This scattering is detrimental because part of the scattered light will enter the spectrograph and give a strong signal at the laser frequency. In bad cases this signal can be five hundred times as strong as the Brillouin components. Even though the half width of the line at the laser frequency will only be 1.5 kMc, there will be quite a bit of signal left 10 kMc away from the center of the unshifted line. This will completely swamp the Brillouin components. A highly polished finish will reduce this scattering substantially. However, even with a good surface polish, the sample can be used only in those positions in which the beam enters and leaves the sample perpendicular to a surface. In addition the intensity of the scattered light seen by the spectrograph is reduced considerably unless the surface through which the scattering is observed is almost perpendicular to the observation direction. It would seem necessary that the sample has to be recut many times to enable one to cover all propagation directions in a certain set of planes, the {110} planes in our case. In addition, the alkali halides present another problem. They are hydroscopic and crystals tend to get clouded surfaces rapidly in humid surroundings. This increases the unwanted scattering at the frequency of the incident radiation by an intolerable amount.

As a solution to both these problems Prof. G. B. Benedek suggested that the samples could be submerged in a mixture of liquids which matches the index of refraction of the particular crystal under observation. After a few preliminary experiments it was found that it is indeed possible to match the indices of refraction of some of the alkali halides well enough so that just one cleaved crystal of each material can be used for observation of the Brillouin spectrum for any propagation direction. It was determined that small surface imperfections can be tolerated and that, as long as the surfaces are smooth, a general wavyness does not cause any problems. Liquids used to match the indices of refraction were diiodomethane, toluene, and methanol with indices of refraction 1.76, 1.50, and 1.33, respectively. The proper mixture was found by the following procedure. KI, for example, has an index of refraction 1.66. The sample was submerged in diiodomethane (methylene iodide) with index of refraction 1.76. A large diameter diverging laser beam was sent through the cube-shaped crystal along its body diagonal. There were then five spots visible on a piece of paper some distance away from the sample, since there was the undeflected part of the beam going through the two corners lying on the body diagonal that is being used and the four beams refracted in going through the faces of the cube. The second liquid (toluene, in the case of KI) was added slowly by means of a hypodermic and the mixture was stirred from time to time. After the constituents had mixed, the spots were observed. This was

continued until only one spot could be seen, at which time all parts of the incident laser beam passed through the crystal undeflected. If one wants to start with an approximate mixture one assumes that the refractivity of the mixture $(n_m - 1)$ is equal to the sum of the refractivities of its pure constituents $(n_1 - 1;\ n_2 - 1)$ each multiplied by the ratio of its mass per unit volume of the mixture to its own density when pure. We have

$$n_m - 1 = (n_1 - 1)\, M_1/(V\rho_1) + (n_2 - 1)\, M_2/(V\rho_2)$$

where M_1 and M_2 are the total masses of the constituents, V is the total volume of the mixture and ρ_1 and ρ_2 are the densities. Since $\rho_1 = M_1/V_1$, $\rho_2 = M_2/V_2$, and $V_1 + V_2 = V$ for a mixture, we find

$$V_1/V = (n_m - n_2)/(n_1 - n_2).$$

From this we find the approximate mixtures for the three crystals treated in this thesis:

Crystal	index of refraction	% V_1	% V_2
KCl	1.488	93% toluene	7% methanol
KI	1.661	62% diiodomethane	38% toluene
RbCl	1.492	95% toluene	5% methanol

As the proportions are temperature dependent and as the liquids evaporate at different rates, it was found more convenient to determine the proportions experimentally. By just adding a few drops at a time it was easy to obtain a proper mixture and to replenish evaporated liquid.

A sample holder was constructed which makes possible observation of elastic waves in the {110} planes with one cleaved sample of the compound being investigated (see Fig. 3.2). There are two advantages in using a cleaved sample rather than one cut at some angle with respect to the cleaved planes: i) cleaved crystals are easily obtainable, ii) with a cleaved sample there is no question as to the angle of the faces and the direction of the <100> axes (usually the cleaved angle is within 20 minutes of arc from the <100> axes).

3.2 Limitations of the equipment

3.2.1 Alignment procedure and discussion of errors

Limitations in the accuracy and precision imposed by the equipment and/or the operating procedure can be best understood by discussing the alignment procedure.

1) Alignment of the incident beam. - First it was determined with the aid of the laser and a precision level that the plane of the spectrograph comprising the entrance slit S_1, the exit slit S_2, the grating and the two spherical mirrors M_1 and M_2 (see Fig. 3.1), was horizontal. The laser was then adjusted by means of the precision level until the laser beam fell into a plane parallel to the plane of the spectrograph. The laser beam was then reflected

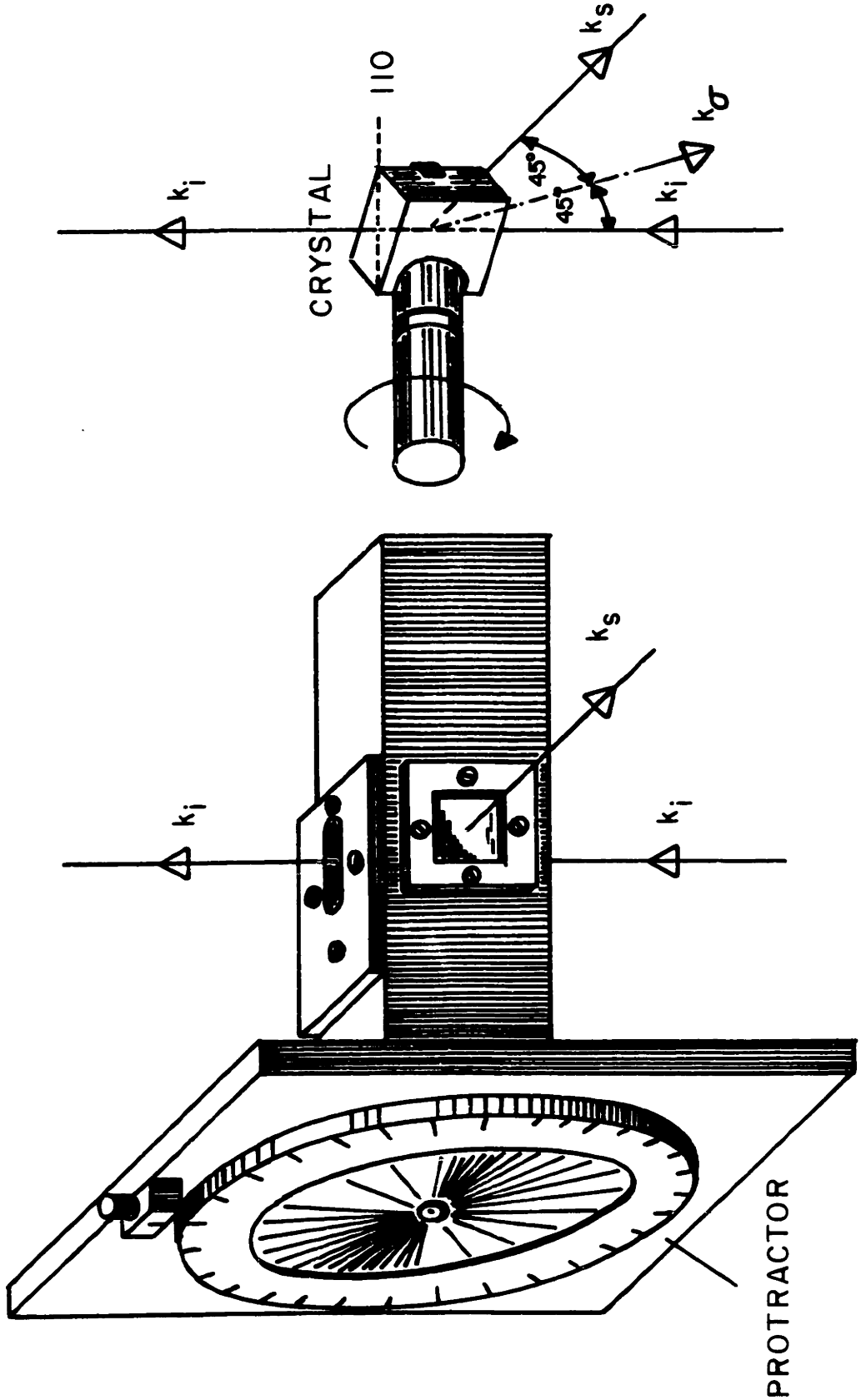

FIG. 3.2 SAMPLE HOLDER AND CLAMP

back into itself from the face of the prism P by rotating this prism. This automatically lined up the incident beam perpendicular to the spectrograph plane, as it should be for 90 degree scattering. In addition, the verticality of the laser beam was checked with a 9 foot plumb line. After these two adjustments the location of the spot formed by the laser beam on the ceiling (9 feet away from the sample) was marked. The lens L_1 was introduced into the beam and adjusted using a pair of micrometers until the beam followed its original path and hit the marked spot on the ceiling.

Due to the fact that the beam now left the sample diverging rapidly because of lens L_1, this last adjustment introduced some error in the scattering angle. The uncertainty in placing the spot on the ceiling correctly was roughly 0.5 inches over a distance of 9 feet corresponding to an uncertainty in the scattering angle of about 0.3 degrees. This is equivalent to an error in frequency of about 0.3%.

2) Alignment of the sample holder. - The sample holder was first made horizontal with the aid of the precision level. Then, the glass front surface of the sample holder (see Fig. 3.2) was lined up perpendicular to the spectrograph in both the horizontal and the vertical planes by reflection of a laser beam off this surface. This laser beam had been aligned previously to follow the entrance axis of the spectrograph, defined by the entrance slit S_1 and the mirror M_1 in Fig. 3.1. The maximum error in this adjustment was a displacement of the reflected beam amounting to 3 inches in 45 feet,

i.e. an error in angle of about 0.2 degrees. This is small compared to some of the other errors introduced and can be completely neglected.

However, a systematic error was introduced at this place in the procedure by the fact that the edges of the sample were not aligned completely with the indicated 0 degree and 90 degree directions on the protractor. This was caused by machining problems. Correction for this "zero-error" was simple, since the correction angle could be measured by letting the aligned laser beam graze the sample and by determining when a sample face was parallel to the beam.

A more serious problem arose when the sample was removed during the experiment. Conceivably it might not have been seated properly when it was replaced. This possibility was eliminated by rechecking some angles for agreement. If the agreement was satisfactory, it was assumed that the crystal had taken up its original position. The sample had to be removed more or less regularly because the liquids had become discolored or dirty. Although the mixed liquids had been cleared of any water by use of some potassium metal, water seemed to be taken up by the mixture after some time. If this was not removed by use of some potassium, the sample started clouding over. It was found that the sample could be wiped with pieces of cotton under the liquid and partially cleaned. But the treatment with potassium and the cleaning procedure introduced small specks of dirt and potassium metal into the liquid. In the case of KI,

diiodomethane had to be used. This liquid becomes discolored after exposure to light.

3) Maximization of intensity. - Whenever the lens L_2 was adjusted to maximize the intensity of the Brillouin components, the angle at which the spectrograph observed the sample was changed slightly in the horizontal plane. If the scattering line originally was not quite in line with the spectrograph axis defined by slit S_1 and mirror M_1, then, the lens L_2 could be moved in the horizontal plane to maximize the intensity. In this case, the light passing through the lens would be refracted slightly and although one is still observing 90 degree scattering, $\underset{\sim}{k}_s$ instead of being in a {110} plane might be slightly away from it causing $\underset{\sim}{k}_\sigma$ to fall just outside a {110} plane. Let us compute the possible error. At the start of the experiment, L_2 was removed and the laser was moved until the incident beam coincided with the spectrograph axis defined by slit S_1 and mirror M_1. The lens L_2 was then replaced and moved until the scattered light went into the spectrograph undeflected. So far everything was lined up properly. But in some runs the lens L_2 had to be moved off the spectrograph axis to give maximum intensity. In that case the scattered light was (a) refracted in going through the glass window and (b) refracted in passing through the lens L_2. Let us assume the biggest displacement of the lens from the dead center was no more than 3 mm. Since this lens was separated from the sample by about 30 cm, the corresponding change in angle was 0.6 degrees. Because the index of refraction of the liquid was

typically between 1.4 and 1.7, this angle was reduced to 0.3 degrees measured from the perpendicular inside the sample upon crossing the air-glass-liquid boundary. Since the slope of the velocity versus direction of propagation curve is never steep, this error is not important. The adjustment was only necessary in a few cases, where the intensities were rather low and best geometrical alignment had to be sacrificed for alignment for maximum intensity. We may assume then that the error of 0.3% due to the error in the sine of the scattering angle dominates all the other errors except the zero-error of the sample position, for which one can correct.

4) Calibration of the spectrograph. - The object of an accurate calibration of the spectrograph was to find an accurate value for the dispersion $d\bar{\nu}/ds$ of the instrument, where $d\bar{\nu}$ is the shift in wavenumbers ($\bar{\nu} = 1/\lambda$) and ds is the corresponding displacement along the focal plane in mm. For the calibration we tried to use two spectral lines falling within the scanning range of the exit slit drive. However, this was made difficult by the fact that at 6328 Å in the tenth order the scanning range of the drive covers only about three to four cm^{-1}. Finally, two neon lines were found which fall close together, one lying in the ninth order and one in the tenth order.

Using these two lines for calibration purposes proved unwise, however, for the following two reasons:

a) The lines fall so close together that accuracy in the wavelength difference between them in tenth order is not good, inasmuch

as one is subtracting two large numbers differing only in the last four decimal places.

b) The lines fall into two different orders. Since line profiles vary sharply in different orders, the maximum of a line can shift to a different wavelength in different orders. Hence, one can expect a discrepancy in wavelength measurements if standards from a lower order are used to derive higher order wavelengths.

To get a correct value for the dispersion we replaced the photoelectric equipment by a photographic plate covering $m\lambda$ from 63200 Å to 63380 Å, where m = order, λ = wavelength. In this wavelength range eight neon lines produced by a 60 cycles a.c. neon discharge at 4000 volts were photographed. A traveling microscope was used to find the accurate distances between various lines along the plate. The average of ten readings for the distance between each pair of lines was used in the calculations. The following wavelengths, determined interferometrically by Burns[12], were used for the photographic calibration:

7024.0500 Å	9th order
5748.2985 Å	11th order
4865.5009 Å	13th order
3515.1900 Å	18th order
6328.1646 Å	10th order
7032.4127 Å	9th order
6334.4279 Å	10th order
3520.4714 Å	18th order

Since the instrument was to be calibrated in the tenth order, all other order lines appearing above will give rise to errors, the error in wavelength being bigger as the order is higher (lower wavelength). Since errors introduced in this way can vary from 0.001 Å to 0.01 Å depending upon the quality of the grating, only the two lines in the tenth order were used. To a good approximation $\Delta\bar{\nu}/\Delta s$ given by these two lines will be the slope of the dispersion curve at the midpoint, i.e. at 6331.2962 Å. By use of the grating formula the quadratic part of the dispersion was found and using this correction the slope $d\bar{\nu}/ds$ at 6328 Å was found. This slope was used as linear dispersion in evaluating the experimental results. The error incurred in using a linear dispersion formula is approximately 0.08 % / cm^{-1} near 6328 Å. Since the biggest shifts measured in this experiment were about 1 cm^{-1}, we are justified in using the linear dispersion formula.

To double check on this procedure a quadratic dispersion curve was fitted to all the spectral lines given above using the theoretical quadratic term and the linear slope at 6331.2962 Å found from the two lines in tenth order. The position of the lines agreed with the predicted position within the 0.01 Å error limit set by use of "other order" lines.

It should be mentioned at this point that both exit slit carriage and photo plate were aligned perpendicular to the light beam diffracted by the grating into the tenth order by reflection of the laser beam back into itself. The reflecting surface consisted of a

small mirror mounted onto the exit slit in the one case and of the front surface of the photo plate in the other case. The error caused due to misalignment here was certainly less than 0.1%.

The results of the calibration measurements are:

a) Calibration obtained from photoelectric scanning

$$d\bar{\nu}/ds = (0.2036 \pm .0010)\ cm^{-1}/mm$$

b) Calibration obtained from the photo plate

$$d\bar{\nu}/ds = (0.2040 \pm .0005)\ cm^{-1}/mm$$

The photoelectric calibration is based on the assumption that the two neon lines used are known in wavelength to the indicated accuracy:

Ne I 7032.4127 $\pm$ 0.0001 Å recorded in the 9th order

Ne I 6328.1646 $\pm$ 0.0001 Å recorded in the 10th order[12].

Since we are interested in the tenth order spectrum, the effective wavelengths and accuracies are:

Ne I 6329.1714 $\pm$ 0.0010 Å (= 0.9 x 7032.4127 Å)

Ne I 6328.1646 $\pm$ 0.0001 Å

The error of 0.0010 Å is assigned to the 7032 Å line as an estimate of the possible error introduced by using lines of different orders for calibration purposes. Although the error can amount to almost 0.01 Å in the worst case for average quality gratings, it should be much smaller for the exceptional quality grating employed in this experiment, especially, since the two calibration lines were in adjacent orders.

An error of 0.25% is assigned to the photo plate calibration to take care of errors induced by the roughness in the driving screw.

This fluctuation was measured by using a dial depth indicator to measure actual displacement of the slit versus number of turns of the driving screw.

The value of the calibration used to evaluate the frequency shifts of the data was that obtained photographically, i.e.

$$d\bar{\nu}/ds = (0.2040 \pm .0005)\ cm^{-1}/mm \quad (0.25\%\ \text{accuracy})$$

3.2.2 Improvement of the signal to noise ratio

In the search for good data two problems appeared:

1) Low signal to noise ratio due to extremely small anode currents.

2) Too much signal at the frequency of the incident radiation. The two problems are related and will be treated at the same time.

The easiest way to improve the signal to noise ratio would have been to employ a more powerful laser, inasmuch as the noise originated mainly in the photo-multiplier tube. A 30 milliwatt laser was therefore used. However this particular laser could only be operated in a configuration giving a beam with a non-spherical wavefront. It was found that

a) there was no gain in signal, since the beam cannot be focussed well enough inside the sample thus giving an image projected on the entrance slit which is many times bigger than the entrance slit with consequent light losses (see 3.1.1) and

b) scattering from inclusions was increased due to the rapid divergence of the beam resulting in a wide central line.

It should be remarked that no chopping was used and the phototube was not cooled. Larger integration times combined with slower sweep speeds would undoubtedly have increased the signal to noise ratio. However, it was not feasible to modify the equipment to obtain slower speeds. In addition, it would have taken an unreasonable amount of time to record the spectra.

The second problem to be discussed is that of the wide central unshifted component of the spectra. After the first few traces had been recorded it was noticed that the central line showed pronounced asymmetry on its wings. It should be pointed out that for most of the traces the Brillouin components had an intensity roughly 1 to 2% that of the unshifted line. The line shape produced by the grating was examined closely by looking at the laser output directly with the spectrograph. The line shape obtained with a 0.25 mm slit under conditions duplicating those existing at the time of the experiment is shown in Fig. 3.3. In addition to the evenly spaced Rowland ghosts one can see a strong (approximately 1%) satellite on the low wavelength side of the line. The ghosts are spurious lines produced by periodic errors in the ruling approximately 1/500 as intense as the parent line while the satellites are spurious lines produced by non-periodic ruling errors, approximately 1/100 as intense as the parent line. In addition, often, 15% of the total intensity goes into grass, scattered light which is not focussed into distinct lines but is spread around the parent lines. This is also caused by non-periodic errors in the ruling.

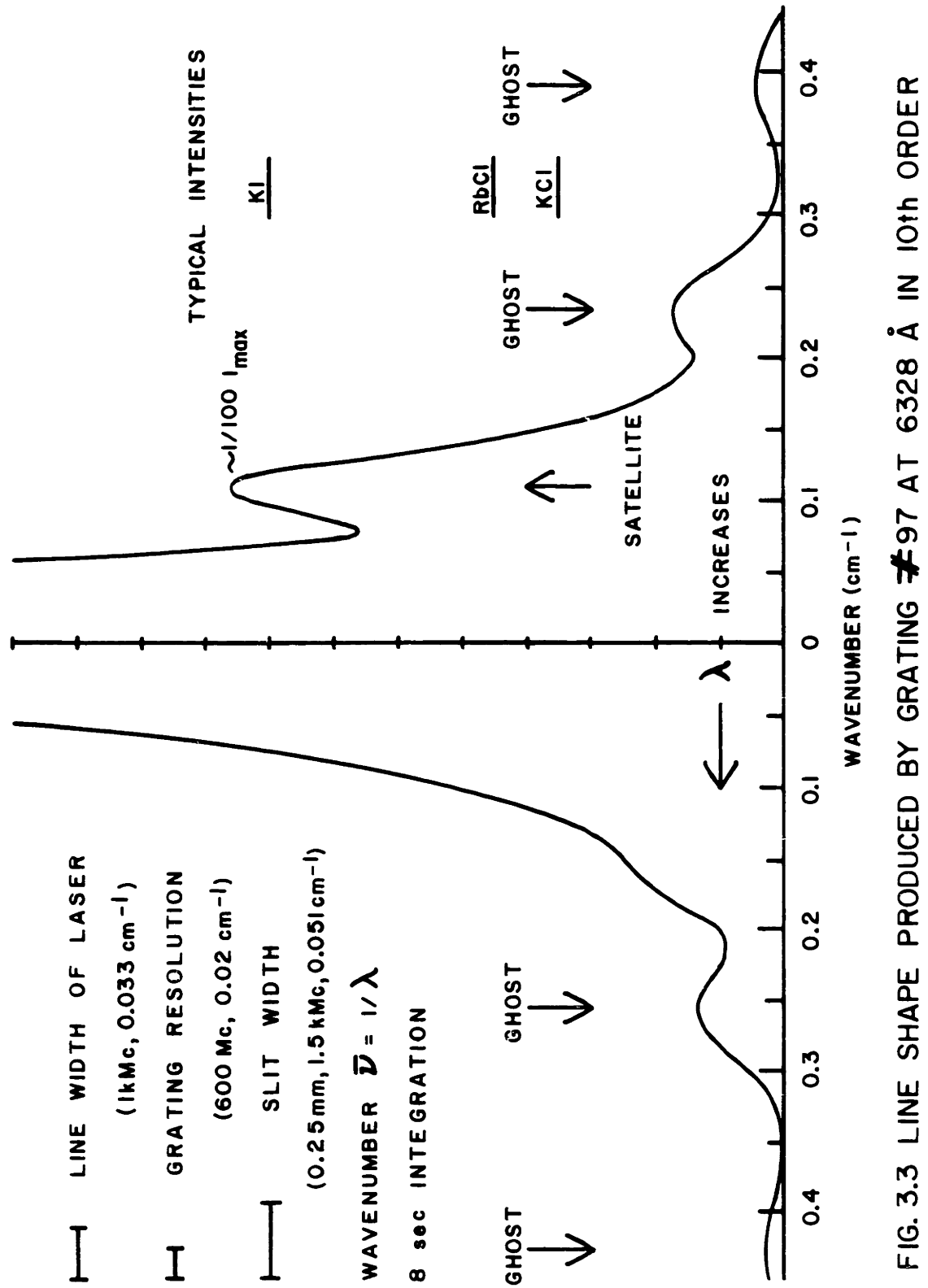

FIG. 3.3 LINE SHAPE PRODUCED BY GRATING #97 AT 6328 Å IN 10th ORDER

For comparison we find from the intensity formula for the Fraunhofer diffraction pattern from an ideal grating[13]

$$I \propto (\sin^2 N\phi)/(\sin^2 \phi) \tag{3.1}$$

that the secondary maxima next to all spectral lines occur approximately at distances Δs_k from the center of the parent line

$$\Delta s_k = \frac{1}{2}(2k + 1)\frac{f\lambda}{W \cos\theta} \tag{3.2}$$

where $k = 1, 2, 3, \ldots\ldots$, W = width of the ruled grating area and θ = grating angle. Of course, the factor $\frac{f\lambda}{W \cos\theta}$ is just the half width of the principal maximum. This is 600 Mc, i.e. the resolution limit of the grating. Hence the first few secondary maxima fall quite close to the parent line, approximately 900 Mc, 1.5 kMc, and 2.1 kMc away from the center. Using Eq. (3.1) the ratio of the intensities of the secondary maxima to the intensity of the parent line can be written as

$$\frac{I_{\text{secondary}}}{I_{\text{primary}}} = \frac{\sin^2 N\phi_{\text{sec.}}}{N^2 \sin^2 \phi_{\text{sec.}}}$$

where $\phi_{\text{sec.}} = \pi\frac{2k + 1}{2N}$, $k = 1, 2, 3, \ldots$. Hence, $\sin^2 N\phi_{\text{sec.}} = 1$ for all $\phi_{\text{sec.}}$ and since $\phi_{\text{sec.}}$ is very small here we may approximate

$\sin^2 \phi_{sec.} = \phi^2_{sec.} = \pi^2 \frac{(2k+1)^2}{2N^2}$. Therefore, the ratio of of the intensities is approximately

$$\frac{I_{secondary}}{I_{primary}} = \frac{4}{\pi^2 (2k+1)^2} \quad .$$

The locations of the first secondary maxima in relation to the primary maximum are given here with intensities relative to the parent line in parentheses:

0 Mc (1), 900 Mc (0.05), 1.5 kMc (0.02), 2.1 kMc (0.008).

In comparison, the satellite occurs at 3 kMc (0.01) and the primary ghosts shown in Fig. 3.3 are located at 7.2 kMc (0.002). At 6.9 kMc the secondary diffraction maximum has a relative intensity of only (0.0008). It is seen that the diffraction pattern is relatively unimportant as far as the lineshape is concerned and that the ghosts and the satellite are stronger than the secondary maxima of the diffraction pattern.

The satellite seen in Fig. 3.3 may be especially pronounced because the grating was used at 72 degrees in auto collimation, well in excess of the 64 degree blaze angle. Masking and refocussing did not improve matters substantially. In addition to this satellite there were other factors responsible for the broad central line. Amongst these one should mention the presence of crystal inclusions, a bad matching of the index of refraction of the liquid mixture and the crystal, use of contaminated liquids and use of badly mixed

liquids. Contamination of the liquids was discussed before. If the mixture had been left for a few days it was found necessary to stir it to mix the components well. Evidently the liquids used did not mix well. Contaminated and badly mixed liquids are bothersome in that particles floating around or density fluctuations in the mixture change the intensity of the light seen by the spectrograph whenever they occur in the incident or scattered beam, therefore making the signal to noise ratio low. It was found that to obtain good traces of the spectra the following points had to be followed closely:

1) A crystal as free from inclusions as possible should be used.

2) Care should be taken in minimizing the dark current and dark current fluctuations in the phototube.

3) The liquids used for matching the index of refraction should be filtered and the sample must be handled so that it will not pick up any moisture.

4) In some cases it is preferable to operate the laser in the hemispherical configuration yielding a uniphase wavefront so that the incident beam is very small in diamter and the number of inclusions illuminated is a minimum.

5) Alignment of the system and maximization of the intensities has to be done very carefully.

3.2.3 Processing of the traces

There was no real problem in resolving the Brillouin components

due to the heavily longitudinal waves. The completely transverse waves were not observable. However, the mixed modes presented a problem. The grating satellite mentioned before fell between the partially transverse peak and the central peak making it difficult to resolve the mixed mode on the low wavelength side of the line. In RbCl it was possible to lower the central line intensity sufficiently so that all five peaks were resolved. However, in KI there was too much scattering from inclusions and the Stokes component was not resolved. In KCl, intensities were so low that the ghosts actually masked the mixed modes. However, by taking a trace of the line shape of the incident laser line directly using the proper integration time and by subtracting this line shape from the unresolved traces, both partially transverse Brillouin peaks were clearly resolved in KI and RbCl (see Fig. 3.4). This tedious subtraction procedure was used on all traces which showed mixed mode peaks.

3.2.4 Data processing

Generally about ten traces were taken for every data point with a maximum number of twentyfive traces for data points yielding low precision. The ten to twentyfive traces for each angle were averaged and their root mean square error was calculated. From the frequency shifts found in this manner the velocities were found by use of Eq. (1.6). The error due to the uncertainty in the scattering angle was included here along with statistical and calibration uncertainties. The indices of refraction and the densities at the temperature at

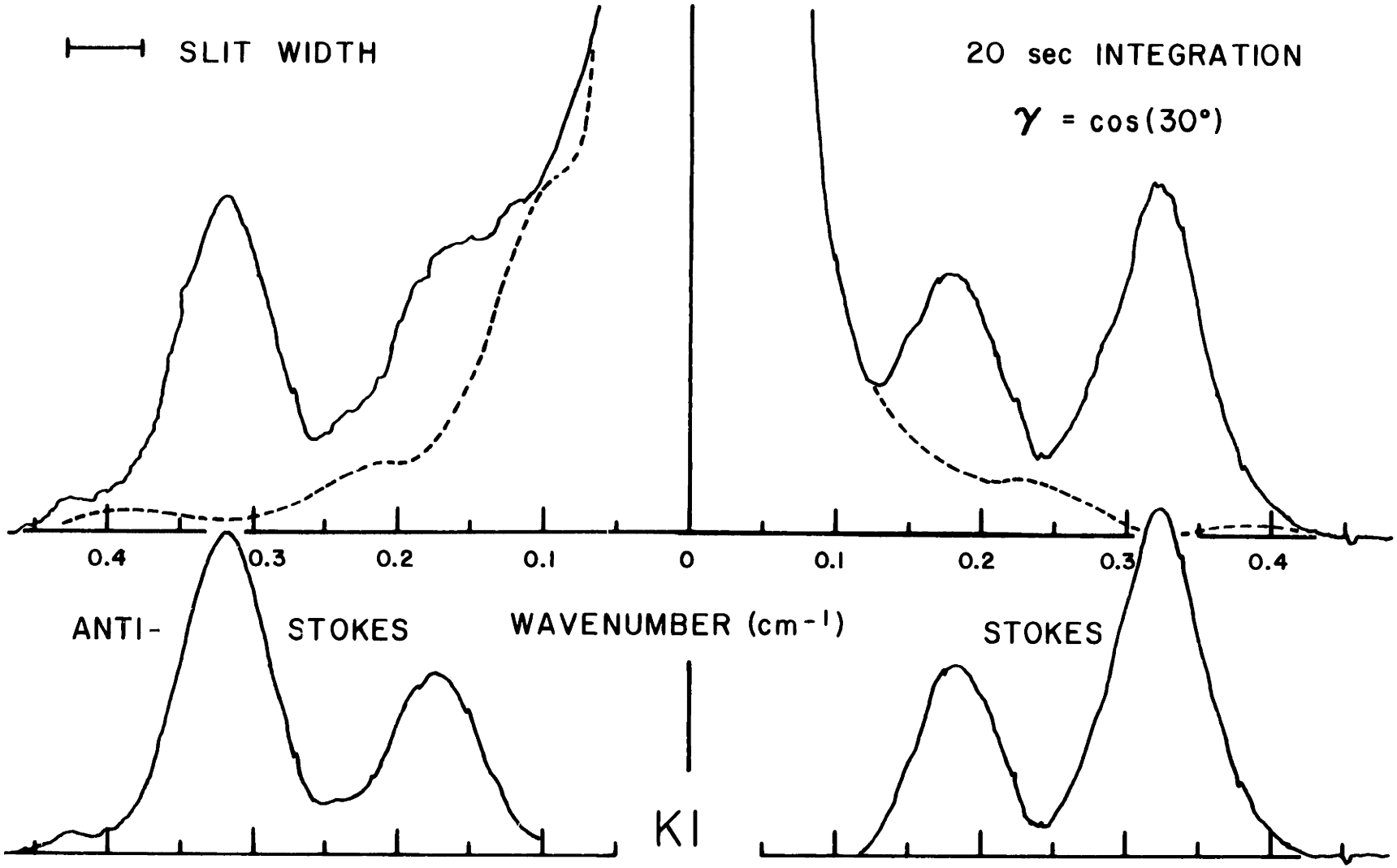

FIG. 3.4 SUBTRACTION OF GHOSTS & SATELLITE

which the experiment was carried out were calculated from values given in Landolt-Börnstein, Zahlenwerte und Funktionen[14] and in the International Critical Tables[15].

3.2.5 Determination of the elastic constants

Starting values for the elastic constants were obtained from the velocities in a few directionswhere the velocities are most sensitive to a particular constant (outlined in 2.2) and from literature values of the constants in the ultrasonic region. A set of from six to ten values for each constant around the starting values was made up. An IBM 709 computer was programmed to compute the root mean square deviation between the experimental velocities and the theoretical curve for all possible combinations of the elastic constants contained in the set mentioned above. After a rough minimum of the root mean square deviation had been located, the finesse of the grid of elastic constants was increased.

Some problems encountered in this procedure will be discussed in the following chapter. Finally, the theoretical curve was plotted using the "best" values of c_{11}, c_{44}, and c_{12} as found by the computer. The experimental values are then shown in comparison.

Chapter IV

RESULTS

4.1 Introduction

The Brillouin spectra for the three alkali halides potassium chloride (KCl), potassium iodide (KI), and rubidium chloride (RbCl) were recorded as a function of propagation direction in the {110} planes. Some of the qualitative features of the spectra can be explained by considering the lattice sizes and physical constants of the crystals.

The three crystals are cubic of the NaCl type with space group O_h^5 - Fm3m. The molecular weights, densities, indices of refraction, lattice constants and compressibilities are listed in Table II. There are four molecules per unit cell in each of the three crystals. The crystal structure is shown in Fig. 4.1.

The intensity of the light scattered by the adiabatic fluctuations in the density can be written in the form

$$I \propto \varepsilon^2 \left(\frac{\partial \ln \varepsilon}{\partial \ln \rho}\right)^2 kT \beta_s \qquad (4.1)$$

TABLE II

Some physical constants for KCl, KI, and RbCl

Crystal	KI	RbCl	KCl(Sylvite)	Reference
Molecular weight	166.0	120.9	74.6	a
Density at 22.5°C (gm/cm^3)	3.124	2.799	1.987	b
Index of refraction at 22.5°C and 6328 Å	1.661	1.492	1.488	c
Lattice constant = 2 x (interionic distance) (Å) (see Fig. 4.1)	7.06	6.55	6.29	d
Compressibility at room temperature (x 10^{-12} $cm^2/dyne$)	8.07 8.33	6.16	5.50	e f

a Handbook of Chemistry and Physics (Chemical Rubber Publishing Company, Cleveland, Ohio, 1960), 41st ed., p. 626, p. 630, p. 640.

b International Critical Tables of Numerical Data in Physics, Chemistry and Technology (McGraw-Hill, 1928), Volume III, p. 43, p. 44.

c Landolt-Börnstein, Zahlenwerte und Funktionen aus Physik-Chemie-Astronomie-Geophysik-Technik (Springer-Verlag, 1962), 6. Auflage, II. Band, 8. Teil, Optische Konstanten, p. 2-421, 2-53 (KI); p. 2-418, 2-51 (KCl); p. 2-57 (RbCl).

d Ibid, I. Band, 4. Teil, Kristalle (1955), p. 93, p. 95.

e K. Spangenberg and S. Haussühl, Zeits. für Kristallographie, 109, 422 (1957).

f M. H. Norwood and C. V. Briscoe, Phys. Rev. 112, 45 (1958).

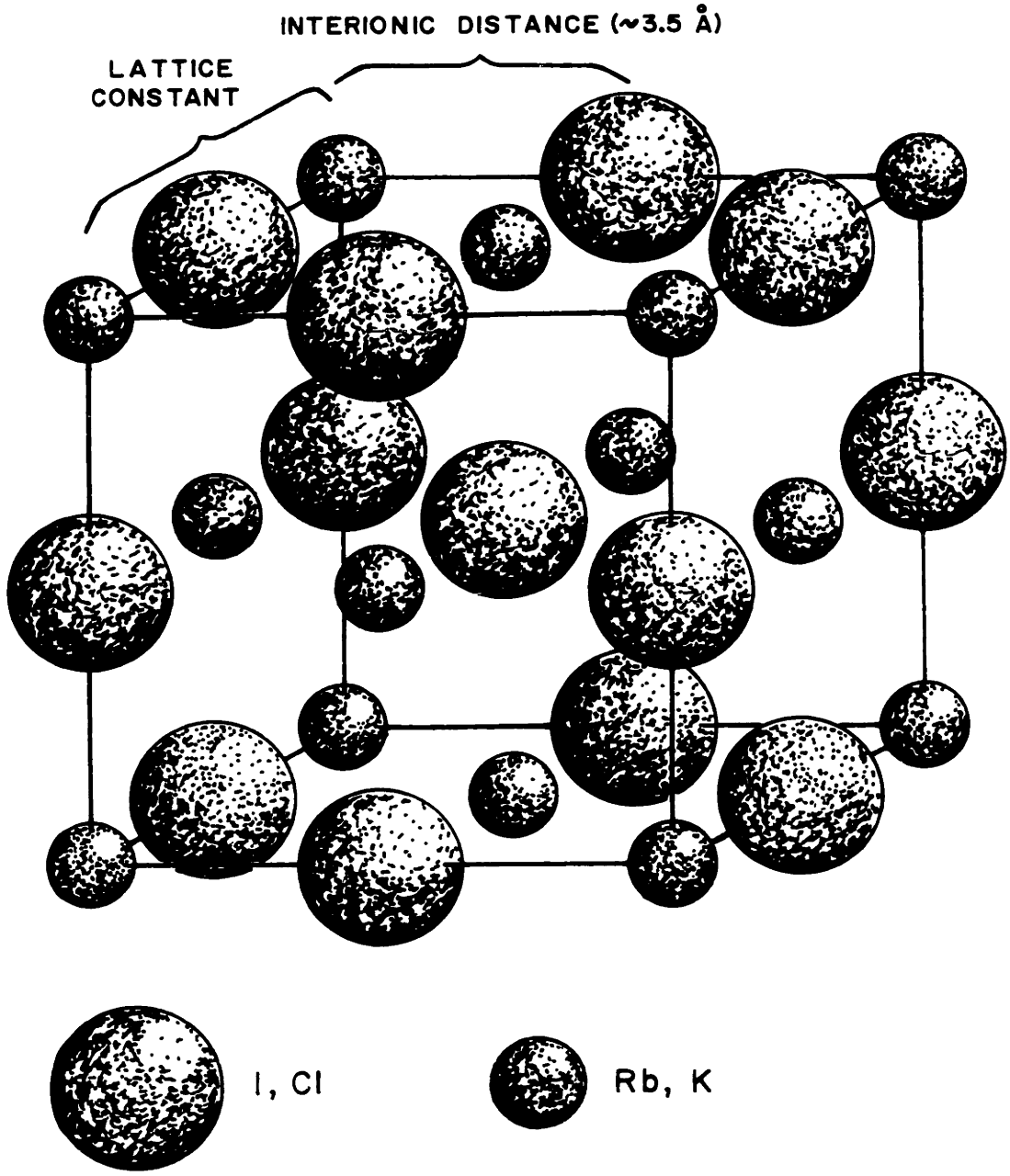

IN RbCl, KI, and KCl

FIG. 4.1 CRYSTAL STRUCTURE OF THE ALKALI HALIDES

where ε is the dielectric constant, ρ the density, and β_s the adiabatic compressibility[16]. If one assumes that $(\frac{\partial \ln \varepsilon}{\partial \ln \rho}) \sim 1$ for the three crystals, the measured ratio of the intensities in KI: RbCl:KCl (2 1/4 : 1 1/4 : 1) agree fairly well with the intensities expected from Eq. (4.1). This is explained more fully in 4.5. The crystals with higher compressibility will be softer and have smaller sound velocities, since

$$\beta_s = 1/(\rho\, v^2(\gamma)) = 1/c_{eff}\,(\gamma) \qquad (4.2)$$

where c_{eff} is the effective elastic constant for a particular direction of propagation. c_{eff} is defined by Eq. (4.2). For example, the sound velocities of longitudinal waves in the <001> direction are found to be 2980, 3650, and 4510 meters per second for KI, RbCl, and KCl, respectively.

4.2 Potassium chloride (KCl)

A single crystal of potassium chloride, 1/2" x 1/2" x 1/2", provided by Prof. Smakula at M.I.T., was used. The sample had transparent faces which became somewhat cloudy after some handling. As expected, the scattering was rather weak and the traces had a low signal to noise ratio compared to those obtained for KI and RbCl. Inasmuch as the sound velocities are highest along the <001> direction, the intensities presented the biggest problem in that direction, since the intensity is proportional to $1/v^2$.

Even though this sample contained few inclusions, the scattering from these inclusions was approximately 150 times as strong in intensity as the Brillouin scattering. As a result, the mixed modes could not be resolved clearly. In some propagation directions the intensities of the Brillouin components were so low that they were hard to distinguish from the grating ghosts (see Fig. 3.3). Only one point on the mixed branch was tabulated in the results. A trace with good signal to noise is reproduced in Fig. 4.2. One can see the longitudinal modes, the strong central line, the grating satellite and the two primary ghosts.

Approximately seventy traces were recorded for seven data points for this crystal. Integration times up to twentyone seconds were used. In Table III the phonon frequency ν_σ and the hypersonic phase velocity v_s of the sound waves are tabulated as a function of the propagation direction in the {110} planes. The angle tabulated in Table III is measured from the <001> direction.

The sound velocities given in Table III were fed to an IBM 709 computer. The computer found the velocity as a function of $\gamma = \cos\theta$ using Eq. (2.8) for the following set of values of c_{11}, c_{44}, and c_{12} :

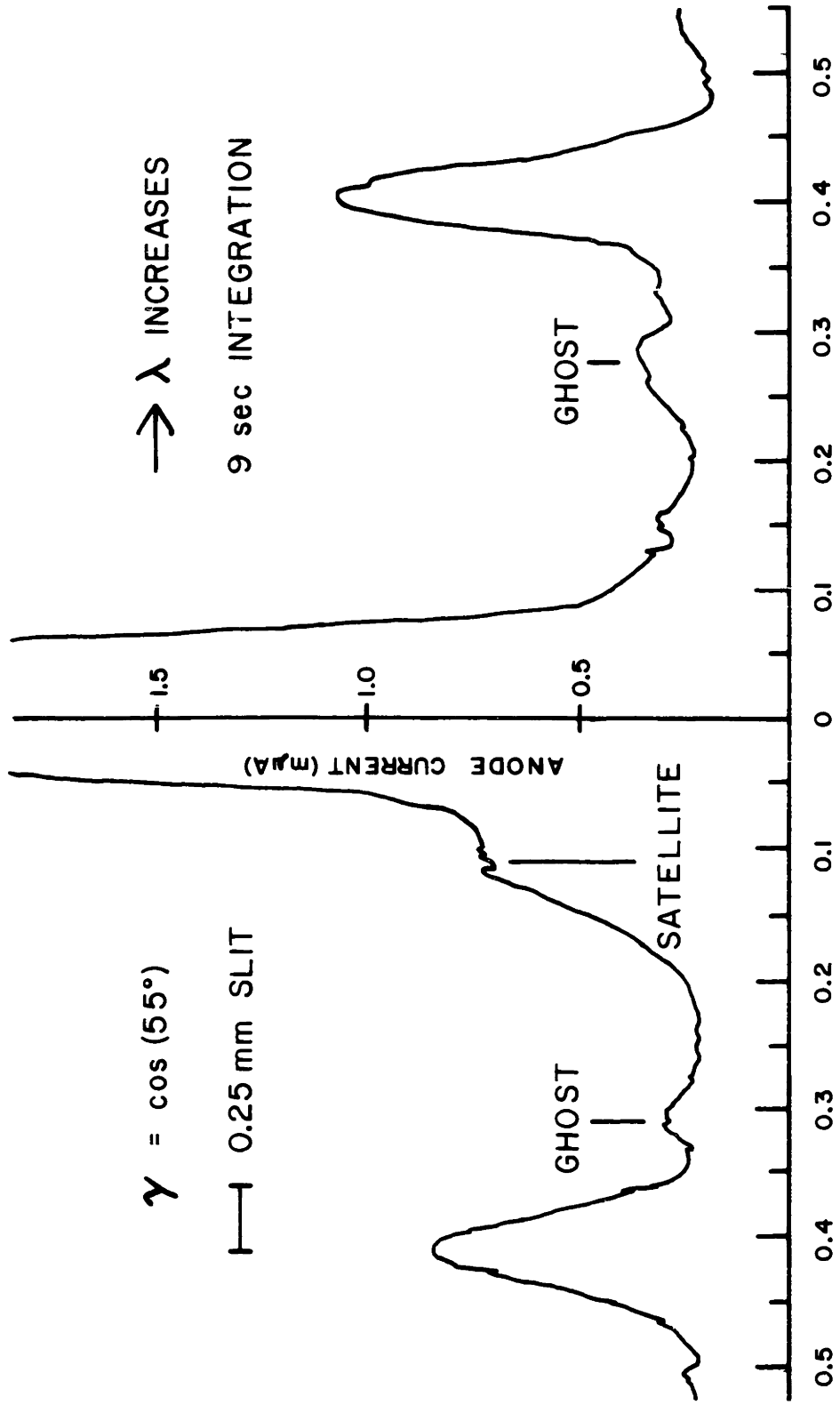

FIG. 4.2 BRILLOUIN SPECTRUM OF KCl

TABLE III

ν_σ and v_s for KCl

Density at 22.8°C = 1.9873 gm/cm^3

Index of refraction at 6328 Å and 22.8°C = 1.4879

Wavelength of phonons = 3007.4 Å

Angle (degrees)	Temperature (°C)	Phonon frequency ν_σ (kMc) (90° scattering)	Error (%)	Hypersonic phase velocity v_s (meters/sec)	Mode
0	22.7	14.993 ± 0.116	0.78	4509 ± 35	L
25	22.6	14.090 ± 0.128	0.91	4237 ± 38	L
35	22.7	13.283 ± 0.101	0.76	3995 ± 30	L
		8.134 ± 0.112	1.4	2446 ± 34	M
45	22.7	12.453 ± 0.082	0.66	3745 ± 25	L
55	22.8	12.121 ± 0.065	0.54	3645 ± 20	L
70	22.6	12.571 ± 0.061	0.49	3780 ± 18	L
90	23.1	12.931 ± 0.063	0.49	3889 ± 19	L

The percentage error quoted in the table for ν_σ and v_s is composed of the root mean square deviation of the traces from the average for each angle (i.e. the statistical fluctuation), of the error in the dispersion (i.e. roughness of the screw, 0.25%), and of the error due to alignment difficulties (approximately 0.30%). Judging by the fit of the theoretical values to the experimental values, the error is actually smaller.

Batch number 1:

c_{11} = 4.02, 4.03, 4.04, 4.05, 4.06, 4.07, 4.08, 4.09, 4.10

c_{44} = 0.66, 0.67, 0.68, 0.69, 0.70, 0.71, 0.72, 0.73, 0.74

c_{12} = 0.47, 0.49, 0.51, 0.53, 0.55, 0.57, 0.59, 0.61, 0.63

Batch number 2:

c_{11} = 4.050, 4.055, 4.060, 4.065, 4.070

c_{44} = 0.58, 0.59, 0.60, 0.61, 0.62, 0.63, 0.64, 0.65, 0.66

c_{12} = 0.63, 0.65, 0.67, 0.69, 0.71, 0.73, 0.75, 0.77, 0.79

(all c's in units of 10^{11} dyne/cm^2)

For each possible combination of elastic constants in these two groups the computer calculated first the velocities for all γ where experimental measurements had been made. Then the computer found the deviation between the experimentally measured velocities and the computed velocities for each γ where an experimental observation had been made. The deviations were squared and added up. This number was divided by m - 1 where m is the number of experimental points. Finally the square root was taken. In the following discussion of the results this procedure will be referred to as finding the root mean square deviation (between the experimental points and the theoretical curve):

$$RMS = \sqrt{\frac{\sum_{p=1}^{m} \delta_p^2}{m - 1}} \qquad (4.3)$$

The minimum root mean square deviation in batch number 1 occurred at $c_{11} = 4.06 \times 10^{11}$ dyne/cm^2, for the longitudinal root. The

minimum root mean square deviation in batch number 2 was found to lie between $c_{11} = 4.06 \times 10^{11}$ dyne/cm^2 and $c_{11} = 4.065 \times 10^{11}$ dyne/cm^2, also for the longitudinal root. Since this particular root is very sensitive to c_{11} in all directions in the {110} planes (see Fig. 2.3), the error should be quite small. It was found that although there is only one absolute minimum found by the computer, the root mean square deviation between the experimental points and the theoretical curve of the velocities stays almost constant near the minimum value for all combinations of the elastic constants for which $2\,c_{44} + c_{12}$ is approximately constant, for the longitudinal branch. This should not surprise us. By looking at Table I one observes that along the <111> and <110> directions the velocities contain c_{44} and c_{12} in the form $2\,c_{44} + c_{12}$. One might expect that, at least between 55 degrees and 90 degrees, these two constants enter in the form $a\,c_{44} + b\,c_{12}$ where a differs not much from 2 and b is approximately 1, both a and b varying slightly with γ. In the appendix it is shown that this is indeed the case. This would imply that a least root mean square fit of the theoretical curve to the data points would only give c_{11} and $2\,c_{44} + c_{12}$ to good accuracy, but not c_{44} and c_{12} separately. By reference to Fig. 2.3 one can see that c_{11} and $2\,c_{44} + c_{12}$ can be found with very good accuracy, inasmuch as v_L is very sensitive to these combinations of constants.

With data on the mixed branch it becomes possible to find the individual magnitudes of c_{12} and c_{44}. By reference to Fig. 2.4 we see that the mixed mode is quite sensitive to c_{44} near 30 degrees. Therefore, c_{44} was determined from this branch and then used to pick out the proper c_{12} from the longitudinal branch. As a result, those values of c_{11}, c_{44}, and c_{12} giving the minimum root mean square deviation for the longitudinal branch were selected as the best values for the elastic constants contained in the data, with the constraint that c_{44} had to give a good fit to the mixed mode.

To show more graphically the dependence of the deviation on the combination of elastic constants $2\,c_{44} + c_{12}$ I have plotted the root mean square deviation for KCl ($c_{11} = 4.06 \times 10^{11}$ dyne/cm^2) in Fig. 4.3 as a function of c_{44} and c_{12}. One observes no really pronounced minimum but rather a valley at $2\,c_{44} + c_{12} = 1.95 \times 10^{11}$ dyne/cm^2. In Table IV the root mean square error is tabulated for $c_{11} = 4.060$, 4.065×10^{11} dyne/cm^2 as a function of c_{44} in the bottom of the valley, i.e. for $2\,c_{44} + c_{12} = 1.95 \times 10^{11}$ dyne/cm^2. It is seen that for the 17 entries between $c_{44} = 0.58 \times 10^{11}$ dyne/cm^2 and $c_{44} = 0.74 \times 10^{11}$ dyne/cm^2 the root mean square deviation changes only by 25%. However, by reference to Table V one sees that as one goes away from the valley along either the c_{44} or the c_{12} axis by just one entry, the deviation increases by the same amount. Hence, the constraint on $2\,c_{44} + c_{12}$ is quite strong but the longitudinal branch gives us no clue to the separate magnitudes

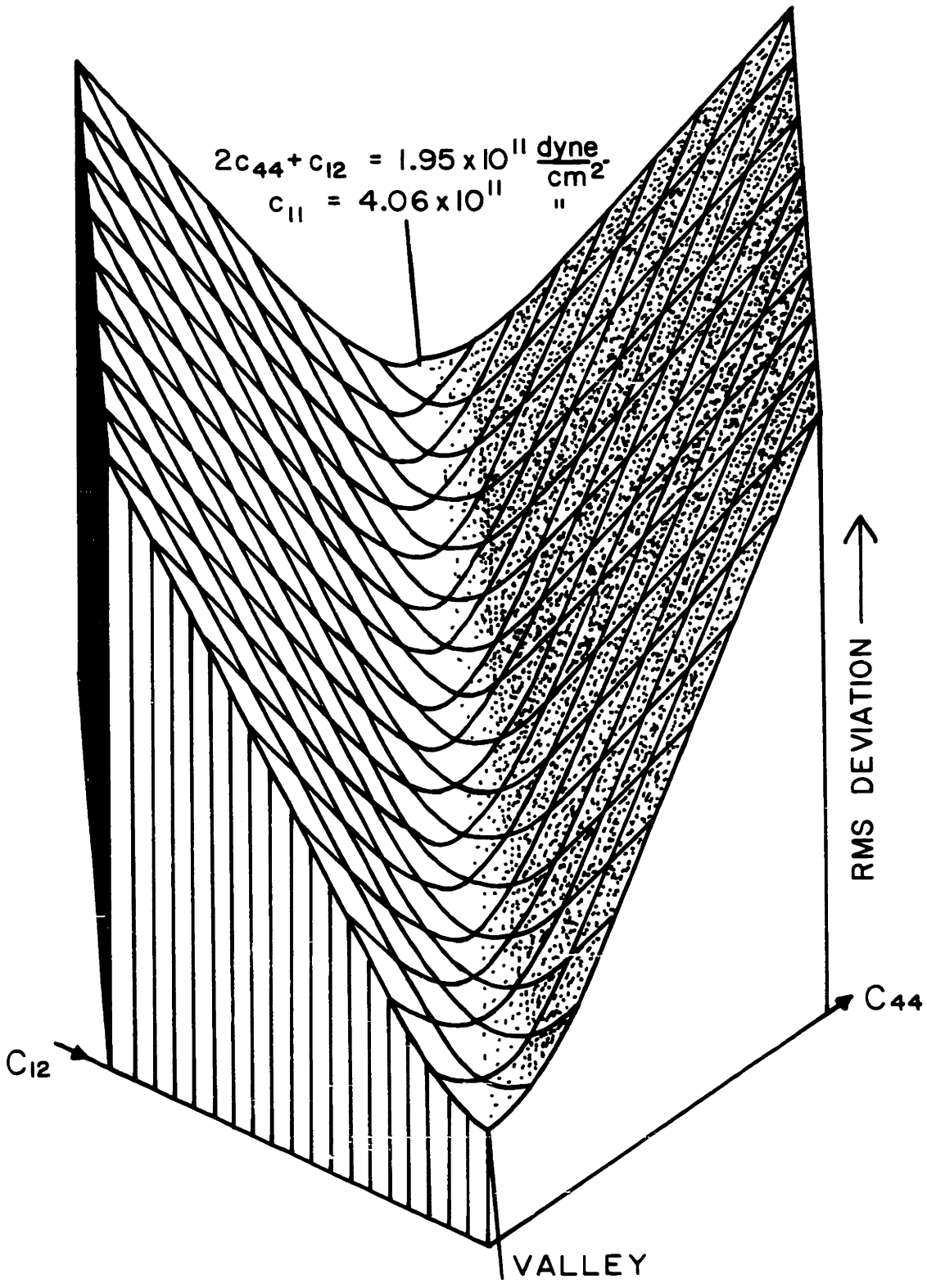

FIG. 4.3 RMS DEVIATION AS A FUNCTION OF c_{44} and c_{12} (LONGITUDINAL MODE)

TABLE IV

RMS deviations for v_L

$c_{11} = 4.06\ (4.065) \times 10^{11}$ dyne/cm^2, $2\,c_{44} + c_{12} = 1.95 \times 10^{11}$ dyne/cm^2

Elastic constant		RMS deviations (meters/second)	
c_{44}	c_{12}	$c_{11} = 4.06$	$c_{11} = 4.065$
0.58	0.79	10.3	10.0
0.59	0.77	10.1	9.92
0.60	0.75	9.94	9.78
0.61	0.73	9.77	9.66
0.62	0.71	9.62	9.53
0.63	0.69	9.46	9.41
0.64	0.67	9.30	9.29
0.65	0.65	9.15	9.18
0.66	0.63	9.00	9.07
0.67	0.61	8.86	
0.68	0.59	8.72	
0.69	0.57	8.58	
0.70	0.55	8.46	
0.71	0.53	8.32	
0.72	0.51	8.21	
0.73	0.49	8.10	
0.74	0.47	7.99	

$$\text{RMS deviation} = \sqrt{\frac{\Sigma\delta^2}{m-1}}\ ,\ m = 7$$

TABLE V

RMS deviations for v_L

Sharpness of minimum along c_{11}, c_{44}, and c_{12} axes

c_{12} = 0.69, c_{44} = 0.63		c_{11} = 4.06, c_{12} = 0.69		c_{11} = 4.06, c_{44} = 0.63	
c_{11}	RMS (m/sec)	c_{44}	RMS (m/sec)	c_{12}	RMS (m/sec)
4.050	10.8	0.58	35.4	0.63	22.2
4.055	9.94	0.59	29.0	0.65	16.6
4.060	9.46	0.60	22.8	0.67	11.8
4.065	9.41	0.61	17.0	0.69	9.46
4.070	9.79	0.62	12.0	0.71	11.1
		0.63	9.46	0.73	15.6
		0.64	11.1	0.75	21.1
		0.65	15.6	0.77	27.1
		0.66	21.2	0.79	33.2

of c_{12} and c_{44}.

We know c_{11} is between 4.060 and 4.065 x 10^{11} dyne/cm^2 and 2 c_{44} + c_{12} = 1.95 x 10^{11} dyne/cm^2. Unfortunately, we have only one data point on the mixed branch for this crystal. By using the grids described before we can find the absolute least root mean square deviation between the one data point and the computed mixed branch. Inasmuch as we know to good accuracy c_{11} and 2 c_{44} + c_{12} from the longitudinal branch we will use those two pieces of information. With these two constraints we get the root mean square errors tabulated in Table VI as a function of c_{44} and c_{12}.

By inspection of Table VI one sees that there is a fairly sharp minimum for c_{12} = 0.69 and c_{44} = 0.63 x 10^{11} dyne/cm^2. So that one can get an idea of the sharpness of the minimum, the root mean square deviations have been given along the c_{12}, c_{44}, and c_{11} axes in Table V. In Fig. 4.4 the root mean square deviation has been plotted for c_{11} = 4.06 x 10^{11} dyne/cm^2 as a function of c_{44} and c_{12} for the mixed mode. It is seen that there is again some sort of valley rather than a minimum. However, this valley is at right angles to the one from the longitudinal branch. Hence, the best fit to both branches will occur where the constraint 2 c_{44} + c_{12} crosses the valley in Fig. 4.4. The point of intersection is indicated in the figure and corresponds to the c_{44} and c_{12} already given.

TABLE VI

Deviations for v_M

$c_{11} = 4.06\ (4.065) \times 10^{11}$ dyne/cm^2, $2c_{44} + c_{12} = 1.95 \times 10^{11}$ dyne/cm^2

Elastic constant		Deviation (meters/second) = δ	
c_{44}	c_{12}	$c_{11} = 4.06$	$c_{11} = 4.065$
0.58	0.79	46.8	45.7
0.59	0.77	37.1	35.9
0.60	0.75	27.4	26.2
0.61	0.73	17.7	16.6
0.62	0.71	8.09	6.94
0.63	0.69	1.49	2.63
0.64	0.67	11.0	12.2
0.65	0.65	20.5	21.6
0.66	0.63	30.0	31.1

TABLE VII

Deviations for v_M

Sharpness of minimum along c_{11}, c_{44}, and c_{12} axes

$c_{12} = 0.69$, $c_{44} = 0.63$		$c_{11} = 4.06$, $c_{12} = 0.69$		$c_{11} = 4.06$, $c_{44} = 0.63$	
c_{11}	Deviation (m/sec)	c_{44}	Deviation (m/sec)	c_{12}	Deviation (m/sec)
4.050	0.789	0.58	31.4	0.63	10.5
4.055	0.352	0.59	24.7	0.65	7.55
4.060	1.49	0.60	18.1	0.67	4.56
4.065	2.63	0.61	11.5	0.69	1.49
4.070	3.76	0.62	4.98	0.71	1.65
		0.63	1.49	0.73	4.87
		0.64	7.91	0.75	8.17
		0.65	14.3	0.77	11.5
		0.66	20.6	0.79	15.0

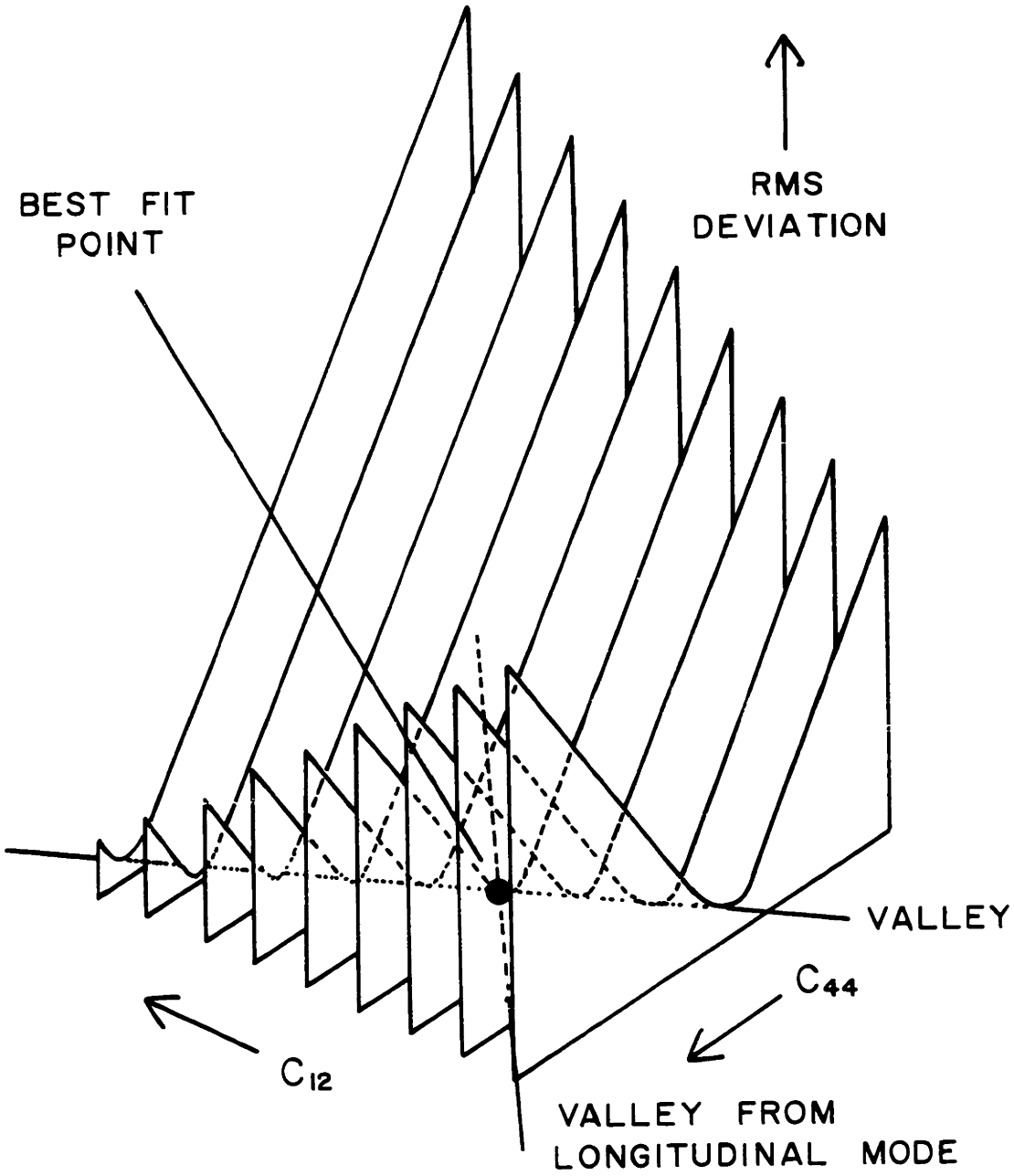

FIG. 4.4 RMS DEVIATION AS A FUNCTION OF c_{44} and c_{12} (MIXED MODE)

In Table VII the deviations along the elastic constant axes are given for the mixed mode. The minimum occurs at $c_{11} = 4.055 \times 10^{11}$ dyne/cm^2, but this branch is not as sensitive to c_{11} as the longitudinal branch. Therefore, we will use only the longitudinal branch to find c_{11}. From Table V the minimum occurs at $c_{11} = 4.064 \times 10^{11}$ dyne/cm^2. Using Eq. (2.8) with $c_{11} = 4.064 \times 10^{11}$ dyne/cm^2, $c_{44} = 0.63 \times 10^{11}$ dyne/cm^2, and $c_{12} = 0.69 \times 10^{11}$ dyne/cm^2 one obtains the velocities of sound given in Table VIII. In Figs. 4.5 and 4.6 I have displayed the values for v_L, v_M and v_T as a function of γ for these values of the elastic constants along with the corresponding experimental velocities.

Inasmuch as the mixed branch data point has big error bars, one can say without qualifications only that

$$c_{11} = (4.064 \pm 0.010) \times 10^{11} \text{ dyne/cm}^2 \ (\pm 0.25\%) \text{ and}$$

$$2\, c_{44} + c_{12} = (1.95 \pm 0.02) \times 10^{11} \text{ dyne/cm}^2$$

The magnitude of the error is estimated qualitatively on the basis of the mesh size of the grid, on the basis of the sharpness of the minimum, and by examination of Figs. 2.3 and 2.4.

If one assumes that the one mixed branch point is centered on the actual velocity curve, one can furthermore say that

TABLE VIII

Sound velocities in KCl

$\rho = 1.9873$ gm/cm^3, $c_{11} = 4.064$, $c_{44} = 0.63$, $c_{12} = 0.69$
(c_{11}, c_{44}, and c_{12} in units of 10^{11} dyne/cm^2)

Angle (degrees)	Experimental velocity (meters/sec)		Theoretical velocity (meters/sec)		
	v_L	v_M	v_L	v_M	v_T
0	4509 ± 35		4522	1780	1780
7.5			4494	1825	1806
15			4412	1948	1878
25	4237 ± 38		4228	2189	2030
30			4111	2322	2121
35	3995 ± 30	2446 ± 34	3985	2448	2218
40			3859	2556	2317
45	3745 ± 25		3750	2627	2414
50			3677	2642	2508
55	3645 ± 20		3655	2587	2596
65			3722	2325	2746
70	3780 ± 18		3774	2165	2805
75			3821	2015	2852
80			3857	1891	2886
90	3889 ± 19		3890	1780	2914

The root mean square deviation between the experimental points and the theoretical curve for the longitudinal branch is 9.24 meters per second.

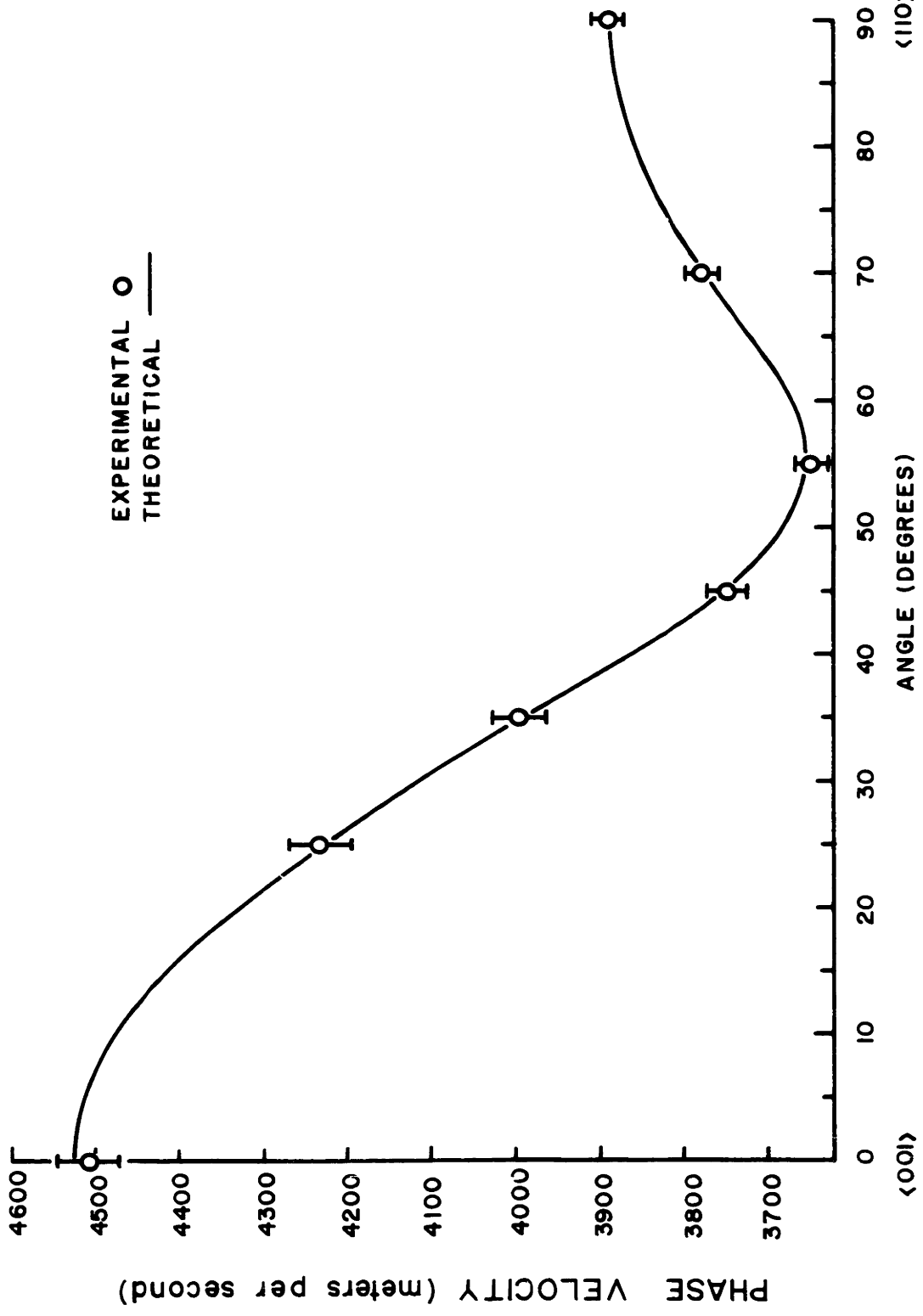

FIG. 4.5 DEPENDENCE OF V_L ON PROPAGATION DIRECTION IN KCl

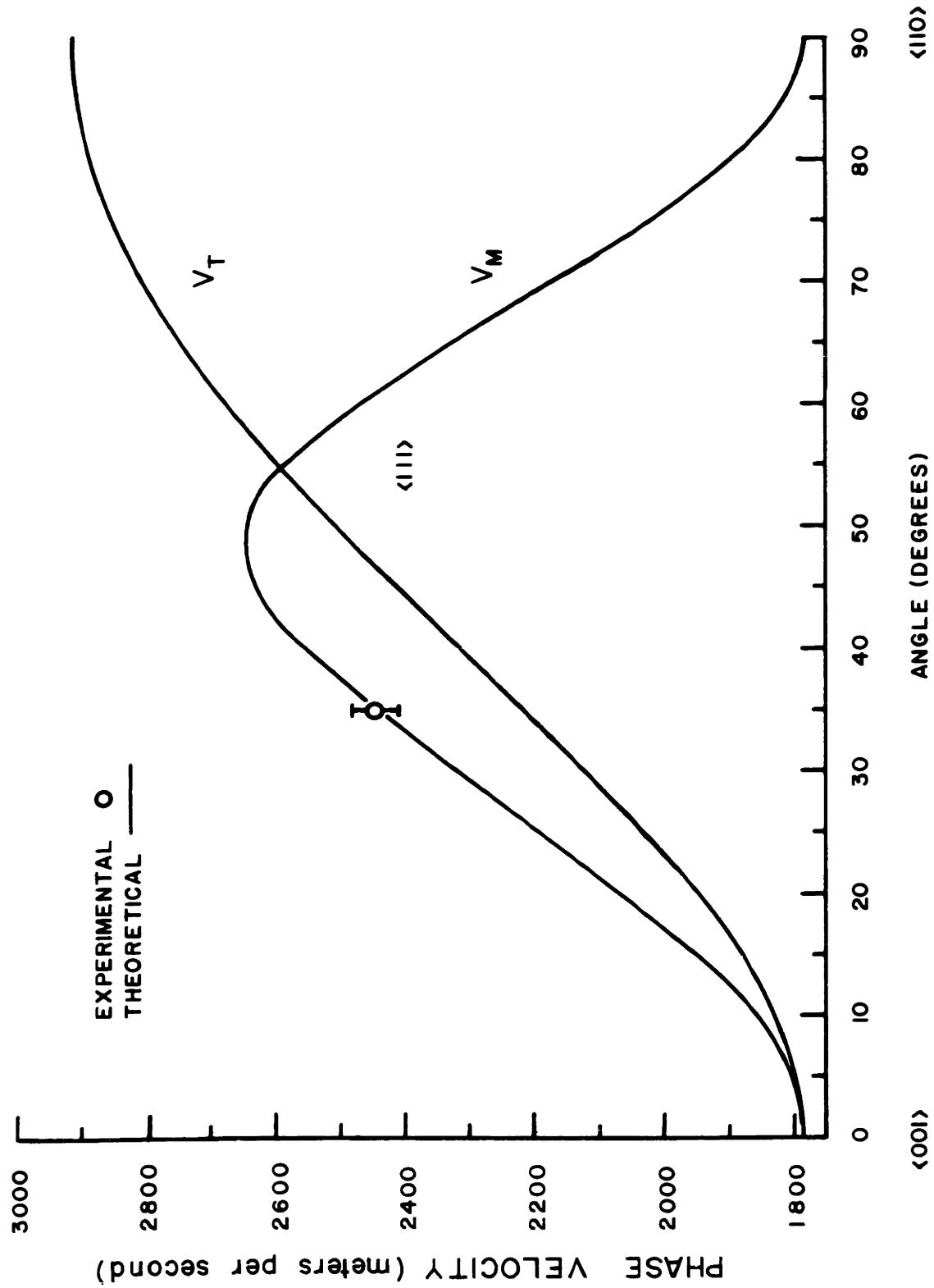

FIG. 4.6 DEPENDENCE OF V_M AND V_T ON PROPAGATION DIRECTION IN KCl

$$c_{44} = (0.63 \pm 0.01) \times 10^{11} \text{ dyne/cm}^2 (\pm 1.6\%) \text{ and}$$

$$c_{12} = (0.69 \pm 0.04) \times 10^{11} \text{ dyne/cm}^2 (\pm 5.8\%)$$

These errors are on the conservative side. In Table IX the ultrasonic values of the elastic constants have been presented along with the present results. It is seen that the elastic constants obtained from this experiment are in good agreement with the ultrasonic values. There does not seem to be a significant amount of dispersion between 9 Mc and 15 kMc.

It should be noted that no attempt was made to weight the data according to the precision with which the various frequency shifts had been determined, since the percentage errors varied at most by a factor of two.

4.3 Rubidium Chloride (RbCl)

A single crystal of rubidium chloride, 3/8" x 3/8" x 5/8", was used in the experiment. The traces obtained for RbCl were generally of higher quality than those for KCl and along some directions they showed a signal to noise ratio that compared favorably with that of the traces for KI.

The intensity of the central line, due largely to reflection of the incident beam from inclusions into the spectrograph, was weaker than in KCl so that the mixed modes were resolved in certain directions of propagation. A trace with comparatively low signal to noise ratio is reproduced in Fig. 4.7. This trace

TABLE IX

Elastic constants for KCl

Frequency	Temperature	c_{11}	c_{44}	c_{12}	$2c_{44} + c_{12}$	Compressibility	Reference	(Year)
	22°C	4.078 ±.008	0.633 ±.006	0.69 ±.014	1.96 ±.03	5.50	a	(1960)
9 Mc	22°C	4.08 ±.014	0.635 ±.003	0.69 ±.034	1.96 ±.04	5.50	b	(1957)
	22.8°C	4.044 ±.012	0.630 ±.003	0.66 ±.06	1.92 ±.07	5.59	c	(1958)
10 kMc - 15 kMc	22.8°C	4.064 ±.01	0.63 ±.01	0.69 ±.04	1.95 ±.02	5.51	this thesis	

$$\text{Compressibility} = \frac{3}{(c_{11} + 2c_{12})}$$

[All elastic constants in units of 10^{11} dyne/cm^2; compressibility in units of 10^{-12} cm^2/dyne]

a S. Haussühl, Zeits. für Physik, 159, 223 (1960)

b K. Spangenberg and S. Haussühl, Zeits. für Kristallographie, 109, 422 (1957)

c M. H. Norwood and C. V. Briscoe, Phys. Rev. 112, 45 (1958)

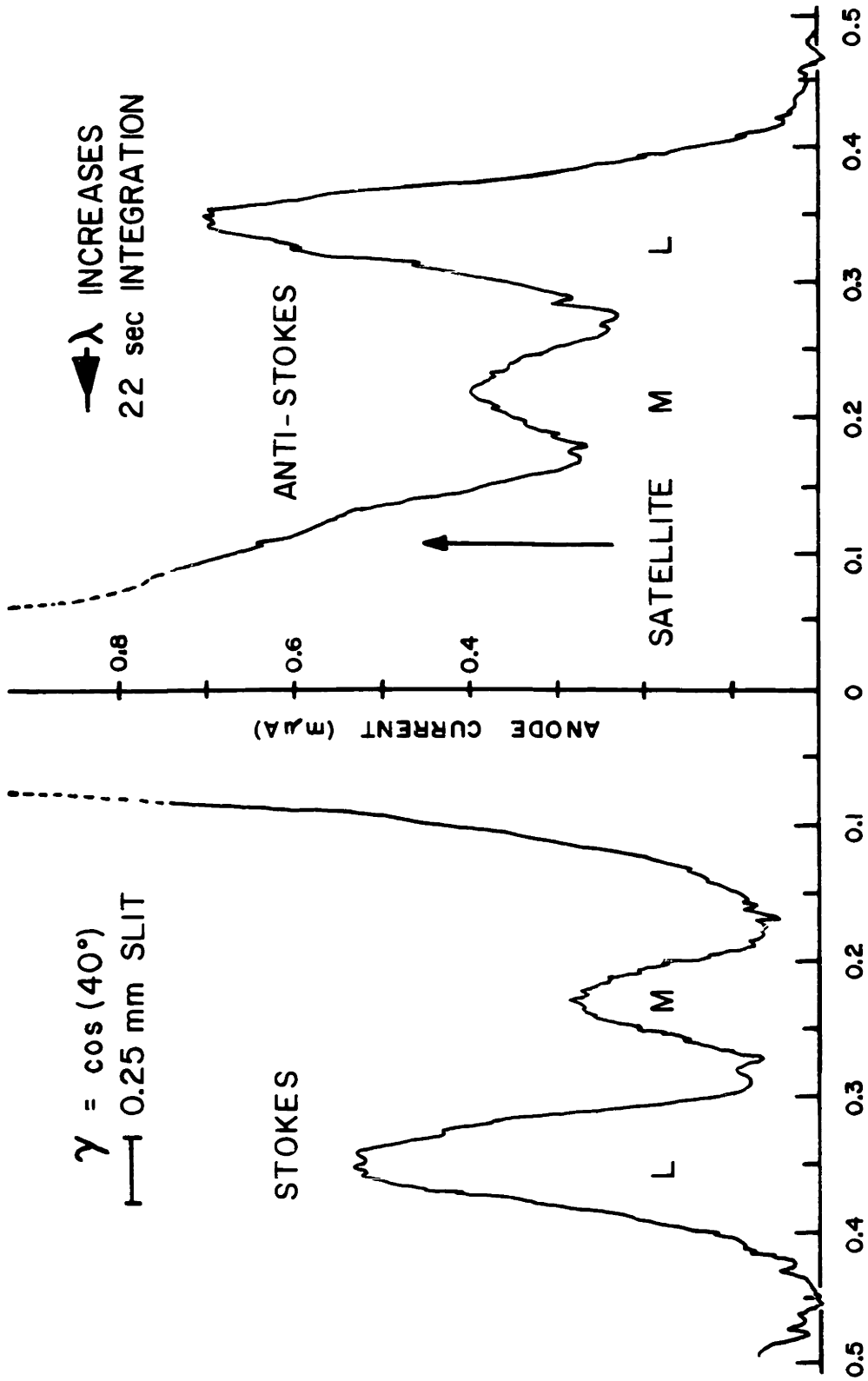

FIG. 4.7 BRILLOUIN SPECTRUM OF RbCl

was chosen because the longitudinal and mixed modes are clearly resolved.

Seventy traces were recorded for nine directions of propagation in this particular crystal. Integration times of up to twentytwo seconds were employed. In Table X the phonon frequency ν_σ and the hypersonic phase velocity v_s of the sound waves are given as a function of the propagation direction in the {110} planes.

The sound velocities given in Table X were again given to the IBM 709 computer so that it could find the root mean square deviation between the experimental velocities in Table X and those velocities found by use of Eq. (2.8) for the following values of c_{11}, c_{44}, and c_{12};

c_{11} = 3.71, 3.72, 3.73, <u>3.74</u>, 3.75, 3.76, 3.77, 3.78, 3.79

c_{44} = 0.520, 0.525, 0.530, 0.535, 0.540, 0.545, 0.550
0.555, 0.560

c_{12} = 0.62, 0.64, 0.66, 0.68, 0.70, 0.72, 0.74, 0.76, 0.78

(all c's in units of 10^{11} dyne/cm^2)

For the longitudinal branch the minimum root mean square deviation occurred at $c_{11} = 3.740 \times 10^{11}$ dyne/cm^2 and did not change much along the bottom of the valley defined by $2\,c_{44} + c_{12} = 1.79 \times 10^{11}$ dyne/cm^2. In Table XI the values of the root mean square deviation in the bottom of the valley are given. In Table XII the root mean square deviation is tabulated for v_M with constraints $c_{11} = 3.74 \times 10^{11}$ dyne/cm^2 and $2\,c_{44} + c_{12} = 1.79 \times 10^{11}$ dyne/cm^2. It is seen that the minimum in the mixed mode

TABLE X

ν_σ and v_s for RbCl

Density at 22.6°C = 2.7986 gm/cm^3

Index of refraction at 6328 Å and 22.6°C = 1.4916

Wavelength of phonons = 2999.9 Å

Angle (degrees)	Temperature (°C)	Phonon frequency ν_σ (kMc) (90° scattering)	Error (%)	Hypersonic phase velocity v_s (meters/sec)	Mode
0	23.1	12.154 ± 0.071	0.59	3646 ± 21	L
25	22.5	11.419 ± 0.059	0.52	3426 ± 18	L
		5.840 ± 0.103	1.8	1752 ± 31	M
30	22.5	11.103 ± 0.071	0.64	3331 ± 21	L
		6.210 ± 0.163	2.6	1863 ± 49	M
35	22.5	10.722 ± 0.071	0.67	3216 ± 21	L
		6.464 ± 0.094	1.4	1939 ± 28	M
40	22.8	10.331 ± 0.072	0.70	3099 ± 22	L
	?	6.752 ± 0.157	2.3	2025 ± 47	M
45	22.3	10.100 ± 0.066	0.65	3030 ± 20	L
		6.752 ± 0.177	2.6	2025 ± 53	M
55	22.4	9.800 ± 0.054	0.55	2940 ± 16	L
70	22.4	10.194 ± 0.055	0.54	3058 ± 16	L
90	22.4	10.511 ± 0.062	0.59	3153 ± 18	L

The percentage error is composed of the root mean square deviation of the traces from the average for each angle, of the error in dispersion, and of the error due to alignment difficulties.

TABLE XI

RMS deviations for v_L

$c_{11} = 3.74 \times 10^{11}$ dyne/cm^2, $2c_{44} + c_{12} = 1.79 \times 10^{11}$ dyne/cm^2

Elastic constant		RMS deviations (meters/second)
c_{44}	c_{12}	$c_{11} = 3.74$
0.555	0.68	10.926
0.545	0.70	10.922
0.535	0.72	10.923
0.525	0.74	10.930

$$\text{RMS deviation} = \sqrt{\frac{\Sigma\delta^2}{m-1}}, \quad m = 9$$

TABLE XII

RMS deviations for v_M

$c_{11} = 3.74 \times 10^{11}$ dyne/cm^2, $2c_{44} + c_{12} = 1.79 \times 10^{11}$ dyne/cm^2

Elastic constant		RMS deviations (meters/second)
c_{44}	c_{12}	$c_{11} = 3.74$
0.555	0.68	47.8
0.545	0.70	43.9
0.535	0.72	42.2
0.525	0.74	43.0

$$\text{RMS deviation} = \sqrt{\frac{\Sigma\delta^2}{m-1}}, \quad m = 4$$

is by no means very sharp. Assuming that the actual minimum is within an area where the root mean square deviation is between the minimum given by the computer and a value 20% higher we find a maximum uncertainty in c_{44} of $\pm$ 0.02 x 10^{11} dyne/cm^2 and a maximum uncertainty in c_{12} of $\pm$ 0.04 x 10^{11} dyne/cm^2. Of course, these errors are better defined by the fact that 2 c_{44} + c_{12} = 1.79 x 10^{11} dyne/cm^2 and hence if c_{12} is too large by amount d, then c_{44} must be too small by d/2. Again, the root mean square deviations are given along the c_{11}, c_{44}, and c_{12} axes for the "best fit" point, so that one can get an idea of the sharpness of the minimum. This data is presented in Table XIII.

Again it was determined by a semi-quantitative study of the sharpness of the minimum and of Figs. 2.3 and 2.4 what the possible uncertainties in the determination of the three elastic constants are. The results are

$$c_{11} = (3.74 \pm 0.01) \times 10^{11} \text{ dyne/cm}^2$$
$$c_{44} = (0.535 \pm 0.020) \times 10^{11} \text{ dyne/cm}^2$$
$$c_{12} = (0.72 \pm 0.04) \times 10^{11} \text{ dyne/cm}^2$$
$$2\,c_{44} + c_{12} = (1.79 \pm 0.02) \times 10^{11} \text{ dyne/cm}^2$$

Using Eq. (2.8) with these elastic constants one obtains the velocities of sound given in Table XIV. In Figs. 4.8 and 4.9

TABLE XIII

RMS deviations for v_L

Sharpness of minimum along c_{11}, c_{44}, and c_{12} axes

c_{12} = 0.72 c_{44} = 0.535		c_{11} = 3.74 c_{12} = 0.72		c_{11} = 3.74 c_{44} = 0.535	
c_{11}	RMS (m/sec)	c_{44}	RMS (m/sec)	c_{12}	RMS (m/sec)
3.71	15.2	0.520	13.3	0.62	28.1
3.72	13.0	0.525	11.9	0.64	23.3
3.73	11.5	0.530	11.1	0.66	18.8
3.74	10.9	0.535	10.9	0.68	14.8
3.75	11.5	0.540	11.4	0.70	11.8
3.76	13.0	0.545	12.5	0.72	10.9
3.77	15.2	0.550	14.1	0.74	12.4
3.78	17.9	0.555	15.9	0.76	15.8
3.79	20.8	0.560	18.0	0.78	20.0

TABLE XIV

Sound velocities in RbCl

$\rho = 2.7986$ gm/cm^3, $c_{11} = 3.74$, $c_{44} = 0.535$, $c_{12} = 0.72$

(c_{11}, c_{44}, and c_{12} in units of 10^{11} dyne/cm^2)

Angle (degrees)	Experimental velocities (meters/sec)		Theoretical velocities (meters/sec)		
	v_L	v_M	v_L	v_M	v_T
0	3646 ± 21		3656	1383	1383
7.5			3633	1420	1404
15			3566	1524	1464
25	3426 ± 18	1752 ± 31	3416	1726	1592
30	3331 ± 21	1863 ± 49	3321	1837	1668
35	3216 ± 21	1939 ± 28	3218	1942	1749
40	3099 ± 22	2025 ± 47	3117	2031	1831
45	3030 ± 20	2025 ± 53	3029	2088	1912
50			2970	2099	1989
55	2940 ± 16		2953	2054	2061
65			3006	1837	2185
70	3058 ± 16		3048	1705	2233
75			3087	1580	2272
80			3117	1476	2300
90	3153 ± 18		3143	1383	2323

The root mean square deviation between the experimental points and the theoretical curve for the longitudinal branch is 11 meters per second.

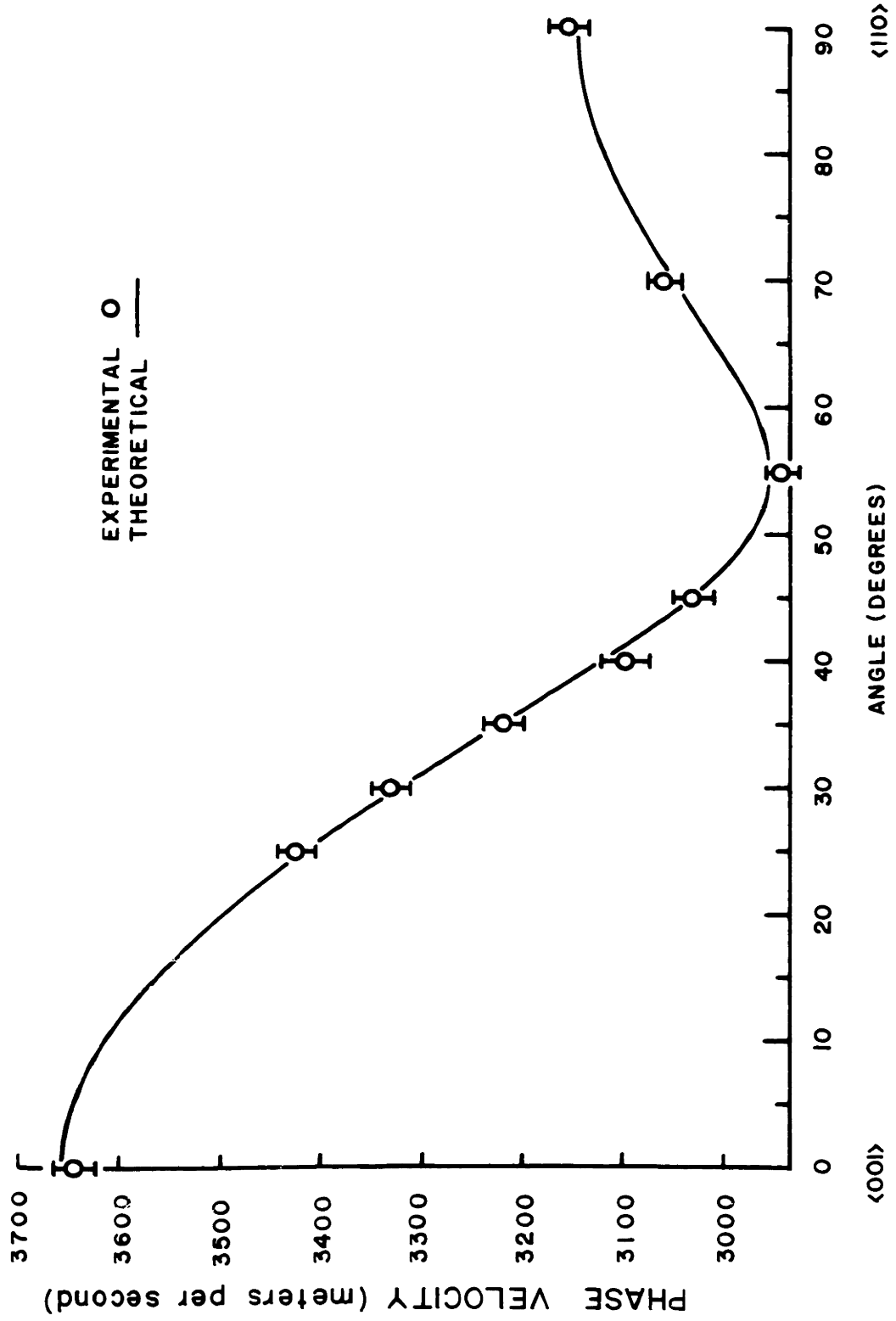

FIG. 4.8 DEPENDENCE OF V_L ON PROPAGATION DIRECTION IN RbCl

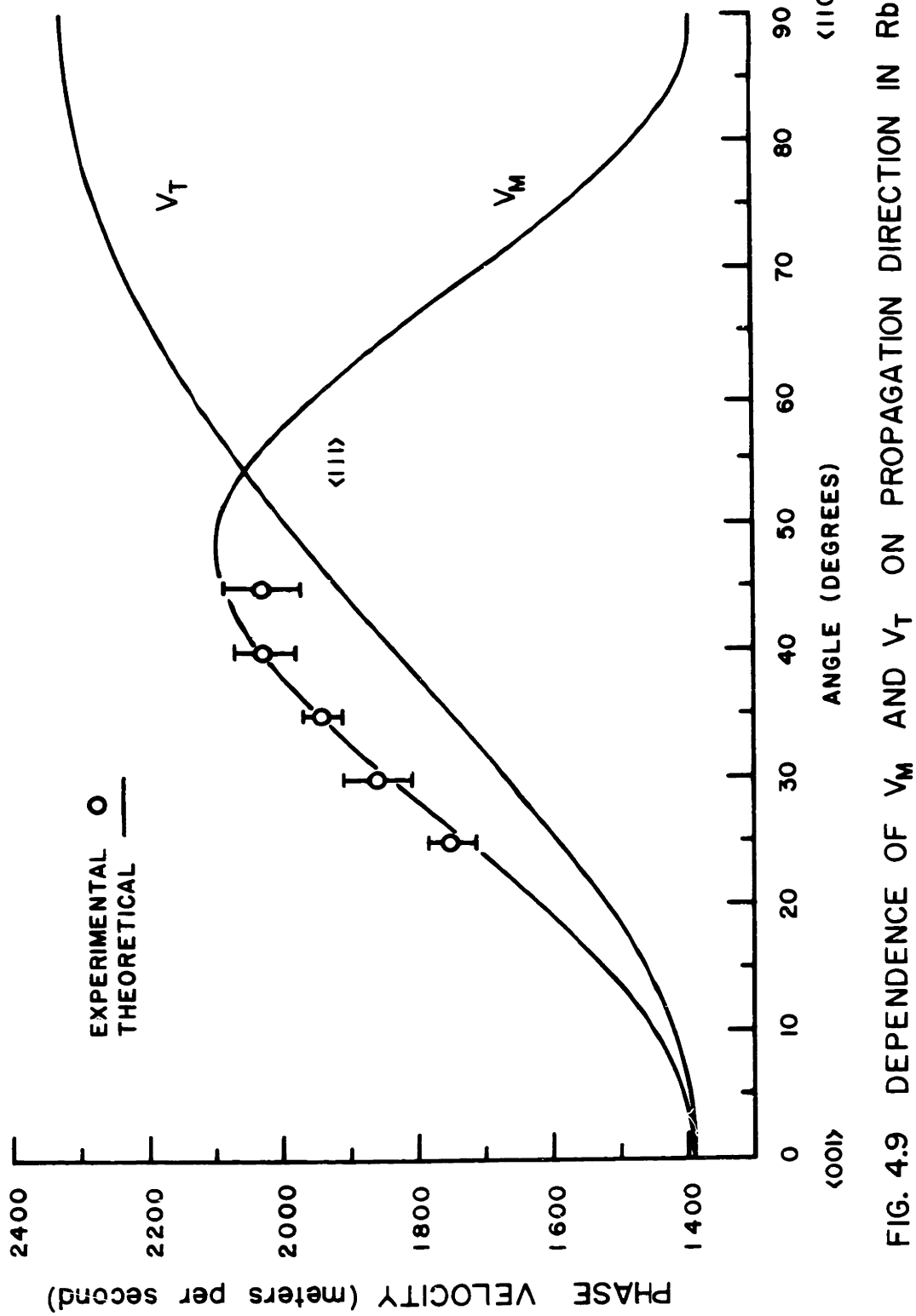

FIG. 4.9 DEPENDENCE OF V_M AND V_T ON PROPAGATION DIRECTION IN RbCl

I have plotted the values for v_L, v_M, and v_T as a function of γ for these values of the elastic constants along with the corresponding experimental velocities. The fit between the experimental points and the theoretical curve is again quite good for the longitudinal mode. The root mean square deviation is 11 meters per second, about half as big as the uncertainty in the individual experimental points. The fit of the experimental points for the mixed branch is not so good. The root mean square deviation for all five experimental points on the mixed root is approximately 37 meters per second, about the size of the individual uncertainties.

For comparison with elastic constants determined previously the ultrasonic values have been listed along with the present results in Table XV. It is seen that with respect to the size of the uncertainties the agreement is not too good. The hypersonic values are too high by about 2.8%, 12%, and 18% for c_{11}, c_{44}, and c_{12}, respectively. The sample of RbCl was compared with a sample obtained from the National Bureau of Standards by x ray diffraction techniques. Unfortunately, the National Bureau of Standards sample was not quite pure with the main impurity being 0.1% to 1.0% potassium. Hence, there are two possible explanations for the large discrepancies between the ultrasonic and the hypersonic elastic constants. Either the sample is very impure. Or there is a significant amount of dispersion present in RbCl. By repeating the ex-

TABLE XV

Elastic constants for RbCl

Frequency	Temperature	c_{11}	c_{44}	c_{12}	$2c_{44} + c_{12}$	Compressibility	Reference	(Year)
	22°C	3.634 ±.007	0.465 ±.005	0.615 ±.012	1.54 ±.02	6.17	a	(1960)
9 Mc	22°C	3.645 ±.013	0.475 ±.002	0.61 ±.03	1.56 ±.03	6.16	b	(1957)
6 kMc - 12 kMc	22.6°C	3.74 ±.01	0.535 ±.02	0.72 ±.04	1.79 ±.02	5.79	this thesis	

$$\text{Compressibility} = \frac{3}{(c_{11} + 2c_{12})}$$

[All elastic constants in units of 10^{11} dyne/cm^2; compressibility in units of 10^{-12} cm^2/dyne]

a S. Haussühl, Zeits. für Physik, 159, 223 (1960)

b K. Spangenberg and S. Haussühl, Zeits. für Kristallographie, 109, 422 (1957)

periment at a different scattering angle one would be able to determine whether there is dispersion, i.e. whether the group velocity is different from the phase velocity.

4.4 Potassium iodide (KI)

A single crystal of potassium iodide, 5/8" x 5/8" x 5/8", supplied by the Harshaw Chemical Company, with window glass polish, was used. The sample originally had completely transparent faces when it was delivered but after some handling the faces became somewhat cloudy. In this respect, KI was the trickiest crystal of the three used in the experiment described here. As expected, potassium iodide was the strongest scatterer of the three crystals. Unfortunately, the sample contained a large number of inclusions giving rise to an extremely strong central line. KI seems to be especially hard to grow in large single crystals without inclusions. It turned out that this particular crystal had one very bad [111] plane cutting across a corner of the cube which contained an impressive number of bubble-like inclusions. This plane was avoided whenever possible but in some directions of propagation the scattering beam had to pass through this plane. Since the central line was so strong and as the splittings in KI are small, it was not possible to resolve the mixed mode on both sides of the central line because the grating satellite overlapped the low wavelength Brillouin component.

So that good measurements of the location of the mixed mode could be obtained, the incident laser line profile as modified by the grating was subtracted out. This procedure was illustrated in Fig. 3.4 for KI. Since the intensity of the unshifted component varied substantially from trace to trace, the laser line had to be fitted to the trace by bringing the base lines in coincidence and by adjusting the intensity axis until there was a good fit between the two curves at all points where the Brillouin spectrum contributed little to the line shape, i.e. between the location of the mixed modes and the center of the spectrum. This procedure worked remarkably well. However, errors could conceivably occur. It was found, that due to the large number of traces analyzed, systematic errors in the location of the mixed modes were minimal. It should be understood that this subtraction procedure was very important, even for the longitudinal mode, since the subtraction procedure shifted these modes slightly away from the center. In Fig. 4.10 four more traces of KI at various propagation directions are shown. One can see how the character of the central line changes with γ and how the mixed modes can be seen at $\gamma = \cos 30°$.

One should note that the central line in the <001> direction is maybe five times stronger than in the other directions shown. This is caused by the fact that for observation in this direction the crystal had to be held in a

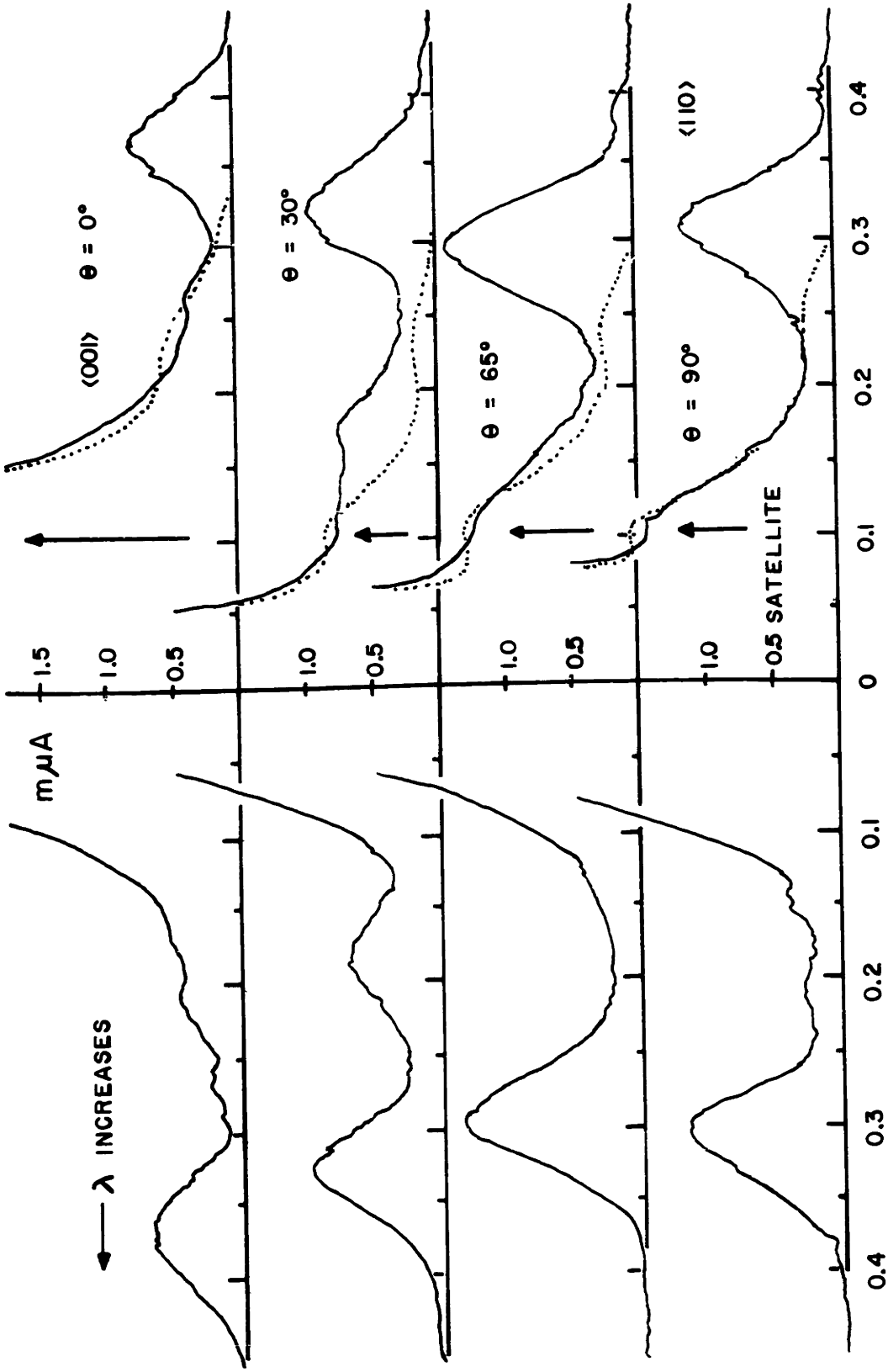

FIG. 4.10 BRILLOUIN SPECTRA OF KI

position where one of its surfaces made a 45 degree angle with both the incident beam and the direction of observation. Therefore, even if the index of refraction was perfectly matched, if the crystal surfaces were clouded over somewhat, some portion of the incident light was reflected directly into the spectrograph. Since the incident beam is very strong compared to the scattered light, not much light had to be reflected to give rise to an extremely strong central line.

The position of the grating satellite is also indicated in Fig. 4.10. One can see how the grating line profile (dotted curve) has to be adjusted in the intensity "direction" to fit the observed line profile. On the actual traces, the amplification was changed near the center of the spectrum so that the position of the maximum of the central line could be recorded. It was found in all cases after corrections for the amount of integration that the Stokes and Anti-Stokes components were shifted equally to either side of the central line within experimental accuracy.

It is also seen that the signal to noise ratio is better for the traces at 65 degrees and at 90 degrees than those at 0 degrees and 30 degrees. This is just a reflection of the $1/v^2$ factor in the intensity formula, Eq. (4.1). All peaks have a width at one half maximum height (half width) of between 0.34 and 0.37 mm compared to a slit size of 0.25 mm. The problems of line width will be discussed in 4.6.

The procedure used in evaluating the traces is the same as that used for KCl and RbCl. 170 traces (at 10 minutes each!) were recorded for eleven directions of propagation in the {110} planes. Integration times for the most part were nine seconds. In Table XVI the phonon frequency ν_σ and the hypersonic phase velocity v_s of the sound waves are given as a function of the propagation direction in the {110} planes.

The velocities presented in Table XVI were analyzed by means of the IBM 709 computer and the root mean square deviation between the experimental velocities and the calculated velocities was found for these elastic constants:

c_{11} = 2.710, 2.715, 2.720, 2.725, <u>2.730</u>, 2.735, 2.740, 2.745, 2.750

c_{44} = 0.350, 0.355, 0.360, 0.365, 0.370, 0.375, 0.380, 0.385, 0.390

c_{12} = 0.38, 0.39, 0.40, 0.41, 0.42, 0.43, 0.44, 0.45, 0.46

(all c's in units of 10^{11} dyne/cm^2)

For the longitudinal branch the minimum root mean square deviation was found to occur at $c_{11} = 2.73 \times 10^{11}$ dyne/cm^2. In Table XVII the values of the root mean square deviation in the bottom of the valley defined by $2\,c_{44} + c_{12} = 1.15 \times 10^{11}$ dyne/cm^2 are listed. In Table XVIII the root mean square deviations are tabulated for v_M with the constraints $c_{11} = 2.73 \times 10^{11}$ dyne/cm^2 and $2\,c_{44} + c_{12} = 1.15 \times 10^{11}$ dyne/cm^2 imposed. It is seen that the minimum in the mixed mode is not very sharp.

TABLE XVI

ν_σ and v_s for KI

Density at 22.4°C = 3.1245 gm/cm^3

Index of refraction at 6328 Å and 22.4°C = 1.6607

Wavelength of phonons = 2694.5 Å

Angle (degrees)	Temperature (°C)	Phonon frequency ν_σ (kMc) (90° scattering)	Error (%)	Hypersonic phase velocity v_s (meters/sec)	Mode
0	22.6	11.051 ± 0.061	0.55	2978 ± 16	L
15	22.6	10.738 ± 0.065	0.60	2893 ± 17	L
25	22.5	10.156 ± 0.069	0.68	2736 ± 19	L
		5.242 ± 0.091	1.7	1412 ± 24	M
30	22.3	9.814 ± 0.064	0.66	2644 ± 17	L
		5.568 ± 0.067	1.2	1500 ± 18	M
35	22.3	9.493 ± 0.058	0.61	2558 ± 16	L
		5.810 ± 0.063	1.1	1565 ± 17	M
40	22.4	9.128 ± 0.043	0.48	2460 ± 12	L
		6.066 ± 0.078	1.3	1635 ± 21	M
45	22.5	8.899 ± 0.047	0.53	2398 ± 13	L
		6.334 ± 0.123	1.9	1707 ± 33	M
55	22.4	8.640 ± 0.045	0.52	2328 ± 12	L
65	22.2	8.828 ± 0.042	0.48	2379 ± 11	L
75	22.4	9.087 ± 0.041	0.45	2448 ± 11	L
90	22.6	9.257 ± 0.042	0.45	2494 ± 11	L

The percentage error is composed of the root mean square deviation of the traces from the average for each angle, of the error in dispersion, and of the error due to alignment difficulties.

TABLE XVII

RMS deviations for v_L

$c_{11} = 2.73 \times 10^{11}$ dyne/cm^2, $2\,c_{44} + c_{12} = 1.15 \times 10^{11}$ dyne/cm^2

Elastic constant		RMS deviations (meters/second)
c_{44}	c_{12}	$c_{11} = 2.73$
0.350	0.45	14.1
0.355	0.44	14.2
0.360	0.43	14.3
0.365	0.42	14.4
0.370	0.41	14.5
0.375	0.40	14.6
0.380	0.39	14.7
0.385	0.38	14.8

$$\text{RMS deviation} = \sqrt{\frac{\Sigma\delta^2}{m-1}}, \quad m = 11$$

TABLE XVIII

RMS deviations for v_M

$c_{11} = 2.73 \times 10^{11}$ dyne/cm^2, $2\,c_{44} + c_{12} = 1.15 \times 10^{11}$ dyne/cm^2

Elastic constant		RMS deviations (meters/second)
c_{44}	c_{12}	$c_{11} = 2.73$
0.350	0.45	33.2
0.355	0.44	29.0
0.360	0.43	25.3
0.365	0.42	22.3
0.370	0.41	20.3
0.375	0.40	19.6
0.380	0.39	20.4
0.385	0.38	22.3

$$\text{RMS deviation} = \sqrt{\frac{\Sigma\delta^2}{m-1}}, \quad m = 5$$

The minimum occurs at $c_{44} = 0.375 \times 10^{11}$ dyne/cm^2 and $c_{12} = 0.40 \times 10^{11}$ dyne/cm^2. If we assume that the actual minimum can occur anyplace where the deviation is between the minimum found by the computer and a value 20% higher, the errors are for $c_{44} \pm 0.015 \times 10^{11}$ dyne/cm^2 and for $c_{12} \pm 0.03 \times 10^{11}$ dyne/cm^2. Here again the possible errors are constrained by $2\,c_{44} + c_{12} = (1.15 \pm 0.02) \times 10^{11}$ dyne/cm^2. The root mean square deviations along the c_{11}, c_{44}, and c_{12} axes for the best fit point are given in Table XIX.

The elastic constants and errors are

$$c_{11} = (2.73 \pm 0.01) \times 10^{11} \text{ dyne/cm}^2$$
$$c_{44} = (0.375 \pm 0.015) \times 10^{11} \text{ dyne/cm}^2$$
$$c_{12} = (0.40 \pm 0.03) \times 10^{11} \text{ dyne/cm}^2$$
$$2\,c_{44} + c_{12} = (1.15 \pm 0.02) \times 10^{11} \text{ dyne/cm}^2$$

Using Eq. (2.8) with these elastic constants one obtains the velocities of sound given in Table XX.

In Figs. 4.11 and 4.12 the values for v_L, v_M, and v_T are plotted as a function of γ for the above values of the elastic constants and the corresponding experimental velocities are shown. The fit between the experimental points and the theoretical curve is seen to be very good for both the longitudinal and the mixed mode. Due to the good quality of the traces and to the small statistical fluctuations, the error bars are quite

TABLE XIX

RMS deviations for v_L

Sharpness of minimum along c_{11}, c_{44}, and c_{12} axes

$c_{12} = 0.40$, $c_{44} = 0.375$		$c_{11} = 2.73$, $c_{12} = 0.40$		$c_{11} = 2.73$, $c_{44} = 0.375$	
c_{11}	RMS (m/sec)	c_{44}	RMS (m/sec)	c_{12}	RMS (m/sec)
2.710	16.9	0.350	21.4	0.38	16.2
2.715	16.0	0.355	19.3	0.39	15.1
2.720	15.2	0.360	17.5	0.40	14.6
2.725	14.8	0.365	16.1	0.41	14.7
2.730	14.6	0.370	15.1	0.42	15.2
2.735	14.7	0.375	14.6	0.43	16.3
2.740	15.1	0.380	14.8	0.44	17.9
2.745	15.7	0.385	15.5	0.45	19.7
2.750	16.5	0.390	16.7	0.46	21.7

TABLE XX

Sound velocities in KI

$\rho = 3.1245$ gm/cm^3, $c_{11} = 2.73$, $c_{44} = 0.375$, $c_{12} = 0.40$

(c_{11}, c_{44}, and c_{12} in units of 10^{11} dyne/cm^2)

Angle (degrees)	Experimental velocities (meters/sec)		Theoretical velocities (meters/sec)		
	v_L	v_M	v_L	v_M	v_T
0	2978 ± 16		2956	1095	1095
7.5			2936	1128	1115
15	2893 ± 17		2879	1216	1170
25	2736 ± 19	1412 ± 24	2749	1389	1285
30	2644 ± 17	1500 ± 18	2665	1484	1354
35	2558 ± 16	1565 ± 17	2572	1577	1425
40	2460 ± 12	1635 ± 21	2478	1658	1498
45	2398 ± 13	1707 ± 33	2394	1716	1570
50			2335	1733	1638
55	2328 ± 12		2316	1696	1702
65	2379 ± 11		2368	1501	1810
70			2407	1382	1853
75	2448 ± 11		2442	1271	1886
80			2469	1178	1911
90	2494 ± 11		2492	1095	1931

The root mean square deviation between the experimental points and the theoretical curve is ± 14.6 meters per second for the longitudinal mode and ± 19.6 meters per second for the mixed mode.

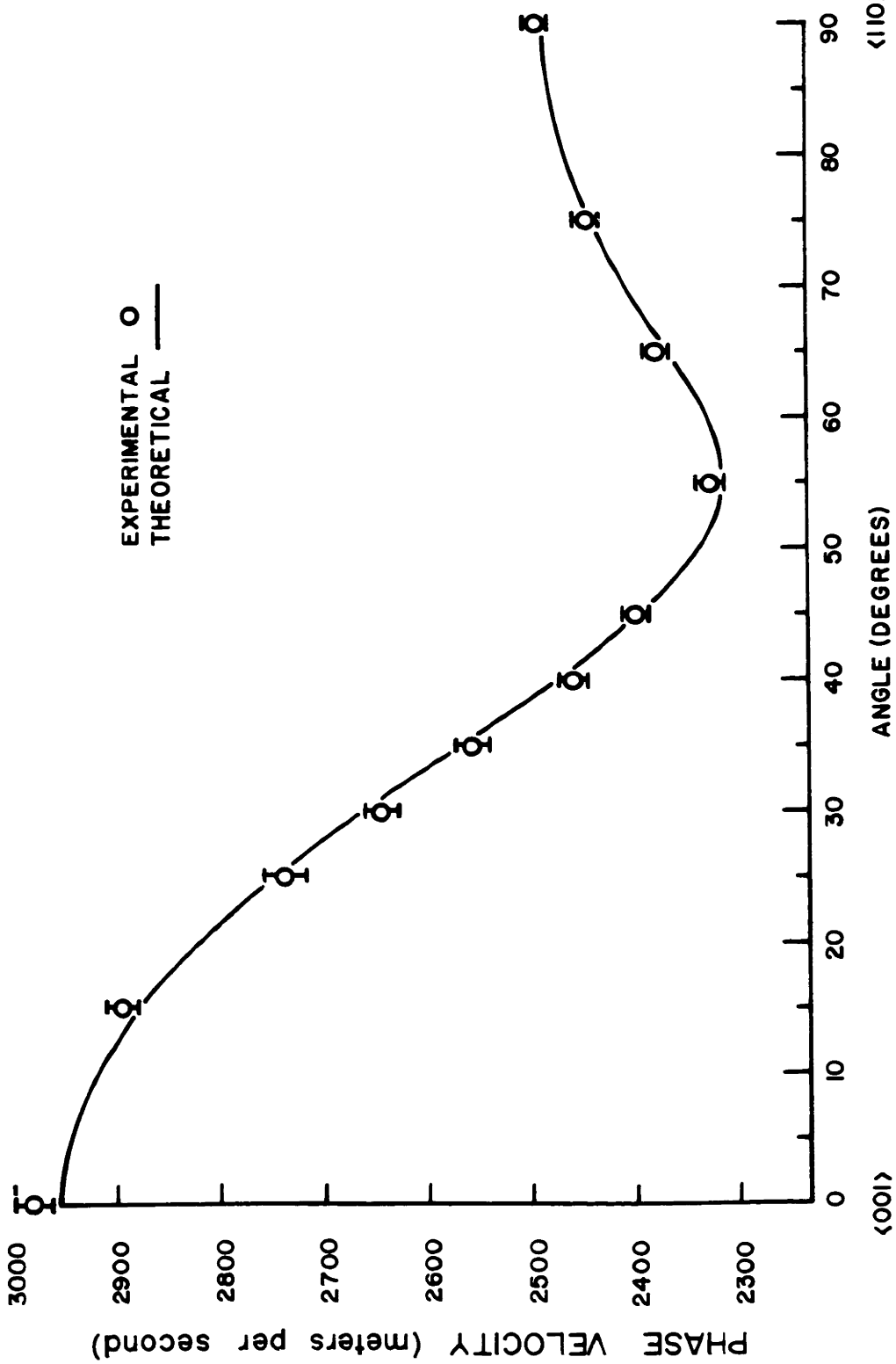

FIG. 4.11 DEPENDENCE OF V_L ON PROPAGATION DIRECTION IN KI

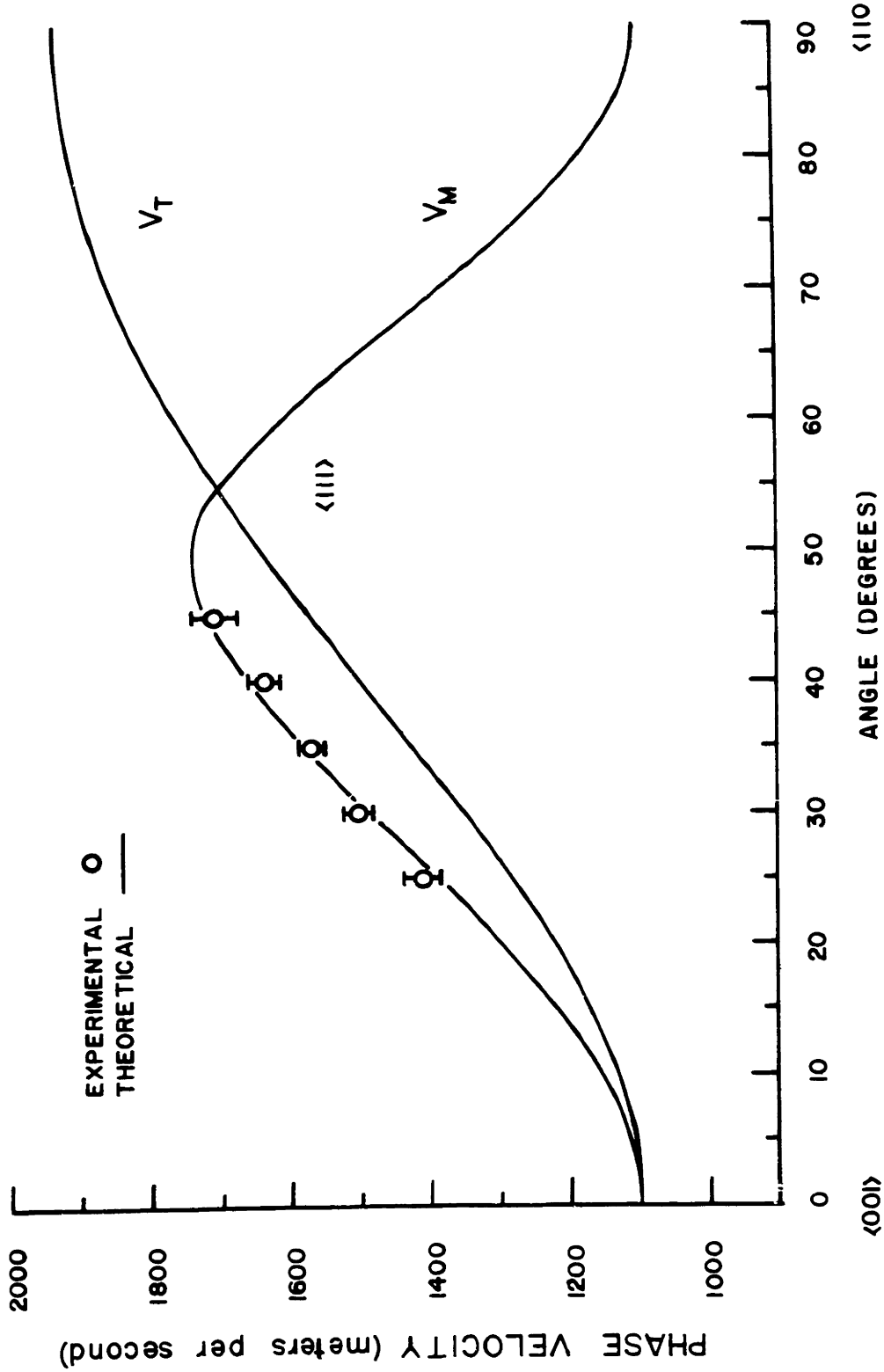

FIG. 4.12 DEPENDENCE OF V_M AND V_T ON PROPAGATION DIRECTION IN KI

small.

Previous results for the elastic constants in KI in the ultrasonic region are given in Table XXI. One sees that the general agreement with results presented in this thesis is quite good and there is no indication of any significant amount of dispersion.

4.5 Intensities

Since the symmetry of the experimental setup varied slightly from crystal to crystal and since the amount of scattered light received by the spectrograph was dependent on the orientation of the crystal, one can make only semi-quantitative observations concerning the relative intensities of the Brillouin components at various angles for the three crystals. It is somewhat easier, on the other hand, to get an idea of the relative intensity of the mixed and longitudinal modes by measuring the ratio in all the traces showing mixed modes. Of course, the ratios of the intensities were measured on the traces after the incident line profile had been subtracted.

For all three crystals the intensity was uniformly high between 50 and 90 degrees and fell off considerably from 50 to 0 degrees for the longitudinal mode. One has to remember that as the crystal is rotated the scattered light is observed through different parts of the surface of the crystal and if

TABLE XXI

Elastic constants for KI

Frequency	Temperature	c_{11}	c_{44}	c_{12}	$2c_{44} + c_{12}$	Compressibility	Reference	(Year)
	22°C	2.76 ±.006	0.37 ±.004	0.45 ±.009	1.19 ±.02	8.20	a	(1960)
9 Mc	22°C	2.775 ±.01	0.38 ±.002	0.47 ±.024	1.23 ±.03	8.07	b	(1957)
	22.4°C	2.72 ±.03	0.364 ±.004	0.45 ±.04	1.18 ±.05	8.33	c	(1958)
5 kMc - 11 kMc	22.4°C	2.73 ±.01	0.375 ±.015	0.40 ±.03	1.15 ±.02	8.50	this thesis	

$$\text{Compressibility} = \frac{3}{(c_{11} + 2\,c_{12})}$$

[All elastic constants in units of 10^{11} dyne/cm^2; compressibility in units of 10^{-12} cm^2/dyne]

a S. Haussühl, Zeits. für Physik, 159, 223 (1960)

b K. Spangenberg and S. Haussühl, Zeits. für Kristallographie, 109, 422 (1957)

c M. H. Norwood and C. V. Briscoe, Phys. Rev. 112, 45 (1958)

the crystal has clouded areas the intensity seen is dependent on the cloudiness of a particular area on the surface. Hence, one can only say that there seems to be a general behavior of the intensity following Eq. (4.1) in that the intensity drops off at high velocities.

It was pointed out before that the average intensities for the three crystals (averaged over all angles) are in the ratio 2 1/4 : 1 1/4 : 1 for KI : RbCl : KCl, respectively. Since the intensity is dependent upon the propagation direction, it is more useful to compare the relative intensities in a few specific directions of propagation. The intensity, Eq. (4.1), can be rewritten as

$$I \propto \left(\frac{\partial \ln \varepsilon}{\partial \ln \rho}\right)^2 \frac{n^4}{\rho v^2} \, kT \qquad (4.4)$$

If we assume $\left(\frac{\partial \ln \varepsilon}{\partial \ln \rho}\right) \sim 1$ for the three crystals, the ratio of the intensities of the longitudinal modes in KI : RbCl : KCl should be given by the ratios of $n^4/\rho v^2$ for the three crystals. In Table XXII these ratios are presented along with the measured ratios for the three directions of propagation.

TABLE XXII

I(KI) : I(RbCl) : I(KCl)

Direction of propagation	<001>	<111>	<110>
$n^4/\rho v^2$	2.3 : 1.1 : 1.0	2.4 : 1.1 : 1.0	2.4 : 1.1 : 1.0
Measured	2.7 : 1.0 : 1.0	2.0 : 1.3 : 1.0	1.7 : 1.1 : 1.0

where the intensity of KCl has been set equal to 1.0 in the three cases. On the same intensity scale, I[CsI] = 2.9 (<110>), I[Water] = 9.7, $I[C(Cl)_4]$ = 13, and I[Toluene] = 32.

Of considerable interest is the behavior of the ratio of the intensities of the longitudinal mode to the mixed mode as a function of γ. This information, unfortunately, is not very complete, since data could be obtained only between 25 degrees and 45 degrees. The ratios are presented here for KI and RbCl as a function of γ in Table XXIII.

It can be shown that the intensity of the Brillouin-scattered light is proportional to $(\underset{\sim}{k}_\sigma \cdot \underset{\sim}{A}_j)^2$ where $\underset{\sim}{k}_\sigma$ is the propagation vector of the elastic wave and $\underset{\sim}{A}_j$ is the polarization vector of the mode j (j = L, T, M). This is exactly the same factor that appears in the theory of diffraction of x rays[17]. In other words, as we said before, only the longitudinal component of the phonon polarization contributes to the scattering. Hence, the complete intensity formula should be of the form

TABLE XXIII

Experimental ratio I_M/I_L as a function of γ

RbCl	Angle $\theta = \cos^{-1}\gamma$ (degrees)	Experimental I_M/I_L
	25	0.64 ± 0.06
	30	0.61 ± 0.08
	35	0.50 ± 0.06
	40	0.34 ± 0.10
	45	0.24 ± 0.04

KI	Angle $\theta = \cos^{-1}\gamma$ (degrees)	Experimental I_M/I_L
	25	0.49 ± 0.06
	30	0.48 ± 0.03
	35	0.46 ± 0.05
	40	0.34 ± 0.04
	45	0.28 ± 0.02

$$I \propto \varepsilon^2 \left(\frac{\partial \ln \varepsilon}{\partial \ln \rho}\right)^2 kT \beta_s (\%L)_j^2 \qquad (4.5)$$

where $(\%L)_j$ is the percentage longitudinal admixture in mode j. These admixtures are found by use of Eqs. (2.11) and (2.12). The values for RbCl and KI are presented in Table XXIV.

It should be noted that the longitudinal admixture in the mixed mode is smaller for RbCl than for KI. In KCl it has about the same magnitude as in RbCl. This low relative intensity together with a strong central line made it so difficult in KCl to observe the mixed modes. Only the point at 35 degrees was recorded. This is the angle at which the longitudinal admixture in the mixed mode is a maximum.

Using Eq. (4.5) we expect the ratio of the intensities of the mixed mode to the longitudinal mode at a given γ to be given by

$$I_M/I_L = v_L^2/v_M^2 \quad (\%L)_M^2/(\%L)_L^2 \qquad (4.6)$$

if we again assume that $\left(\frac{\partial \ln \varepsilon}{\partial \ln \rho}\right) \sim 1$. The relevant numbers are given in Table XXV. It is seen that I_M/I_L is indeed proportional to $v_L^2/v_M^2 \quad (\%L)_M^2/(\%L)_L^2$ but the constant of proportionality is A = 2.65 for RbCl and A = 1.65 for KI, where A is defined by

$$\left(\frac{I_M}{I_L}\right)_{expt.} = A \left(\frac{v_L}{v_M} \frac{\%L_M}{\%L_L}\right)^2.$$

TABLE XXIV

Longitudinal admixtures

RbCl	Angle θ (degrees)	$\%L_L$	$\%L_M$	$\%L_M/\%L_L$	$(\%L_M/\%L_L)^2$
	25	97.3	23.1	0.237	0.0562
	30	96.7	25.5	0.264	0.0697
	35	96.5	26.0	0.269	0.0724
	40	97.1	24.0	0.247	0.0610
	45	98.3	18.4	0.187	0.0350
KI	Angle θ (degrees)	$\%L_L$	$\%L_M$	$\%L_M/\%L_L$	$(\%L_M/\%L_L)^2$
	25	96.2	26.2	0.272	0.0740
	30	95.4	29.3	0.307	0.0942
	35	94.9	31.3	0.330	0.109
	40	95.4	29.3	0.307	0.0942
	45	97.2	23.5	0.242	0.0586

TABLE XXV

Calculated ratio I_M/I_L as a function of γ

Angle $\theta = \cos^{-1}\gamma$ (degrees)	$(\%L_M/\%L_L)^2$	$(v_L/v_M)^2$	A	$A(\%L_M/\%L_L)^2 x (v_L/v_M)^2$	$(I_M/I_L)_{exp.}$
RbCl					
25	0.0562	3.92	2.65	0.58	0.64 ± 0.06
30	0.0697	3.27	2.65	0.60	0.61 ± 0.08
35	0.0724	2.74	2.65	0.52	0.50 ± 0.06
40	0.0610	2.36	2.65	0.38	0.34 ± 0.10
45	0.0350	2.10	2.65	0.19	0.24 ± 0.04
KI					
25	0.0740	3.92	1.65	0.48	0.49 ± 0.06
30	0.0942	3.22	1.65	0.50	0.48 ± 0.03
35	0.109	2.66	1.65	0.48	0.46 ± 0.05
40	0.0942	2.23	1.65	0.35	0.34 ± 0.04
45	0.0586	1.95	1.65	0.19	0.28 ± 0.02

Both the experimental I_M/I_L and the computed values of I_M/I_L for RbCl and KI are plotted in Figs. 4.13 and 4.14. It is seen that there is good agreement between experiment and theory except for the point at 45 degrees. The fact that the constant of proportionality A is not 1 seems to indicate that there is attenuation of the sound waves.

4.6 Line widths

The line widths were largely independent of angle and averaged to

$$W_{half} = (0.35 \pm 0.02) \text{ mm for KI}$$

$$W_{half} = (0.36 \pm 0.03) \text{ mm for KCl}$$

$$W_{half} = (0.38 \pm 0.04) \text{ mm for RbCl}$$

Clearly, the same factors seem to be determining the half width in the three crystals. We have mentioned before that the half width of the line is a function of a number of factors. More explicitly, the observed half width is the half width of a complex profile formed from the convolution of five separate functions. They are expressions representing

a) the entrance slit

b) the exit slit

c) the diffracted line profile of the grating

d) the line width of the source

e) and the errors of the spectrometer mirrors.

In this experiment the entrance slit and the exit slit both had a 0.25 mm width. The natural line width of the source was 1 kMc.

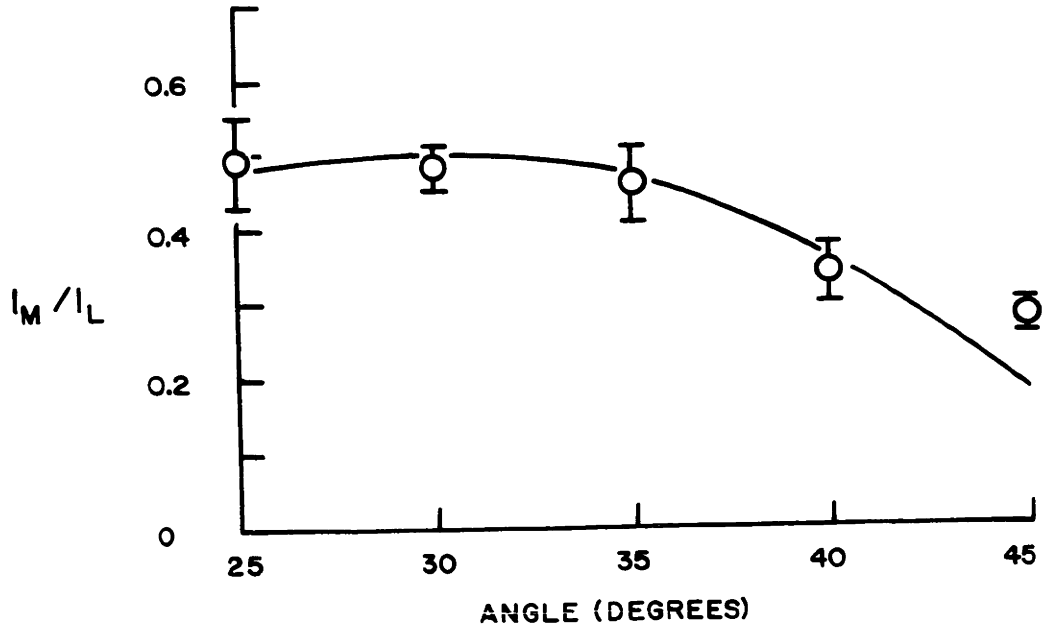

FIG. 4.13 I_M / I_L FOR RbCl

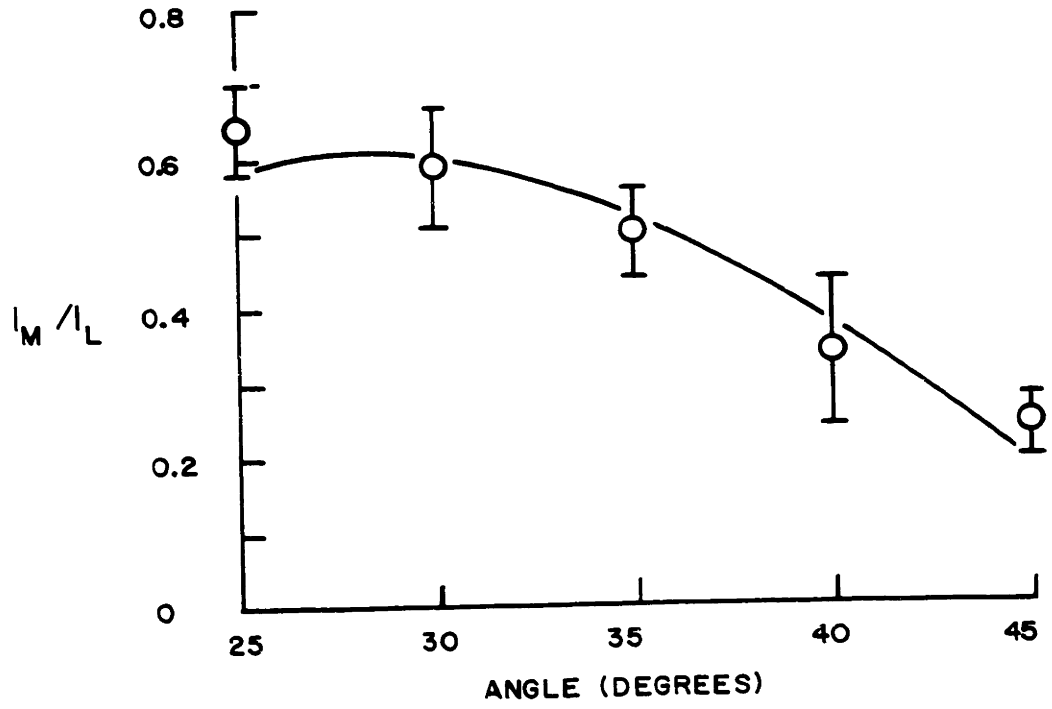

FIG. 4.14 I_M / I_L FOR KI

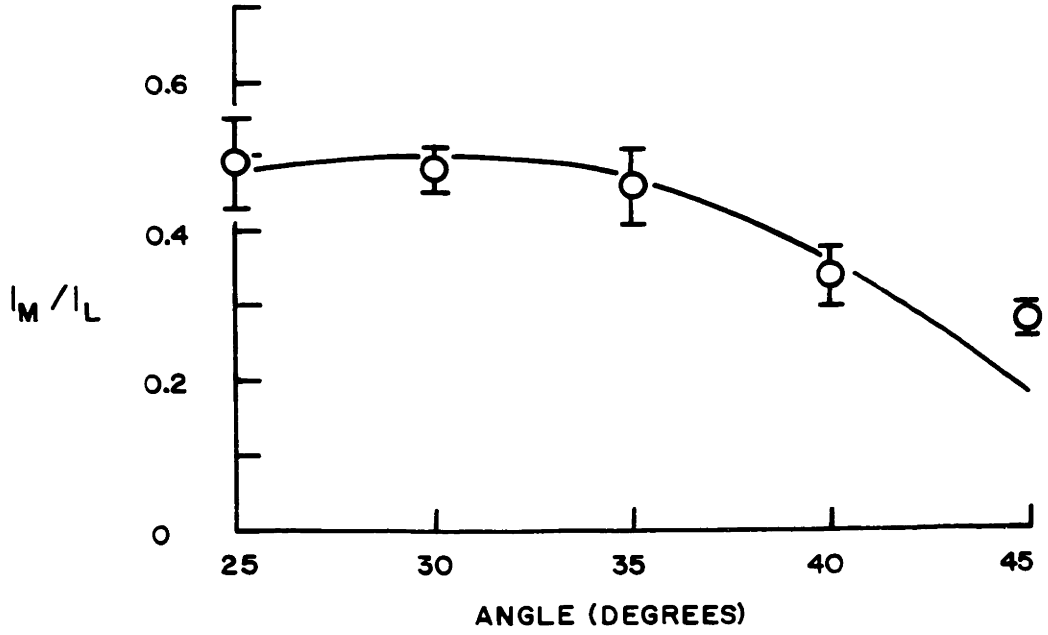

FIG. 4.13 I_M / I_L FOR RbCl

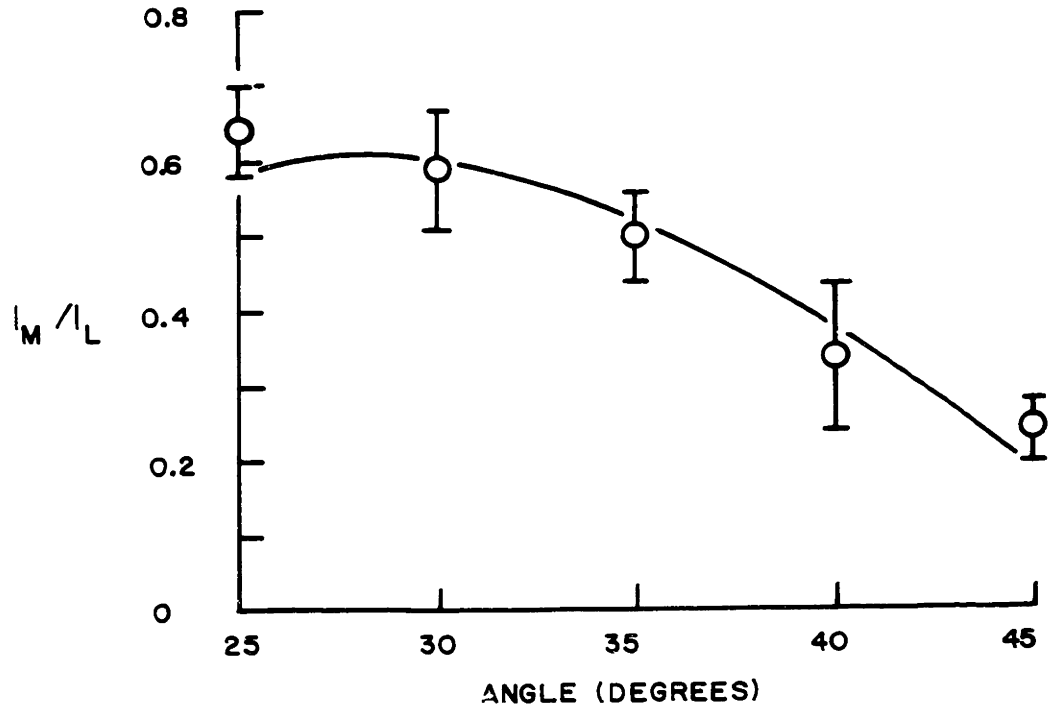

FIG. 4.14 I_M / I_L FOR KI

However due to the fact that a large solid angle of light was admitted into the spectrograph the natural line width of the laser was effectively broadened. This broadening is roughly 780 Mc for KCl, 580 Mc for KI, and 640 Mc for RbCl. the variation in broadening with propagation direction due to the large acceptance angle is only about 20% between 0 degrees and 55 degrees. Hence we would not expect to see this. It is not obvious how this broadening will affect the line width of the scattering. Let us assume that the square of the final source line width is equal to the sum of the squares of the laser line width and of the broadening. This gives a broadened line width of 1.2 kMc. We will treat the diffracted line profile and the errors of the spectrograph together as instrumental line width. This is 600 Mc corresponding to the resolving limit of the grating spectrograph in tenth order at 6328 Å.

It has been shown by Jaquinot[18] that under normal conditions it is a good approximation to assume that the total observed half width can be evaluated as the square root of the sum of the squares of the constituent half widths:

$$(W_{total})^2 = (W_{slit\ 1})^2 + (W_{slit\ 2})^2 + (W_{instrum.})^2 + (W_{source})^2$$

$$W_{slit\ 1} = W_{slit\ 2} = 0.25 \text{ mm} \simeq 1.5 \text{ kMc}$$

$$W_{instrumental} = 0.098 \text{ mm} = 600 \text{ Mc}$$

$$W_{source} = 0.20 \text{ mm} = 1.2 \text{ kMc}$$

and hence $W_{total} \approx 0.42$ mm = 2.6 kMc, in good agreement with the measured half widths.

Chapter V

PROPOSED FURTHER WORK

5.1 Limitations of the present work

This thesis was limited to the discussion of a particular application of Brillouin scattering using a new technique with possibilities which are becoming more obvious every day. Inasmuch as the treatment given here was limited to a small problem and as the techniques are still in their infancy, there are two obvious ways of continuing from here. One way of going on would be to use the present equipment with minor modifications to investigate the dispersion curve in the hypersonic region by changing the scattering angle and to continue work in other crystals with possibly a different choice of crystal planes. The other way of continuing would consist of either a major modification of the equipment to make it possible to see line widths for an investigation of acoustic phonon lifetimes or of a switch to different equipment such as a Fabry-Perot interferometer with its inherently higher resolving power.

If a spectrograph is to be used for future work in this area it should be kept in mind that in this experiment intensities were marginal dictating the rather wide slit sizes. In other words,

equipment with higher efficiency and better resolution is desirable.

Since either a modification of the present equipment or a switch to a Fabry-Perot interferometer will simplify future experiments, the steps necessary for such modifications will be described next.

5.2 Improvements in the apparatus and technique

5.2.1 Alignment

It was found that alignment is extremely critical. Hence, it is suggested that before any further work is undertaken,

a) the spectrograph should be realigned so that the theoretical resolving power is utilized even in lower orders and so that light is not lost inside the spectrograph due to bad alignment.

b) a practical system be devised for aligning the scatterer and for positioning the various lenses used in sending the scattered light into the spectrograph.

5.2.2 Improvement in the resolving power and the luminosity of the spectrograph

The resolving power of the spectrograph can be increased by a factor of two by using two gratings in series or by using a double pass arrangement. This method has been discussed by Jenkins and Alvarez[19] for an n-pass arrangement (n = 1,...,7). If two gratings are used and if both are blazed at 64 degrees, this has the added advantage of making it possible to use both

gratings at 64 degrees thus raising the luminosity considerably, since the efficiency of the grating is highest near the blaze angle.

Another possibility would be to have a grating blazed at 72 degrees so that it could be used there in tenth order most efficiently. This was suggested by G. W. Stroke[20].

The M.I.T. spectrograph has especially large light losses because of its long focal length. This large (12 meters) projection distance is required if one wants to take photographic plates due to the limitations imposed by grain size. However, with photoelectric equipment projection distances may be shortened with a resultant gain in luminosity. This is brought about, since the luminosity decreases with the square of the projection distance and the slit size increases linearly with projection distance as the distance is increased.

Unfortunately, alignment problems become more acute as the slit sizes become smaller when one wants better resolving power. By using two gratings in series one could obtain an instrumental resolution of about 300 Mc at 6328 Å. This may be good enough for observing phonon lifetimes.

Another problem encountered was that of grating satellites. Recent advances in the quality of gratings[21] make one believe that gratings will be available soon that are superior in many respects to the grating which has been used in this experiment.

5.2.3 Screw drive

The drive was found to be rather deficient in accuracy and reproducibility. It is my feeling that with a better driving screw the statistical errors between the traces could be reduced considerably thus necessitating fewer traces and cutting the errors in the frequencies and in the velocities to maybe 0.1%.

It should be pointed out here that the phototube was found sufficient in every respect. Cooling might improve the signal to noise ratio, a help in getting good traces.

5.2.4 Fabry-Perot interferometer

In most respects the Fabry-Perot interferometer is suited to this work ideally. Since one is working with one particular wavelength of light one does not need to employ a premonochromator. The free spectral range can present problems but the resolving power available does sound attractive (possibility of resolving 150 Mc with not too much difficulty). Furthermore, the efficiency of the Fabry-Perot is very high. Alignment, however, may present even more problems than the alignment of the spectrograph did.

5.3 Behavior of the dispersion curve

It is certainly a simple extension of the work presented here to plot out the dispersion curve in the hypersonic region and to find $d\nu/dk$, the group velocity. One must ask whether this would be very fruitful inasmuch as there is little indication of any significant amount of dispersion in this region. Inasmuch as RbCl shows large discrepancies between the ultrasonic and

hypersonic elastic constants, this is recommended as a first candidate.

It might also be useful to work out the roots of the velocity determinant for all directions in cubic crystals to find out whether there are any more useful planes than the {110} planes as far as determination of the elastic constants is concerned.

5.4 Conclusion

It is hoped that this treatment has lined out the possibilities of this new method in a rapidly expanding field. As more powerful lasers become available (at lower wavelengths), more and more experiments will become feasible.

With some refinement in technique this could be a powerful method of determining elastic constants and their temperature dependence in the hypersonic region.

APPENDIX

Solution of the velocity determinant in the {110} planes

The velocity determinant, Eq. (2.6), can be written

$$\begin{vmatrix} A - E & C & D \\ C & A - E & D \\ D & D & B - E \end{vmatrix} = 0 \qquad (A.1)$$

where $A = 1/2\ [c_{11} + c_{44} + \gamma^2(c_{44} - c_{11})]$

$$B = c_{44} + \gamma^2(c_{11} - c_{44})$$

$$C = 1/2\ (1 - \gamma^2)\ (c_{12} + c_{44}) \qquad (A.2)$$

$$D = \gamma \sqrt{1/2\ (1 - \gamma^2)}\ \ (c_{12} + c_{44})$$

$$E = \rho v^2$$

By rearranging rows and columns we obtain:

$$\begin{vmatrix} 2(A - C - E) & -(A - C - E) & 0 \\ -(A - C - E) & A - E & D \\ 0 & D & B - E \end{vmatrix} = 0 \qquad (A.3)$$

$$(A - C - E)[(B - E)(A + C - E) - 2\,D^2] = 0$$

The three roots of this polynomial are:

$$E_T = A - C \tag{A.4}$$

and

$$E_{\substack{L(+)\\M(-)}} = 1/2\,[A + B + C \pm \sqrt{(A + B + C)^2 - 4(AB + BC - 2\,D^2)}] \tag{A.5}$$

But

$$A + B + C = 1/2\,[4\,c_{44} + c_{11} + c_{12} + \gamma^2(c_{11} - 2\,c_{44} - c_{12})] \tag{A.6}$$

$$\sqrt{(A + B + C)^2 - 4(AB + BC - 2\,D^2)} =$$

$$\{1/4(c_{11} + c_{12})^2 + \gamma^2(4\,c_{44}^2 - 3/2\,c_{11}^2 + 7/2\,c_{12}^2 + c_{11}c_{44} + 9\,c_{12}c_{44} - 2\,c_{12}c_{11}) + \gamma^4(9/4\,c_{11}^2 - 3\,c_{44}^2 - 15/4\,c_{12}^2 - 3\,c_{11}c_{44} - 9\,c_{12}c_{44} + 3/2\,c_{12}c_{11})\}^{1/2} \tag{A.7}$$

and

$$A - C = 1/2\,[c_{11} - c_{12} + \gamma^2(2\,c_{44} + c_{12} - c_{11})] \tag{A.8}$$

Using Eqs. (A.6) and (A.7), (A.8) in Eqs. (A.4) and (A.5) we find the velocities

$$v_T = \sqrt{1/(2\rho)\,[c_{11} - c_{12} + \gamma^2(2\,c_{44} + c_{12} - c_{11})]} \tag{A.9}$$

and

$$v_{\substack{L(+)\\M(-)}} = \sqrt{1/(4\rho)}\,[4\,c_{44} + c_{11} + c_{12} + \gamma^2(c_{11} - 2\,c_{44} - c_{12})$$

$$\pm \{(c_{11} + c_{12})^2 + (2\,c_{44} + c_{12} - c_{11})[\gamma^2(8\,c_{44} + 14\,c_{12} + 6\,c_{11})$$

$$- \gamma^4(6\,c_{44} + 15\,c_{12} + 9\,c_{11})]\}^{1/2}]^{1/2} \qquad \text{(A.10)}$$

Eigenvectors of the velocity determinant

Let us now consider the polarizations corresponding to the velocities, Eqs. (A.9) and (A.10). Consider Eq. (A.4). Upon substitution of (A.4) into (A.1) we find

$$\begin{bmatrix} C & C & D \\ C & C & D \\ D & D & B - A + C \end{bmatrix} \begin{bmatrix} A_1 \\ A_2 \\ A_3 \end{bmatrix} = 0$$

By inspection we see that the eigenvector having components A_1, A_2, and A_3 must be of the form (after normalization):

$$\underset{\sim}{A}_T = (1/\sqrt{2},\ -1/\sqrt{2},\ 0) \qquad \text{(A.11)}$$

This is a transverse polarization always perpendicular to the z-axis.

Secondly consider the root E_L, Eq. (A.5). If we let

$$K = (A + B + C)^2 - 4(AB + BC - 2\,D^2)$$

$$E_L = 1/2\ (A + B + C + \sqrt{K})$$

After letting $M = 1/2\ (A - B)$ and $N = -\ 1/2\ (C + \sqrt{K})$, Eq. (A.1) reduces to

$$\begin{bmatrix} M + N & C & D \\ C & M + N & D \\ D & D & -M + N \end{bmatrix} \begin{bmatrix} A_1 \\ A_2 \\ A_3 \end{bmatrix} = 0$$

and the unnormalized eigenvector is

$$\underset{\sim}{A}'_L = (1,\ 1,\ 4D/(A - B + C + \sqrt{K})) \qquad (A.12)$$

This is a mixed longitudinal and transverse mode with polarization in the {110} plane.

Finally consider E_M, Eq. (A.5). Let $P = -\ 1/2\ (C - \sqrt{K})$ and (A.1) reduces to

$$\begin{bmatrix} M + P & C & D \\ C & M + P & D \\ D & D & P - M \end{bmatrix} \begin{bmatrix} A_1 \\ A_2 \\ A_3 \end{bmatrix} = 0$$

and the unnormalized eigenvector is

$$\underset{\sim}{A}'_M = (1,\ 1,\ 4D/(A - B + C - \sqrt{K})\ ) \qquad (A.13)$$

This is another longitudinal and transverse mixed mode with polarization in the {110} plane, perpendicular to $\underset{\sim}{A}'_L$.

Let us rewrite (A.12) and (A.13) in normalized form. Write

$$\underset{\sim}{A}_{L,\ M} = (1,\ 1,\ P_{L,\ M})\ (2 + P^2_{L,\ M})^{-1/2} \qquad (A.14)$$

where

$$P_{\substack{L,\ M \\ (+,\ -)}} = 4D/(A - B + C \pm \sqrt{K})$$

However,

$$E_{\substack{L,\ M \\ (+,\ -)}} = 1/2\ (A + B + C \pm \sqrt{K})$$

and so

$$P_{L,\ M} = 4D/(2\ E_{L,\ M} - 2\ B)$$

$$P_{L,\ M} = \frac{\gamma\sqrt{2(1 - \gamma^2)}\ \ (c_{12} + c_{44})}{\rho v^2_{L,\ M} - c_{44} - \gamma^2(c_{11} - c_{44})} \qquad (A.15)$$

and $P_L P_M = -2$, easily shown by substitution.

Of course, along the <110> and <001> directions there is degeneracy and the two polarization vectors perpendicular to $\underset{\sim}{A}_L$ are not fixed in the plane perpendicular to $\underset{\sim}{A}_L$. Nevertheless, it is useful to choose the two vectors such that $\underset{\sim}{A}_T$ is always perpendicular to the {110} planes, $\underset{\sim}{A}_L$ and $\underset{\sim}{A}_M$ always being in those planes. It turns out that the L-root is almost completely longitudinal, the M-root shows longitudinal admixtures from 0% to 30%

depending upon the propagation direction, and $\underset{\sim}{A}_T$ is always completely transverse.

The percentage longitudinal admixture is defined by

$$\%L = 100 \times \underset{\sim}{A}\cdot\underset{\sim}{k}/|\underset{\sim}{k}|$$

where $\underset{\sim}{A}$ is the unit polarization vector and

$$\underset{\sim}{k} = k(\sqrt{1/2\ (1 - \gamma^2)}\ \hat{x} + \sqrt{1/2\ (1 - \gamma^2)}\ \hat{y} + \gamma\hat{z})$$

With Eq. (A.14) we find

$$\%L_{L,\,M} = 100\ \{\sqrt{2(1 - \gamma^2)} + \gamma P_{L,\,M}\}\ (2 + P^2_{L,\,M})^{-1/2} \qquad (A.16)$$

and the angle θ which the polarization makes with the propagation direction $\underset{\sim}{k}$ is given by

$$\theta = \cos^{-1}\ (\%L/100) = \cos^{-1}\ (\underset{\sim}{A}\cdot\underset{\sim}{k}/|\underset{\sim}{k}|) \qquad (A.17)$$

Sensitivity of v_L to the combination of elastic constants $2c_{44} + c_{12}$

The object is to show that v_L is sensitive only to the combination of elastic constants $2c_{44} + c_{12}$ and to c_{11}. We have found that $2c_{44} + c_{12}$ = constant will give approximately the same velocity regardless of the individual values of c_{44} and c_{12}. We want to show that this is consistent with the derivatives of v_L with respect to the elastic constants. We deduce $2dc_{44} + dc_{12} = 0$. If this condition is to be obeyed, then if c_{44} increases by the amount a, c_{12} must decrease by the amount 2a. So that the velocity does not change in this process,

$$dv_L/dc_{12} = 1/2\ dv_L/dc_{44} \qquad (A.18)$$

We can say that if we find Eq. (A.18) to hold fairly well for all γ, we expect $2c_{44} + c_{12}$ to be approximately constant. In Table XXVI I have presented the percentage difference between $2dv_L/dc_{12}$ and dv_L/dc_{44} as a function of γ. By studying Fig. 2.3 one finds that v_L is most sensitive to $2c_{44} + c_{12}$ between 40 and 80 degrees so that in the region where v_L is sensitive to the above combination, $2c_{44} + c_{12}$ = constant is obeyed quite well. This relation does not hold for the mixed mode and, therefore, we may use that mode to determine c_{12} and c_{44} separately.

TABLE XXVI

Percentage difference between dv_L/dc_{12} and 1/2 dv_L/dc_{44} as a function of propagation direction

Angle	Percentage discrepancy between dv_L/dc_{12} and 1/2 dv_L/dc_{44}
0	0%
15	20%
25	17%
35	12%
45	4%
55	0%
65	1.4%
75	1.3%
90	0%

REFERENCES

1. R. S. Krishnan, Proc. Ind. Acad. Sci. A 41, 91 (1955).

2. R. W. James, The Optical Principles of the Diffraction of X Rays (G. Bell and Sons, Ltd., London, 1958).

3. B. N. Brockhouse and A. T. Stewart, Rev. Mod. Phys. 30, 236 (1958).

4. L. Brillouin, Ann. de Phys. 17, 88 (1922).

5. E. F. Gross, Zeits. für Phys. 63, 685 (1930).

6. C. V. Raman and B. V. R. Rao, Nature 135, 761 (1935).

   C. V. Raman and B. V. R. Rao, Nature 141, 242 (1938).

   C. V. Raman and C. S. Venkateswaran, Nature 142, 250 (1938).

   R. S. Krishnan, Proc. Ind. Acad. Sci. A 26, 399 (1947).

   R. S. Krishnan, Proc. Ind. Acad. Sci. A 26, 450 (1947).

   R. S. Krishnan, Nature 159, 740 (1947).

   V. Chandrasekharan, Proc. Ind. Acad. Sci. A 32, 379 (1950).

   R. S. Krishnan and V. Chandrasekharan, Proc. Ind. Acad. Sci. A 31, 427 (1950).

   R. S. Krishnan and V. Chandrasekharan, Nature 165, 406 (1950).

   R. S. Krishnan, Nature 165, 933 (1950).

7. G. B. Benedek, J. B. Lastovka, K. Fritsch, and T. Greytak, J. Opt. Soc. Am. 54, 1284 (1964).

8. R. Y. Chiao and B. P. Stoicheff, J. Opt. Soc. Am. 54, 1286 (1964).

9. A. D. B. Woods, B. N. Brockhouse, R. A. Cowley, Phys. Rev. 131, 1025 (1963).

10. C. Kittel, Introduction to Solid State Physics (John Wiley and Sons, Inc., New York, 1960), pp. 85 - 92.

11. Jules de Launay, "The Theory of Specific Heats and Lattice Vibrations" in Solid State Physics, Advances in Research and Applications, Vol. 2 (1956), p. 266.

12. K. Burns, K. B. Adams, and J. Longwell, J. Opt. Soc. Am. 40, 339 (1950).

13. F. A. Jenkins and H. E. White, Fundamentals of Optics (McGraw-Hill Book Company, Inc., 1957), p. 330.

14. Landolt-Börnstein, Zahlenwerte und Funktionen aus Physik-Chemie-Astronomie-Geophysik-Technik, 6. Auflage, II. Band, 8. Teil, Optische Konstanten.

15. International Critical Tables of Numerical Data in Physics, Chemistry and Technology (McGraw-Hill Book Company, Inc., New York, 1926).

16. I. Fabelinskii, Usp. Fiz. Nauk 63, 355 (1957).

17. R. W. James, The Optical Principles of the Diffraction of X Rays (G. Bell and Sons, Ltd., London, 1958), p. 208.

18. P. Jaquinot, J. Opt. Soc. Am. 44, 761 (1954).

19. F. A. Jenkins and L. W. Alvarez, J. Opt. Soc. Am. 42, 699 (1952).

20. G. W. Stroke, J. Opt. Soc. Am. 51, 1321 (1961).

21. Quarterly Status Report # 1, AF19(628)-3994, Research directed toward the development of an improved process for optical grating ruling, M.I.T. Spectroscopy Laboratory with Electronics Research Directorate, Air Force Research Laboratories Office of the Aerospace Research, USAF.